REVIEW ARTICLE



Optimal Local Truncation Error Method for Solution of Partial Differential Equations on Irregular Domains and Interfaces Using Unfitted Cartesian Meshes: Review

A. Idesman¹

Received: 17 January 2023 / Accepted: 25 May 2023 / Published online: 7 July 2023 © The Author(s) under exclusive licence to International Center for Numerical Methods in Engineering (CIMNE) 2023

Abstract

The review of the optimal local truncation error method (OLTEM) for the numerical solution of PDEs is presented along with some new developments of OLTEM. First, we explain the basic ideas of OLTEM for the 1-D wave equation and then we extend them to the time-dependent PDEs (the scalar wave and heat equations as well as a system of the elastodynamics equations) and to the time-independent PDEs (the Poisson and Helmholtz equations as well as a system of the elastostatics equations) in the 2-D and 3-D cases for homogeneous, inhomogeneous and heterogeneous materials. The main advantages of OLTEM are the optimal (maximum possible) accuracy of discrete equations and the use of unfitted Cartesian meshes for irregular domains and interfaces. For example, for heterogeneous materials with irregular interfaces, OLTEM with 2-D 25-point stencils (similar to those for quadratic finite elements) provides the 11-th and 10-th orders of accuracy for the Poisson and elasticity equations, i.e, a huge increase in accuracy by 8 and 7 orders compared to quadratic finite elements without additional computational costs. Another advantage of OLTEM is a special procedure for the imposition of the boundary and interface conditions without the introduction of additional unknowns. These conditions at a small number of the selected boundary and interface points are added to the local truncation error as the constraints with Lagrange multipliers. This special procedure does not introduce additional unknowns on the boundaries and interfaces (only the unknowns at internal Cartesian grid points are used), does not change the width of cut stencils, allows unfitted meshes and provides a high accuracy of cut stencils. For time-dependent PDEs, OLTEM offers a rigorous approach for the calculation of the diagonal mass matrix in terms of the coefficients of the stiffness matrix that is based on the accuracy considerations. A new OLTEM post-processing procedure for the calculation of the spatial derivatives of the primary function that is based on the use of original PDEs significantly increases the accuracy of the spatial derivatives. For example, we have obtained the 10-th order of accuracy for stresses calculated by OLTEM with 25-point stencils applied to 2-D elastostatics problems with heterogeneous materials and irregular interfaces. New developments of OLTEM related to numerical high-order boundary conditions for cut stencils as well as to the accurate calculation of the primary functions and their derivatives at any point of the domain are presented. The comparison of accuracy of OLTEM and FEM at similar stencils is also analyzed. Numerical results show that at the engineering accuracy, OLTEM can reduce the number of degrees of freedom by 1000-1,000,000 times compared to that for finite elements at similar stencils.

1 Introduction

Accurate and fast numerical solutions of partial differential equations (PDEs) describing many mechanical phenomena is one of the main objectives of computational mechanics.

 Complex irregular geometry including irregular boundaries and interfaces represents difficulties in the development of reliable numerical methods for PDEs. The modern numerical methods such as the finite element method, the finite volume method, the isogeometric elements, the spectral elements and similar techniques are widely used for the solution of different PDEs on irregular geometry. These methods use powerful mesh generators for the automatic spatial discretization of irregular geometry with conforming meshes. However, in the case of very complex geometries, these conforming meshes may include 'bad'



Department of Mechanical Engineering, Texas Tech University, Lubbock, TX 79409-1021, USA

elements (e.g., the elements with small angles) that lead to very inaccurate numerical results. Along with the accuracy considerations, another very important feature of any numerical method is the computation time (computational costs) needed for achieving a given accuracy of numerical results. For example, many numerical techniques for irregular domains are derived using some weak formulations (e.g., based on the Galerkin approaches). However, in many cases these approaches do not provide the optimal accuracy of the derived discrete equations. For example, it is known that finite elements of order p provide the p+1order of accuracy in the L^2 norm. However, in our papers [1-3] we showed that for the same structure of the discrete equations, new 'quadratic' elements (p = 2) provide the 18-th order of accuracy for the Poisson equation and the 10-th order of accuracy for the elasticity equations on regular domains with uniform meshes as well as the 11-th and 10-th order of accuracy for the Poisson and elasticity equations for heterogeneous materials with irregular interfaces.

To resolve the above-mentioned issues with the mesh generation on irregular geometry, many numerical techniques have been developed with simple uniform meshes such as the embedded finite difference method, the cut finite element method, the finite cell method, the Cartesian grid method, the immersed interface method, the virtual boundary method, the embedded boundary method, etc. For example, the techniques based on the finite element formulations (such as the cut finite element method, the finite cell method, the virtual boundary method and others) yield the p + 1 order of accuracy even with small cut cells generated due to complex irregular boundaries (e.g., see [4–10] and many others). The main advantage of the embedded boundary method developed in [11-15] is the use of simple Cartesian meshes. The boundary conditions or fluxes in this technique are interpolated using the Cartesian grid points and this leads to the increase in the stencil width for the grid points located close to the boundary (the numerical techniques developed in [11–15] provide just the second order of accuracy for the global solution). Interesting finite element techniques with simple unfitted meshes has been developed in [16-21] for the Poisson equation with irregular interfaces. However, these techniques provide the p+1 order of accuracy for highorder immersed, generalized and extended finite elements of order p as well as they introduce additional degrees of freedom for the consideration of the interface conditions.

Recently, we have developed an optimal local truncation method (OLTEM) for the numerical solution of PDEs on regular ([1, 2, 22–24]) and irregular ([25–33]) domains and irregular interfaces ([34–38]). The main objectives in the development of OLTEM are to use trivial unfitted

Cartesian meshes for irregular domains and interfaces as well as to provide the maximum possible accuracy of discrete equations used for the discretization of PDEs. In this paper we will review OLTEM for different PDEs presented in our above-mentioned papers as well as we will show some new developments and the applications of OLTEM. We should also note that the derivation of OLTEM with compact stencils includes a Taylor series expansion of unknown functions. The review of Taylorseries based numerical methods (including the generalized finite difference method (GFD), the particle strength method, the moving least square method and the interpolating moving least square method) as well as their comparison with the finite element method is given in the recent paper [39]; see also the numerous references there. One of the main differences between OLTEM and the generalized finite difference method is in the approach for the determination of the coefficients of discrete equations. In contrast to the approximation of the spatial derivatives as in GFD, in OLTEM we maximize the accuracy of each discrete equation by the calculation of the optimal values of the coefficients of the discrete equations with the use of the corresponding PDE. For example, in the case of a system of PDEs, all PDEs are used for the calculation of the coefficients of one discrete equation. This provides the maximum possible accuracy of the discrete equations of OLTEM. Another big difference is the imposition of the boundary and interface conditions. In OLTEM, these conditions are applied at a small number of the selected boundary and interface points as the constraints for the local truncation error. This procedure does not introduce additional unknowns on the boundaries and interfaces, allows unfitted meshes and provides the high accuracy of cut stencils.

In Sect. 2, we explain the ideas and the derivation of OLTEM for the simple 1-D wave equation. This includes the introduction of the local truncation error of stencil equations, the calculation of the stencil coefficients for the 3-point, 5-point and 7-point stencils (similar to those for linear quadratic and cubic finite elements) for homogeneous materials, the calculation of the diagonal mass matrix, the consideration of the wave equation with nonzero body forces, the extension of OLTEM to heterogeneous materials. In Sect. 3 we extend OLTEM to the general 2-D and 3-D cases for the time-dependent scalar wave and heat equations with homogeneous, inhomogeneous and heterogeneous materials as well as for a system of elastodynamics equations with homogeneous and heterogeneous materials. The development of OLTEM for the time independent Poisson, Helmholtz and elasticity equations with homogeneous and heterogeneous materials is presented in Sect. 4. The post-processing procedure for the calculation of the spatial derivatives of the primary



functions at grid points that is based on OLTEM is described in Sect. 5. This paper includes also new developments of OLTEM. A new OLTEM procedure for the calculation the primary function and its derivatives at any point of the domain is presented in Sect. 6. New numerical high-order Dirichlet and Neumann boundary conditions for cut stencils that provide the same order of the local truncation error as that for the 2-D 25-point regular stencils has been developed in Sect. 7. The comparison of accuracy of OLTEM and FEM showing a huge increase in accuracy for OLTEM is given in Sect. 8. The main features and advantages of OLTEM are summarized in the concluding remarks in Sect. 9. For the derivation of many analytical expressions presented below we use the computational program "Mathematica".

2 OLTEM for 1-D Wave Equation

Wave propagation in an 1-D homogeneous medium is described by the following scalar wave equation:

$$\frac{\partial^2 u}{\partial t^2} - c^2 \frac{\partial^2 u}{\partial x^2} = f,\tag{1}$$

where u is the displacement, c is the wave velocity, f(x, t) is the loading term.

2.1 Introduction of the Local Truncation Error

According to the new approach we assume that a stencil equation for the wave equation after the space discretization with a uniform mesh can be written as an ordinary differential equation (a semidiscrete equation):

$$\sum_{i=1}^{L} \left(h^2 m_i \frac{d^2 u_i^{num}}{dt^2} + k_i u_i^{num} \right) = \bar{f}, \tag{2}$$

where u_i^{num} and $\frac{d^2 u_i^{num}}{dt^2}$ are the numerical solution for function u and its second order time derivative at the grid points, m_i and k_i are the unknown coefficients to be determined (they will be determined by the minimization of the local truncation error for Eq. (2), see below), L is the number of the grid points included into the stencil, h is the mesh size along the x- axis, \bar{f} is the discretized loading term. Many numerical techniques such as the finite difference method, the finite element method, the finite volume method, the isogeometric elements, the spectral elements, different meshless methods and others can be finally reduced to a system of the stencil equations, Eq. (2), with some specific coefficients m_i and k_i . For OLTEM used below, we consider the semi-discrete equations without the time discretization. After the derivation of the coefficients of the semidiscrete equations, any existing time-integration method can be used for the time integration of the semidiscrete equations. The initial conditions used for the time integration of the semidiscrete equations are similar to those for other numerical methods (e.g., for FEM).

Let us introduce the local truncation error used with the new approach. The replacement of the numerical values of the function u_i^{num} and its second order time derivatives $\frac{d^2 u_i^{num}}{dt^2}$ at the grid points in Eq. (2) by the exact solution u_i and $\frac{d^2 u_i}{dt^2}$ to the wave equation, Eq. (1), at the grid points leads to the residual of this equation called the local truncation error e in space for the semidiscrete equation, Eq. (2):

$$e = \sum_{i=1}^{L} \left(h^2 m_i \frac{d^2 u_i}{dt^2} + k_i u_i \right) - \bar{f}.$$
 (3)

Considering the difference between Eqs. (3) and (2) we can get

$$e = \sum_{i=1}^{L} \left\{ h^{2} m_{i} \left[\frac{d^{2} u_{i}}{dt^{2}} - \frac{d^{2} u_{i}^{num}}{dt^{2}} \right] + k_{i} [u_{i} - u_{i}^{num}] \right\}$$

$$= \sum_{i=1}^{L} (h^{2} m_{i} \bar{e}_{i}^{v} + k_{i} \bar{e}_{i}),$$
(4)

where $\bar{e}_i = u_i - u_i^{num}$ and $\bar{e}_i^v = \frac{d^2 u_i}{dt^2} - \frac{d^2 u_i^{num}}{dt^2}$ are the errors of function u and its order time derivative at the grid points i. As can be seen from Eq. (4), the local truncation error e is a linear combination of the errors of the function u and its order time derivative at the grid points i which are included into the stencil equation. We will use the unknown stencil coefficients m_i and k_i in Eq. (4) in order to minimize the local truncation error e in Eq. (4).

2.2 3-Point Stencils for the 1-D Wave Equation with Zero Load (f=0) on Uniform Meshes (Comparison OLTEM with FEM)

After the space discretization of Eq. (1) with zero load $(f = \bar{f} = 0)$ on a uniform mesh of size h, a 3-point stencil for each internal grid point can be introduced as follows: (see Fig. 1):

$$h^{2}\left(m_{1}\frac{d^{2}u_{1}^{num}}{dt^{2}} + m_{2}\frac{d^{2}u_{2}^{num}}{dt^{2}} + m_{3}\frac{d^{2}u_{3}^{num}}{dt^{2}}\right) + \left(k_{1}u_{1}^{num} + k_{2}u_{2}^{num} + k_{3}u_{3}^{num}\right) = 0,$$
(5)

where the coefficients m_i and k_i (i = 1, 2, 3) should be

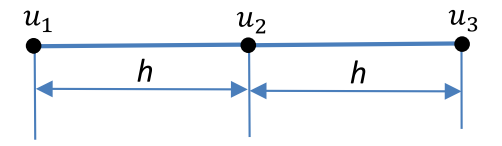


Fig. 1 The spatial locations of the grid points i (i = 1, 2, 3) contributing to the 3-point stencil for the grid point 2



(6)

determined, superscript 'num' corresponds to the numerical value of the function. The 3-point stencil in Eq. (5) is similar to that for linear finite elements with the stencil coefficients calculated through the elemental mass and stiffness matrices. The stencil coefficients for the conventional linear finite elements are:

$$m_1 = \frac{1}{6c^2}$$
, $m_2 = \frac{2}{3c^2}$, $m_3 = \frac{1}{6c^2}$, $k_1 = -1$, $k_2 = 2$, $k_3 = -1$.

The local truncation error e for the 3-point stencil is obtained by the replacement of the numerical value of function u_i^{num} in Eq. (5) by the exact value u_i at the grid points i (i = 1, 2, 3):

$$e = h^{2} \left(m_{1} \frac{d^{2}u_{1}}{dt^{2}} + m_{2} \frac{d^{2}u_{2}}{dt^{2}} + m_{3} \frac{d^{2}u_{3}}{dt^{2}} \right) + (k_{1}u_{1} + k_{2}u_{2} + k_{3}u_{3}).$$

$$(7)$$

Using the partial differential equation, Eq. (1), the time derivatives of the exact solution at the grid points can be replaced by the spatial derivatives as follows:

$$\frac{\partial^2 u_1}{\partial t^2} = c^2 \frac{\partial^2 u_1}{\partial x^2}, \qquad \frac{\partial^2 u_2}{\partial t^2} = c^2 \frac{\partial^2 u_2}{\partial x^2},
\frac{\partial^2 u_3}{\partial t^2} = c^2 \frac{\partial^2 u_3}{\partial x^2},$$
(8)

Then, the expression for the local truncation error, Eq. (5), can be simplified with the help of Eq. (8) as follows:

$$e = h^{2}c^{2} \left(m_{1} \frac{\partial^{2} u_{1}}{\partial x^{2}} + m_{2} \frac{\partial^{2} u_{2}}{\partial x^{2}} + m_{3} \frac{\partial^{2} u_{3}}{\partial x^{2}} \right) + (k_{1}u_{1} + k_{2}u_{2} + k_{3}u_{3}).$$

$$(9)$$

Next, let us expand the local truncation error, Eq. (9), into a Taylor series by the expansion of the exact solution for u_i and $\frac{\partial^2 u_i}{\partial x^2}$ at the grid points i=1 and i=3 into a Taylor series in the vicinity of point i=2 at small $h \ll 1$ as follows (see Fig. 1 for the locations of the grid points):

$$u_{1} = u(x_{1} = x_{2} - h) = u_{2} - \frac{\partial u_{2}}{\partial x}h + \frac{\partial^{2} u_{2}}{\partial x^{2}} \frac{h^{2}}{2!} - \frac{\partial^{3} u_{2}}{\partial x^{3}} \frac{h^{3}}{3!} + \frac{\partial^{4} u_{2}}{\partial x^{4}} \frac{h^{4}}{4!} - \dots$$
(10)

$$u_{3} = u(x_{3} = x_{2} + h) = u_{2} + \frac{\partial u_{2}}{\partial x}h + \frac{\partial^{2} u_{2}}{\partial x^{2}}\frac{h^{2}}{2!} + \frac{\partial^{3} u_{2}}{\partial x^{3}}\frac{h^{3}}{3!} + \frac{\partial^{4} u_{2}}{\partial x^{4}}\frac{h^{4}}{4!} + \dots$$
(11)

$$\frac{\partial^{2} u_{1}}{\partial x^{2}} = \frac{\partial^{2} u}{\partial x^{2}} (x_{1} = x_{2} - h) = \frac{\partial^{2} u_{2}}{\partial x^{2}}
- \frac{\partial^{3} u_{2}}{\partial x^{3}} h + \frac{\partial^{4} u_{2}}{\partial x^{4}} \frac{h^{2}}{2!} - \frac{\partial^{5} u_{2}}{\partial x^{5}} \frac{h^{3}}{3!} + \frac{\partial^{6} u_{2}}{\partial x^{6}} \frac{h^{4}}{4!} - \dots$$
(12)

$$\frac{\partial^{2} u_{3}}{\partial x^{2}} = \frac{\partial^{2} u}{\partial x^{2}} (x_{3} = x_{2} + h) = \frac{\partial^{2} u_{2}}{\partial x^{2}}
+ \frac{\partial^{3} u_{2}}{\partial x^{3}} h + \frac{\partial^{4} u_{2}}{\partial x^{4}} \frac{h^{2}}{2!} + \frac{\partial^{5} u_{2}}{\partial x^{5}} \frac{h^{3}}{3!} + \frac{\partial^{6} u_{2}}{\partial x^{6}} \frac{h^{4}}{4!} + \dots$$
(13)

Inserting Eqs. (10)-(13) into Eq. (9) we get the following Taylor series for the local truncation error:

$$e = u_{2}[k_{1} + k_{2} + k_{3}] + h \frac{\partial u_{2}}{\partial x}[k_{3} - k_{1}]$$

$$+ \frac{1}{2}h^{2} \frac{\partial^{2}u_{2}}{\partial x^{2}}[k_{1} + k_{3} + 2c^{2}(m_{1} + m_{2} + m_{3})]$$

$$+ \frac{1}{6}h^{3} \frac{\partial^{3}u_{2}}{\partial x^{3}}[k_{3} - k_{1} + 6c^{2}(m_{3} - m_{1})]$$

$$+ \frac{1}{24}h^{4} \frac{\partial^{4}u_{2}}{\partial x^{4}}[k_{1} + k_{3} + 12c^{2}(m_{1} + m_{3})]$$

$$+ \frac{1}{120}h^{5} \frac{\partial^{5}u_{2}}{\partial x^{5}}[k_{3} - k_{1} + 20c^{2}(m_{3} - m_{1})]$$

$$+ \frac{1}{720}h^{6} \frac{\partial^{6}u_{2}}{\partial x^{6}}[k_{1} + k_{3} + 30c^{2}(m_{1} + m_{3})] + O(h^{7}).$$
(14)

Equation (14) can be rewritten in the following form:

$$e = u_{2}b_{1} + h\frac{\partial u_{2}}{\partial x}b_{2} + \frac{1}{2}h^{2}\frac{\partial^{2}u_{2}}{\partial x^{2}}b_{3} + \frac{1}{6}h^{3}\frac{\partial^{3}u_{2}}{\partial x^{3}}b_{4} + \frac{1}{24}h^{4}\frac{\partial^{4}u_{2}}{\partial x^{4}}b_{5} + \frac{1}{120}h^{5}\frac{\partial^{5}u_{2}}{\partial x^{5}}b_{6} + \frac{1}{720}h^{6}\frac{\partial^{6}u_{2}}{\partial x^{6}}b_{7} + O(h^{7}),$$

$$(15)$$

where the b_i coefficients are the linear combinations of the 6 stencil coefficients m_i and k_i (i = 1, 2, 3). The b_i coefficients can be easily found by the comparison of Eqs. (14) and (15). Due to the use of Eq. (8), the local truncation error in Eqs. (9), (14) and (15) does not include the time derivatives. We should mention that Eq. (14) provides the local truncation error for any numerical method with the 3-point stencil equation, Eq. (5), independent of the technique used for the derivation of the stencil coefficients in Eq. (5). For example, inserting the stencil coefficients for linear finite elements given by Eq. (6) into Eq. (14), we can find that linear finite elements provide the fourth order of the local truncation error:

$$e_{FE} = \frac{h^4}{12} \frac{\partial^4 u_2}{\partial x^4} + O(h^6). \tag{16}$$

Next, we will show that linear finite elements do not provide the optimal order of accuracy for the the 3-point stencil equation, Eq. (5). Below we derive the stencil coefficients of the 3-point stencil equation, Eq. (5), for OLTEM that are based on the minimization of the local



truncation error. Equating the first five coefficients b_i (i = 1, 2, ..., 5) with the smallest orders of h in Eq. (15) to zero we get the following linear system of five algebraic equations for finding the stencil coefficients:

$$b_{1} = k_{1} + k_{2} + k_{3} = 0, b_{2} = k_{3} - k_{1} = 0,$$

$$b_{3} = k_{1} + k_{3} + 2c^{2}(m_{1} + m_{2} + m_{3}) = 0,$$

$$b_{4} = k_{3} - k_{1} + 6c^{2}(m_{3} - m_{1}) = 0,$$

$$b_{5} = k_{1} + k_{3} + 12c^{2}(m_{1} + m_{3}) = 0.$$

$$(17)$$

Solving this system, we can find the following coefficients m_i and k_i (i = 1, 2, 3) of the stencil equation, Eq. (5), for OLTEM:

$$m_1 = \frac{a}{24c^2},$$
 $m_2 = \frac{5a}{12c^2},$ $m_3 = \frac{a}{24c^2},$ $k_1 = -\frac{a}{2},$ $k_2 = a,$ $k_3 = -\frac{a}{2},$ (18)

where a is an arbitrary coefficient.

Remark 1 The multiplication of each term of the stencil equation, Eq. (5), by any scalar does not change this equation, i.e, only five coefficients m_i and k_i are independent and should be determined in Eq. (5). Therefore, we use five algebraic equations for their calculations (see Eq. (17)). This fact is also reflected by the existence of the arbitrary multiplier a in Eq. (18) that does not affect the results and, for convenience, can be taken as $k_2 = a = 1$.

Inserting the coefficients m_i and k_i (i = 1, 2, 3) for OLTEM (see Eq. (18)) into Eq. (14) we get the local truncation error for OLTEM (we use $k_2 = a = 1$):

$$e_{OLTEM} = \frac{h^6}{480} \frac{\partial^6 u_2}{\partial x^6} + O(h^8). \tag{19}$$

As can be seen from Eqs. (16) and (19), OLTEM with the 3-point stencils improves the accuracy by two orders compared to that for linear finite elements with the same 3-point stencils. The difference between OLTEM and FEM is just in the values of the stencil coefficients m_i and k_i (i = 1, 2, 3).

2.3 Extension of OLTEM to High-Order Stencils for the 1-D Wave Equation on Uniform Meshes

Here, we consider the extension of OLTEM derived in Sect. 2.2 to 5-point and 7-point stencils on uniform Cartesian meshes with the mesh size h. Similar to Eq. (5), the 5-point stencil can be written as follows:

$$h^{2}\left(m_{1}\frac{d^{2}u_{1}^{num}}{dt^{2}} + m_{2}\frac{d^{2}u_{2}^{num}}{dt^{2}} + m_{3}\frac{d^{2}u_{3}^{num}}{dt^{2}} + m_{4}\frac{d^{2}u_{4}^{num}}{dt^{2}} + m_{5}\frac{d^{2}u_{5}^{num}}{dt^{2}}\right) + \left(k_{1}u_{1}^{num} + k_{2}u_{2}^{num} + k_{3}u_{3}^{num} + k_{4}u_{4}^{num} + k_{5}u_{5}^{num}\right) = 0,$$

$$(20)$$

where the coefficients m_i and k_i (i = 1, 2, 3, 4, 5) should be

determined. The 5-point stencil in Eq. (20) is similar to that for quadratic finite elements with the stencil coefficients calculated through the elemental mass and stiffness matrices. Similar to the derivations given by Eqs. (7)-(14), a Taylor series for the local truncation error for the 5-point stencil in the vicinity of the stencil central grid point with the coordinate x_3 is:

$$e = u_{2}b_{1} + h\frac{\partial u_{3}}{\partial x}b_{2} + \frac{1}{2}h^{2}\frac{\partial^{2}u_{3}}{\partial x^{2}}b_{3}$$

$$+ \frac{1}{6}h^{3}\frac{\partial^{3}u_{3}}{\partial x^{3}}b_{4} + \frac{1}{24}h^{4}\frac{\partial^{4}u_{3}}{\partial x^{4}}b_{5}$$

$$+ \frac{1}{120}h^{5}\frac{\partial^{5}u_{3}}{\partial x^{5}}b_{6} + \frac{1}{720}h^{6}\frac{\partial^{6}u_{3}}{\partial x^{6}}b_{7}$$

$$+ \frac{1}{5040}h^{7}\frac{\partial^{7}u_{3}}{\partial x^{7}}b_{8} + \frac{1}{40320}h^{8}\frac{\partial^{8}u_{3}}{\partial x^{8}}b_{9}$$

$$+ \frac{1}{362880}h^{9}\frac{\partial^{9}u_{3}}{\partial x^{9}}b_{10} + \frac{1}{3628800}h^{10}\frac{\partial^{10}u_{3}}{\partial x^{10}}b_{11} + O(h^{11}),$$
(21)

where similar to Eq. (15) the b_i coefficients are the linear combinations of the 10 stencil coefficients m_i and k_i (i = 1, 2, ..., 5). Equating the first nine coefficients b_i (i = 1, 2, ..., 9) with the smallest orders of h in Eq. (21) to zero with $k_3 = 1$ (see Remark 1) we get the following linear system of nine algebraic equations for finding the stencil coefficients:

$$b_{1} = k_{1} + k_{2} + k_{3} + k_{4} + k_{5} = 0,$$

$$b_{2} = -2k_{1} - k_{2} + k_{4} + 2k_{5} = 0,$$

$$b_{3} = (4k_{1} + k_{2} + k_{4} + 4k_{5} + 2c^{2}(m_{1} + m_{2} + m_{3} + m_{4} + m_{5})) = 0,$$

$$b_{4} = (-8k_{1} - k_{2} + k_{4} + 8k_{5} + 6c^{2}(-2m_{1} - m_{2} + m_{4} + 2m_{5})) = 0,$$

$$b_{5} = (16k_{1} + k_{2} + k_{4} + 16k_{5} + 12c^{2}(4m_{1} + m_{2} + m_{4} + 4m_{5})) = 0,$$

$$b_{6} = (-32k_{1} - k_{2} + k_{4} + 32k_{5} + 20c^{2}(-8m_{1} - m_{2} + m_{4} + 8m_{5})) = 0,$$

$$b_{7} = (64k_{1} + k_{2} + k_{4} + 64k_{5} + 30c^{2}(16m_{1} + m_{2} + m_{4} + 16m_{5})) = 0,$$

$$b_{8} = (-128k_{1} - k_{2} + k_{4} + 128k_{5} + 42c^{2}(-32m_{1} - m_{2} + m_{4} + 32m_{5})) = 0,$$

$$b_{9} = (256k_{1} + k_{2} + k_{4} + 256k_{5} + 56c^{2}(64m_{1} + m_{2} + m_{4} + 64m_{5})) = 0,$$

$$b_{10} = (-512k_{1} - k_{2} + k_{4} + 512k_{5} + 72c^{2}(-128m_{1} - m_{2} + m_{4} + 128m_{5})) = 0,$$

$$k_{10} = (-512k_{1} - k_{2} + k_{4} + 512k_{5} + 72c^{2}(-128m_{1} - m_{2} + m_{4} + 128m_{5})) = 0,$$

$$k_{10} = (-512k_{1} - k_{2} + k_{4} + 512k_{5} + 72c^{2}(-128m_{1} - m_{2} + m_{4} + 128m_{5})) = 0,$$

$$k_{11} = (-512k_{1} - k_{2} + k_{4} + 512k_{5} + 72c^{2}(-128m_{1} - m_{2} + m_{4} + 128m_{5})) = 0,$$

$$k_{12} = (-512k_{1} - k_{2} + k_{4} + 512k_{5} + 72c^{2}(-128m_{1} - m_{2} + m_{4} + 128m_{5})) = 0,$$

$$k_{12} = (-512k_{1} - k_{2} + k_{4} + 512k_{5} + 72c^{2}(-128m_{1} - m_{2} + m_{4} + 128m_{5})) = 0,$$

$$k_{13} = (-512k_{1} - k_{2} + k_{4} + 512k_{5} + 72c^{2}(-128m_{1} - m_{2} + m_{4} + 128m_{5})) = 0,$$

Solving this system, we can find the following coefficients m_i and k_i (i = 1, 2, 3, 4, 5) of the stencil equation, Eq. (20), for OLTEM:



$$m_{1} = \frac{23}{4770c^{2}}, m_{2} = \frac{344}{2385c^{2}}, m_{3} = \frac{131}{265c^{2}}, m_{4}$$

$$= \frac{344}{2385c^{2}}, m_{5} = \frac{23}{4770c^{2}}, k_{1} = -\frac{31}{318}, k_{2}$$

$$= -\frac{64}{159}, k_{3} = 1, k_{4} = -\frac{64}{159},$$

$$k_{5} = -\frac{31}{318}.$$
(23)

Inserting the coefficients m_i and k_i (i = 1, 2, 3, 4, 5) for OLTEM (see Eq. (23)) into Eq. (21) we get the local truncation error for OLTEM:

$$e_{OLTEM} = \frac{79h^{10}}{6010200} \frac{\partial^{10}u_3}{\partial x^{10}} + O(h^{11}). \tag{24}$$

Repeating similar derivations for the 7-point stencil, we will get the following coefficients m_i and k_i (i = 1, 2, 3, 4, 5, 6, 7) for OLTEM:

$$m_{1} = \frac{1857}{3252620c^{2}}, m_{2} = \frac{55161}{1626310c^{2}}, m_{3}$$

$$= \frac{989739}{3252620c^{2}}, m_{4} = \frac{543981}{813155c^{2}}, m_{5}$$

$$= \frac{989739}{3252620c^{2}}, m_{6} = \frac{55161}{1626310c^{2}}, m_{7}$$

$$= \frac{1857}{3252620c^{2}}, k_{1} = -\frac{7069}{464660}, k_{2} = -\frac{8019}{33190}, k_{3}$$

$$= -\frac{22599}{92932}, k_{4} = 1, k_{5} = -\frac{22599}{92932}, k_{6}$$

$$= -\frac{8019}{33190}, k_{7} = -\frac{7069}{464660}$$
(25)

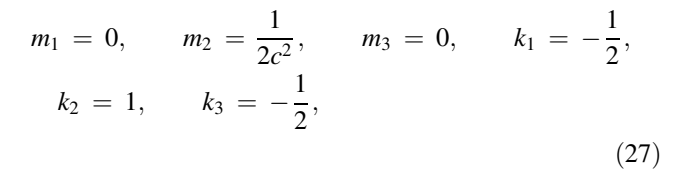
with the following local truncation error:

$$e_{OLTEM} = \frac{114669h^{14}}{1302349048000} \frac{\partial^{14}u_4}{\partial x^{14}} + O(h^{15}). \tag{26}$$

It can be also shown that OLTEM with the (2p+1)-point stencils $(p=1,2,\ldots)$ can provide 4p+2 order of the local truncation error e_{OLTEM} for the 1-D wave equation.

2.4 OLTEM with the Diagonal Mass Matrix

OLTEM with the diagonal mass matrix can be derived as a particular case of the non-diagonal mass matrix presented in Sects. 2.2 and 2.3. For the 3-point stencil with the diagonal mass matrix, the non-diagonal mass matrix coefficients are zero, i.e, $m_1 = m_3 = 0$ in Eqs. (5), (7), (9), (15). Equating the first three coefficients b_i (i = 1, 2, 3) with the smallest orders of h in Eq. (15) to zero with $k_2 = 1$ (see Remark 1), we get the following coefficients m_i and k_i (i = 1, 2, 3) for OLTEM with the 3-point stencil and the diagonal mass matrix:



with the following local truncation error:

$$e_{OLTEM} = \frac{h^4}{24} \frac{\partial^4 u_2}{\partial x^4} + O(h^5). \tag{28}$$

It is interesting to note that from the equation $b_3 = 0$ [see Eq. (17)] it follows that

$$m_2 = -\frac{1}{2c^2}(k_1 + k_3) \tag{29}$$

for the diagonal mass matrix ($m_1 = m_3 = 0$), i.e, the diagonal mass matrix is expressed in terms of the coefficients k_1 and k_3 of the stiffness matrix. This formula, Eq. (29), is valid for any 3-point stencil independent of the numerical method, i.e., with any other value for the diagonal mass term m_2 in the diagonal mass matrix, the order of the local truncation error of Eq. (5) will be smaller (the error will be greater).

Repeating similar derivations for the 5-point and 7-point stencils (we will zero the first five coefficients $b_i = 0$, i = 1, 2, ..., 5 in Eq. (21) for the 5-point stencil and the first seven coefficients $b_i = 0$, i = 1, 2, ..., 7 in the expression for the local truncation error for the 7-point stencil), we will get the following coefficients m_i and k_i for OLTEM with the diagonal mass matrix:

$$m_1 = 0,$$
 $m_2 = 0,$ $m_3 = \frac{2}{5c^2},$ $m_4 = 0,$ $m_5 = 0,$
 $k_1 = \frac{1}{30},$ $k_2 = -\frac{8}{15},$ $k_3 = 1,$
 $k_4 = -\frac{8}{15},$ $k_5 = \frac{1}{30},$ (30)

with the local truncation error:

$$e_{OLTEM} = \frac{h^6}{225} \frac{\partial^6 u_3}{\partial x^6} + O(h^7)$$
 (31)

for the 5-point stencil as well as

$$m_1 = 0,$$
 $m_2 = 0,$ $m_3 = 0,$
 $m_4 = \frac{18}{49c^2},$
 $m_5 = 0,$ $m_6 = 0,$ $m_7 = 0,$
 $k_1 = -\frac{1}{245},$ $k_2 = \frac{27}{490},$ $k_3 = -\frac{27}{49},$ $k_4 = 1,$
 $k_5 = -\frac{27}{49},$ $k_6 = \frac{27}{490},$ $k_7 = -\frac{1}{245},$ (32)

with the local truncation error:



$$e_{OLTEM} = \frac{9h^8}{13720} \frac{\partial^8 u_4}{\partial x^8} + O(h^9)$$
 (33)

for the 7-point stencil. It can be also shown that OLTEM with the (2p+1)-point stencils $(p=1,2,\ldots)$ and the diagonal mass matrix can provide 2p+2 order of the local truncation error e_{OLTEM} for the 1-D wave equation.

2.5 Extension of OLTEM with the 3-Point Stencils to the 1-D Wave Equation with Non-zero Load Term $f \neq 0$

In this case, the non-zero discretized load term \bar{f} should be added to the stencil equation, Eq. (5), as follows:

$$h^{2}\left(m_{1}\frac{d^{2}u_{1}^{num}}{dt^{2}} + m_{2}\frac{d^{2}u_{2}^{num}}{dt^{2}} + m_{3}\frac{d^{2}u_{3}^{num}}{dt^{2}}\right) + (k_{1}u_{1}^{num} + k_{2}u_{2}^{num} + k_{3}u_{3}^{num}) = \bar{f}.$$
(34)

Below we show how to define the load term \bar{f} . The local truncation error e_f for the 3-point stencil with nonzero load term \bar{f} can be obtained by the replacement of the numerical value of function u_i^{num} in Eq. (34) by the exact value u_i at the grid points i (i = 1, 2, 3):

$$e_f = h^2 \left(m_1 \frac{d^2 u_1}{dt^2} + m_2 \frac{d^2 u_2}{dt^2} + m_3 \frac{d^2 u_3}{dt^2} \right) + \left(k_1 u_1 + k_2 u_2 + k_3 u_3 \right) - \bar{f}.$$
(35)

Using the partial differential equation, Eq. (1), the time derivatives of the exact solution at the grid points can be replaced by the spatial derivatives as follows:

$$\frac{\partial^2 u_1}{\partial t^2} = c^2 \frac{\partial^2 u_1}{\partial x^2} + f_1,$$

$$\frac{\partial^2 u_2}{\partial t^2} = c^2 \frac{\partial^2 u_2}{\partial x^2} + f_2,$$

$$\frac{\partial^2 u_3}{\partial t^2} = c^2 \frac{\partial^2 u_3}{\partial x^2} + f_3,$$
(36)

where $f_1 = f(x = x_1, t)$, $f_2 = f(x = x_2, t)$, $f_3 = f(x = x_3, t)$ are the values of the load at three grid points. Then, the expression for the local truncation error, Eq. (35), can be simplify with the help of Eq. (36) as follows:

$$e_{f} = \left[h^{2}c^{2}(m_{1}\frac{\partial^{2}u_{1}}{\partial x^{2}} + m_{2}\right]$$

$$\frac{\partial^{2}u_{2}}{\partial x^{2}} + m_{3}\frac{\partial^{2}u_{3}}{\partial x^{2}}) + (k_{1}u_{1} + k_{2}u_{2} + k_{3}u_{3})\right]$$

$$+ \left[h^{2}(m_{1}f_{1} + m_{2}f_{2} + m_{3}f_{3}) - \bar{f}\right]$$

$$= e + \left[h^{2}(m_{1}f_{1} + m_{2}f_{2} + m_{3}f_{3}) - \bar{f}\right],$$
(37)

where the expression in the first square brackets in Eq. (37) is the local truncation error e for the case of zero load term f; see Eq. (9). We will define the discretized load term f by

zeroing the expression in the second square brackets in Eq. (37):

$$\bar{f} = h^2(m_1 f_1 + m_2 f_2 + m_3 f_3) = h^2 \sum_{i=1}^3 m_i f_i = h^2 \sum_{i=1}^L m_i f_i,$$
(38)

where the last equality in Eq. (38) is the expression for the discretized load term for the *L*-point stencils. Then, it also follows from Eq. (37) that $e_f = e$. This means that first the stencil coefficients m_i and k_i are calculated for the case of zero load term $f = \bar{f} = 0$ as described in Sects. 2.2–2.4. Then, the discretized load term \bar{f} is calculated by Eq. (38).

2.6 Extension of OLTEM with the 3-Point Stencils to the 1-D Wave Equation for Heterogeneous Materials

Wave propagation in a composite domain $\Omega = \bigcup \Omega_l$ $(l = 1, 2, ..., \overline{N}$ where \overline{N} is the total number of subdomains) is described by the following scalar wave equation in each subdomain Ω_l :

$$\frac{\partial^2 u_l}{\partial t^2} - c_l^2 \frac{\partial^2 u_l}{\partial x^2} = f_l, \tag{39}$$

where the wave velocity c_l is assumed to be a piecewise constant function (c_l is a constant for each subdomains Ω_l). At the interface G (G is a point in the 1-D case) between any two subdomains, the following interface conditions for the function and flux are applied:

$$u_G^* - u_G^{**} = \delta_1, \qquad e_* \frac{\partial u_G^*}{\partial x} - e_{**} \frac{\partial u_G^{**}}{\partial x} = \delta_2,$$
 (40)

where e_* and e_{**} are the corresponding material constants, $\delta_1(t)$ and $\delta_2(t)$ are the given jumps for the function and for the flux, the symbols * and ** correspond to the quantities on the opposite sides from the interface for the corresponding subdomains Ω_l (of course, the composite domain under consideration can include any number of different materials). For zero jumps $\delta_1(t) = \delta_2(t) = 0$, the functions u_l are continuous across the interfaces but have the discontinuous spatial derivatives across the interfaces. The functions f_l can be discontinuous across the interfaces.

For the derivation of OLTEM for heterogeneous materials, we assume that the mesh is sufficiently fine in order to include only one interface between different materials within any 3-point stencil; see Fig. 2. The case of the 3-point stencil inside the homogeneous material considered in Section 2.2 also follows from this stencil when point G coincides with the end point 1 or 3 of the 3-point stencil; see Fig. 2 for $\xi = \pm 1$. The coordinates x_1 and x_3 of the points 1 and 3 of the 3-point stencil and the coordinate x_G of the interface point G are (see Fig. 2):



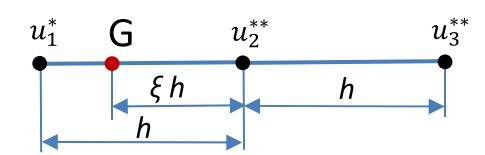


Fig. 2 The spatial locations of the grid points i (i = 1, 2, 3) and the interface G between two materials for the 3-point stencil

$$x_3 = x_2 + h,$$
 $x_1 = x_2 - h,$ $x_G = x_2 - \xi h,$ (41)

where $-1 \le \xi \le 1$.

The 3-point stencil equation for homogeneous materials, Eq. (5), can be modified for heterogeneous materials as follows:

$$h^{2}\left\{m_{1}\left[a_{1}\frac{d^{2}u_{1}^{*,num}}{dt^{2}}+(1-a_{1})\frac{d^{2}u_{1}^{**,num}}{dt^{2}}\right]\right.$$

$$+m_{2}\left[a_{2}\frac{d^{2}u_{2}^{*,num}}{dt^{2}}+(1-a_{2})\frac{d^{2}u_{2}^{**,num}}{dt^{2}}\right]$$

$$+m_{3}\left[a_{3}\frac{d^{2}u_{3}^{*,num}}{dt^{2}}+(1-a_{3})\frac{d^{2}u_{3}^{**,num}}{dt^{2}}\right]$$

$$+k_{1}\left[a_{1}u_{1}^{*,num}+(1-a_{1})u_{1}^{**,num}\right]$$

$$+k_{2}\left[a_{2}u_{2}^{*,num}+(1-a_{2})u_{2}^{**,num}\right]$$

$$+k_{3}\left[a_{3}u_{3}^{*,num}+(1-a_{3})u_{3}^{**,num}\right]=\bar{f},$$
(42)

where the coefficients $a_i = 1$ if the grid point i belongs to material * and $a_i = 0$ if the grid point i belongs to another material * (i.e., only one variable $u_i^{*,num}$ or $u_i^{**,num}$ (i = 1, 2, 3) is included into Eq. (42) for each grid point, e.g., $a_1 = 1$ and $a_2 = a_3 = 0$ for the stencil shown in Fig. 2. As can be seen, the 3-point stencil, Eq. (42), includes the same number of the stencil coefficients m_i and k_i (i = 1, 2, 3) as that for the homogeneous case, Eq. (5).

The local truncation error e follows from Eq. (42) by the replacement of the numerical solution $u_i^{*,num}$, $u_i^{**,num}$ (i = 1, 2, 3) by the exact solution u_i^* , u_i^{**} :

$$e = h^{2} \left\{ m_{1} \left[a_{1} \frac{d^{2}u_{1}^{*}}{dt^{2}} + (1 - a_{1}) \frac{d^{2}u_{1}^{**}}{dt^{2}} \right] \right.$$

$$\left. + m_{2} \left[a_{2} \frac{d^{2}u_{2}^{*}}{dt^{2}} + (1 - a_{2}) \frac{d^{2}u_{2}^{**}}{dt^{2}} \right] \right.$$

$$\left. + m_{3} \left[a_{3} \frac{d^{2}u_{3}^{*}}{dt^{2}} + (1 - a_{3}) \frac{d^{2}u_{3}^{**}}{dt^{2}} \right] \right\}$$

$$\left. + k_{1} \left[a_{1}u_{1}^{*} + (1 - a_{1})u_{1}^{**} \right] + k_{2} \left[a_{2}u_{2}^{*} + (1 - a_{2})u_{2}^{**} \right] \right.$$

$$\left. + k_{3} \left[a_{3}u_{3}^{*} + (1 - a_{3})u_{3}^{**} \right] - \bar{f}.$$

$$(43)$$

In contrast to homogeneous materials, the stencil equation and the local truncation error for heterogeneous materials given by Eqs. (42) and (43) include two different functions u^* and u^{**} . One of the ideas of the new approach for heterogeneous materials is to include the interface conditions for the exact solution into the expression for the local truncation error, Eq. (43), as the constraints in order to couple the functions u^* and u^{**} :

$$e = h^{2} \left\{ m_{1} \left[a_{1} \frac{d^{2}u_{1}^{*}}{dt^{2}} + (1 - a_{1}) \frac{d^{2}u_{1}^{**}}{dt^{2}} \right] \right.$$

$$+ m_{2} \left[a_{2} \frac{d^{2}u_{2}^{*}}{dt^{2}} + (1 - a_{2}) \frac{d^{2}u_{2}^{**}}{dt^{2}} \right]$$

$$+ m_{3} \left[a_{3} \frac{d^{2}u_{3}^{*}}{dt^{2}} + (1 - a_{3}) \frac{d^{2}u_{3}^{**}}{dt^{2}} \right] \right\}$$

$$+ k_{1} \left[a_{1}u_{1}^{*} + (1 - a_{1})u_{1}^{**} \right] + k_{2} \left[a_{2}u_{2}^{*} + (1 - a_{2})u_{2}^{**} \right]$$

$$+ k_{3} \left[a_{3}u_{3}^{*} + (1 - a_{3})u_{3}^{**} \right] - \bar{f}$$

$$+ \left[q_{1} \left(u_{G}^{*} - u_{G}^{**} - \delta_{1} \right) + h q_{2} \left(e_{*} \frac{\partial u_{G}^{*}}{\partial x} - e_{**} \frac{\partial u_{G}^{**}}{\partial x} - \delta_{2} \right) \right.$$

$$+ h^{2} q_{3} \left(\frac{\partial^{2}u_{G}^{*}}{\partial t^{2}} - \frac{\partial^{2}u_{G}^{**}}{\partial t^{2}} - \frac{\partial^{2}\delta_{1}}{\partial t^{2}} \right)$$

$$+ h^{3} q_{4} \left(e_{*} \frac{\partial^{3}u_{G}^{*}}{\partial t^{2}\partial x} - e_{**} \frac{\partial^{3}u_{G}^{**}}{\partial t^{2}\partial x} - \frac{\partial^{2}\delta_{2}}{\partial t^{2}} \right)$$

$$+ h^{4} q_{5} \left(\frac{\partial^{4}u_{G}^{*}}{\partial t^{4}} - \frac{\partial^{4}u_{G}^{**}}{\partial t^{4}} - \frac{\partial^{4}\delta_{1}}{\partial t^{4}} \right) \right], \tag{44}$$

where the unknown coefficients q_i (i = 1, 2, ..., 5) can be considered as the Lagrange multipliers and they will be used for the minimization of the local truncation error in Eq. (44), the expressions in parenthesis after q_1 and q_2 are the interface conditions (see Eq. (40), the expressions in parenthesis after q_3 , q_4 and q_5 are the time derivatives of the interface conditions (the time derivatives of the leftand right-hand sides of Eq. (40)). Therefore, the expressions after the coefficients q_i (i = 1, 2, ..., 5) in Eq. (44) are zero and Eqs. (43) and (44) yield the same local truncation error e. We should mention that we use the even orders of the time derivatives of the interface conditions in Eq. (44) in order to finally express the time derivatives in terms of the spatial derivatives using the partial differential equation (see the derivations below). However, we do not have these limitations for the heat equation which is formulated in terms of the first time derivative (e.g., see Sect. 3.1 below).

To derive the coefficients m_i and k_i (i = 1, 2, 3) in Eq. (44), first we replace the time derivatives of the exact solution in the expression for the local truncation error e in Eq. (44) by the space derivatives using the partial differential equation, Eq. (39), as follows (we assume that



functions u^* and u^{**} are sufficiently smooth in the corresponding subdomains including the interface):

$$\frac{\partial^{2} u_{i}^{*}}{\partial t^{2}} = c_{*}^{2} \frac{\partial^{2} u_{i}^{*}}{\partial x^{2}} + f_{i}^{*},$$

$$\frac{\partial^{2} u_{i}^{**}}{\partial t^{2}} = c_{**}^{2} \frac{\partial^{2} u_{i}^{**}}{\partial x^{2}} + f_{i}^{**},$$

$$\frac{\partial^{3} u_{G}^{*}}{\partial t^{2}} = c_{**}^{2} \frac{\partial^{3} u_{G}^{*}}{\partial x^{3}} + f_{i}^{**},$$

$$\frac{\partial^{3} u_{G}^{*}}{\partial x \partial t^{2}} = c_{**}^{2} \frac{\partial^{3} u_{G}^{*}}{\partial x^{3}} + \frac{\partial^{6} f_{G}^{*}}{\partial x},$$

$$\frac{\partial^{3} u_{G}^{*}}{\partial x} = c_{**}^{2} \frac{\partial^{3} u_{G}^{**}}{\partial x^{3}} + \frac{\partial^{6} f_{G}^{**}}{\partial x^{3}},$$

$$\frac{\partial^{3} u_{G}^{*}}{\partial x^{3}} = c_{**}^{2} \frac{\partial^{3} u_{G}^{**}}{\partial x^{3}} + \frac{\partial^{6} f_{G}^{**}}{\partial x^{3}},$$

$$\frac{\partial^{6} u_{G}^{*}}{\partial x^{3}} = c_{**}^{2} \frac{\partial^{6} u_{G}^{**}}{\partial x^{3}} + \frac{\partial^{6} f_{G}^{**}}{\partial x^{3}},$$

$$\frac{\partial^{6} u_{G}^{*}}{\partial x^{3}} = c_{**}^{2} \frac{\partial^{6} u_{G}^{**}}{\partial x^{3}} + \frac{\partial^{6} u_{G}^$$

$$\frac{\partial^{4} u_{G}^{*}}{\partial t^{4}} = c_{*}^{2} \frac{\partial^{4} u_{G}^{*}}{\partial x^{2} \partial t^{2}} + \frac{\partial^{2} f_{G}^{*}}{\partial t^{2}}
= c_{*}^{4} \frac{\partial^{4} u_{G}^{*}}{\partial x^{4}} + c_{*}^{2} \frac{\partial^{2} f_{G}^{*}}{\partial x^{2}} + \frac{\partial^{2} f_{G}^{*}}{\partial t^{2}}, \quad \frac{\partial^{4} u_{G}^{**}}{\partial t^{4}}
= c_{**}^{2} \frac{\partial^{4} u_{G}^{**}}{\partial x^{2} \partial t^{2}} + \frac{\partial^{2} f_{G}^{**}}{\partial t^{2}}
= c_{**}^{4} \frac{\partial^{4} u_{G}^{*}}{\partial x^{4}} + c_{**}^{2} \frac{\partial^{2} f_{G}^{**}}{\partial x^{2}} + \frac{\partial^{2} f_{G}^{**}}{\partial t^{2}}.$$
(47)

Equation (45) is the original partial differential equation applied at the three grid points and one interface point. Equations (46) and (47) are obtained by the differentiation of Eq. (45) with respect to x and t as well as by the replacement of the time derivatives in Eq. (47) using Eq. (45).

Inserting Eqs. (45–47) into Eq. (44) we get the following local truncation error in space for OLTEM that does not include the time derivatives:

$$e = h^{2} \left\{ m_{1} \left[a_{1} c_{*}^{2} \frac{\partial^{2} u_{1}^{*}}{\partial x^{2}} + (1 - a_{1}) c_{**}^{2} \frac{\partial^{2} u_{1}^{**}}{\partial x^{2}} \right] \right.$$

$$+ m_{2} \left[a_{2} c_{*}^{2} \frac{\partial^{2} u_{2}^{*}}{\partial x^{2}} + (1 - a_{2}) c_{**}^{2} \frac{\partial^{2} u_{2}^{**}}{\partial x^{2}} \right]$$

$$+ m_{3} \left[a_{3} c_{*}^{2} \frac{\partial^{2} u_{3}^{*}}{\partial x^{2}} + (1 - a_{3}) c_{**}^{2} \frac{\partial^{2} u_{3}^{**}}{\partial x^{2}} \right] \right\}$$

$$+ k_{1} \left[a_{1} u_{1}^{*} + (1 - a_{1}) u_{1}^{**} \right] + k_{2} \left[a_{2} u_{2}^{*} + (1 - a_{2}) u_{2}^{**} \right]$$

$$+ k_{3} \left[a_{3} u_{3}^{*} + (1 - a_{3}) u_{3}^{**} \right]$$

$$+ \left[q_{1} \left(u_{G}^{*} - u_{G}^{**} \right) + h q_{2} \left(e_{*} \frac{\partial u_{G}^{*}}{\partial x} - e_{**} \frac{\partial u_{G}^{**}}{\partial x} \right)$$

$$+ h^{2} q_{3} \left(c_{*}^{2} \frac{\partial^{2} u_{G}^{*}}{\partial x^{2}} - c_{**}^{2} \frac{\partial^{2} u_{G}^{**}}{\partial x^{2}} \right)$$

$$+ h^{3} q_{4} \left(e_{*} c_{*}^{2} \frac{\partial^{3} u_{G}^{*}}{\partial x^{3}} - e_{**} c_{**}^{2} \frac{\partial^{3} u_{G}^{**}}{\partial x^{3}} \right)$$

$$+ h^{4} q_{5} \left(c_{*}^{4} \frac{\partial^{4} u_{G}^{*}}{\partial x^{4}} - c_{**}^{4} \frac{\partial^{4} u_{G}^{**}}{\partial x^{4}} \right) \right], \tag{48}$$

as well as the discretized load term f:

$$\bar{f} = h^{2} \sum_{i=1}^{L} m_{i} [a_{i} f_{i}^{*} + (1 - a_{i}) f_{i}^{**}] + h^{2} q_{3} (f_{G}^{*} - f_{G}^{**})
+ h^{3} q_{4} (e_{*} \frac{\partial f_{G}^{*}}{\partial x} - e_{**} \frac{\partial f_{G}^{**}}{\partial x}) + h^{4} q_{5} (c_{*}^{2} \frac{\partial^{2} f_{G}^{*}}{\partial x^{2}} + \frac{\partial^{2} f_{G}^{*}}{\partial t^{2}}
- c_{**}^{2} \frac{\partial^{2} f_{G}^{**}}{\partial x^{2}} - \frac{\partial^{2} f_{G}^{**}}{\partial t^{2}}) - (q_{1} \delta_{1} + h q_{2} \delta_{2} + h^{2} q_{3} \frac{\partial^{2} \delta_{1}}{\partial t^{2}}
+ h^{3} q_{4} \frac{\partial^{2} \delta_{2}}{\partial t^{2}} + h^{4} q_{5} \frac{\partial^{4} \delta_{1}}{\partial t^{4}}),$$
(49)

where the last expression in the parenthesis in Eq. (49) corresponds to the contribution due to the non-zero jump conditions in Eq. (40). So far, in our papers [2, 3, 24, 34, 36, 37] on OLTEM for heterogeneous materials, we have used zero jumps $\delta_1 = \delta_2 = 0$ in the interface conditions. However, non-zero jumps affect just the discretized load term \bar{f} and can be easily included into the numerical procedure (e.g., see Eq. (49)).

Next, similar to Sect. 2.2 let us expand the local truncation error, Eq. (48), into a Taylor series by the expansion of the exact solution for u_i^* , u_i^{**} , $\frac{\partial^2 u_i^*}{\partial x^2}$ and $\frac{\partial^2 u_i^{**}}{\partial x^2}$ at the grid points i = 1, 2, 3 into a Taylor series in the vicinity of the interface point G at small $h \ll 1$ as follows:

$$v_{i} = v_{G} + \frac{\partial v_{G}}{\partial x} r_{i} + \frac{\partial^{2} v_{G} r_{i}^{2}}{\partial x^{2}} \frac{r_{i}^{2}}{2!} + \frac{\partial^{3} v_{G} r_{i}^{3}}{\partial x^{3}} \frac{\partial^{4} v_{G} r_{i}^{4}}{\partial x^{4}} \frac{\partial^{4} v_{G}}{4!} + \dots,$$
(50)

where $r_i = x_i - x_G$ (e.g., $r_1 = (\xi - 1)h$, $r_2 = \xi h$, $r_3 = (\xi + 1)h$ in Fig. 2), the function v_i in Eq. (50) is u_i^* , u_i^{**} , $\frac{\partial^2 u_i^*}{\partial x^2}$, $\frac{\partial^2 u_i^{**}}{\partial x^2}$ (i = 1, 2, 3). Inserting Eq. (50) into Eq. (48) we get the following Taylor series of the local truncation error in space for OLTEM:

$$e = b_{1}u_{G}^{*} + b_{2}u_{G}^{**} + h\left[b_{3}\frac{\partial u_{G}^{*}}{\partial x} + b_{4}\frac{\partial u_{G}^{**}}{\partial x}\right] + h^{2}\left[b_{5}\frac{\partial^{2}u_{G}^{*}}{\partial x^{2}} + b_{6}\frac{\partial^{2}u_{G}^{*}}{\partial x^{2}}\right] + h^{3}\left[b_{7}\frac{\partial^{3}u_{G}^{*}}{\partial x^{3}} + b_{8}\frac{\partial^{3}u_{G}^{**}}{\partial x^{3}}\right] + h^{4}\left[b_{9}\frac{\partial^{4}u_{G}^{*}}{\partial x^{4}} + b_{10}\frac{\partial^{4}u_{G}^{**}}{\partial x^{4}}\right] + h^{5}\left[b_{11}\frac{\partial^{5}u_{G}^{*}}{\partial x^{5}} + b_{12}\frac{\partial^{5}u_{G}^{**}}{\partial x^{5}}\right] + h^{6}\left[b_{13}\frac{\partial^{6}u_{G}^{*}}{\partial x^{6}} + b_{14}\frac{\partial^{6}u_{G}^{**}}{\partial x^{6}}\right] + O(h^{7}),$$

$$(51)$$

where the coefficients b_p (p=1,2,...) are expressed in terms of the coefficients m_i , k_i , q_j (i=1,2,3 and j=1,2,...,5) and the distance ξ ; see our paper [34] for the details. We should mention again that by the use of the wave equation, Eqs. (45–47), the time derivatives in the expression for the local truncation error in Eq. (51) are excluded. In order to minimize the order of the local truncation error in Eq. (51), we will zero the first 10 coefficients $b_p=0$ (p=1,2,...,10) for the smallest power of h. From these 10 algebraic equations and the



condition $k_2 = 1$ (see the Remark 1) we can find the 11 coefficients m_i , k_i , q_j (i = 1, 2, 3 and j = 1, 2, ..., 5) as well as we get the fifth order of the local truncation error in Eq. (51); see our paper [34] for the details. For example, for the location of the interface point shown in Fig. 2 with $a_1 = 1$ and $a_2 = a_3 = 0$, we get the following coefficients m_i , k_i , q_j (i = 1, 2, 3 and j = 1, 2, ..., 5):

meet the corresponding PDE, Eq. (39), and can be extended outside their subdomains). In this case we expand the exact solution for u_i^* , u_i^{**} , $\frac{\partial^2 u_i^*}{\partial x^2}$ and $\frac{\partial^2 u_i^{**}}{\partial x^2}$ at the grid points i=1 and i=3 into a Taylor series in the vicinity of point i=2 at small $h \ll 1$ using Eqs. (10) - (13) as well as we expand the exact solution for u_G^* , u_G^{**} , $\frac{\partial^2 u_G^*}{\partial x^2}$, $\frac{\partial^2 u_G^*}{\partial x^2}$, $\frac{\partial^3 u_G^*}{\partial x^3}$, $\frac{\partial^3 u_G^*}{\partial x^4}$ and $\frac{\partial^4 u_G^*}{\partial x^4}$

$$\begin{split} m_1 &= \frac{e_*(c_*^1, e_*(\xi-1)^4 + 2c_*^2c_{**}^2(3e_*\xi(\xi+1) + e_{**}(-2\xi^2 + \xi+1))(\xi-1)^2 + c_*^4(e_*\xi(\xi^3 + 2\xi^2 - 1) + e_{**}(-4\xi^4 - 2\xi^3 + 6\xi^2 + \xi-1)))}{\overline{d}}, \\ m_2 &= \frac{1}{\overline{d}}[c_{**}^4 e_*(-\xi e_{**} + e_{**} + 5e_*) \\ (\xi+1))(\xi-1)^4 - 2c_*^2c_{**}^2 e_*(e_{**}(5\xi^3 + 5\xi^2 - 6\xi - 4) \\ &- e_*\xi(\xi^2 + 3\xi + 2))(\xi-1)^2 + c_*^4(e_{**}^2(8\xi^3 + 24\xi^2 + 20\xi + 5)(\xi-1)^2 + e_*^2 \\ \xi(\xi+1)^2(\xi^2 + 3\xi + 1) + e_*e_{**}(-5\xi^5 - 15\xi^4 - 4\xi^3 + 14\xi^2 + 9\xi + 1))], \\ m_3 &= \frac{1}{\overline{d}}[c_{**}^4 e_*(e_{**}(\xi-1) - 5e_*\xi)(\xi-1)^4 - 2c_*^2c_{**}^2 e_* \\ (-5e_{**}\xi^2 + e_*(\xi+1)\xi \\ &+ e_{**})(\xi-1)^3 + c_*^4(-e_{**}^2(8\xi^3 - 4\xi - 1)(\xi-1)^2 + e_*^2\xi^2(-\xi^3 + 2\xi + 1) \\ &+ e_*e_{**}\xi(5\xi^4 - 5\xi^3 - 6\xi^2 + 4\xi + 2))], \\ k_1 &= -\frac{e_*}{\xi e_* + e_*} + e_{**} - e_{**}\xi , \\ k_2 &= 1, \quad k_3 = -\frac{-\xi e_{**}}{\xi e_* + e_*} + e_{**} + e_{**}\xi , \\ q_1 &= \frac{e_*}{\xi e_* + e_*} + e_{**} - e_{**}\xi , \\ q_2 &= \frac{\xi-1}{\xi e_* + e_*} + e_{**} - e_{**}\xi , \\ q_3 &= \frac{e_*(5c_{**}^4 + e_*(\xi-1)^4 - 4c_*^2c_{**}^2 e_*(2\xi+1)(\xi-1)^3 + c_*^4(e_{**}(4\xi^4 + 2\xi^3 - 6\xi^2 - \xi + 1) - e_*\xi(\xi^3 + 2\xi^2 - 1)))}{d}, \\ q_4 &= \frac{(\xi-1)(c_*^4 e_*(\xi-1)^4 - 4c_*^2c_{**}^2 e_*\xi(\xi+1)(\xi-1)^3 + c_*^4(e_{**}(4\xi^4 + 2\xi^3 - 6\xi^2 - \xi + 1) - e_*\xi(\xi^3 + 2\xi^2 - 1)))}{d}, \\ q_5 &= -\frac{e_*(\xi-1)^2(c_*^2(5e_*\xi(\xi+1) + e_{**}(-2\xi^2 + \xi + 1)(\xi-1)^2 + c_*^4(e_{**}(4\xi^4 + 2\xi^3 - 6\xi^2 - \xi + 1) - e_*\xi(\xi^3 + 2\xi^2 - 1)))}{2d}, \\ \end{cases}$$

with

$$\bar{d} = 12c_*^2 c_{**}^2 (\xi e_* + e_* + e_{**} - e_{**} \xi) (c_{**}^2 e_* (\xi - 1)^2 + c_*^2 e_* \xi (\xi + 1) + c_*^2 e_{**} (-2\xi^2 + \xi + 1)).$$

It can be checked that for $\xi=1$ in Fig. 2 (homogeneous materials), Eq. (52) yields the same m_i , k_i (i=1,2,3) stencil coefficients as those given by Eq. (18).

Remark 2 We should mention that the local truncation error, Eq. (48), can be also expanded into a Taylor series in the vicinity of the central grid point i = 2 (we assume that the unknown functions u^* and u^{**} are sufficiently smooth,

at the interface point G into a Taylor series in the vicinity of point i = 2 at small $h \ll 1$ as follows:

$$v_{G} = v_{2} - \frac{\partial v_{2}}{\partial x} (\xi h) + \frac{\partial^{2} v_{2}}{\partial x^{2}} \frac{(\xi h)^{2}}{2!} - \frac{\partial^{3} v_{2}}{\partial x^{3}} \frac{(\xi h)^{3}}{3!} + \frac{\partial^{4} v_{2}}{\partial x^{4}} \frac{(\xi h)^{4}}{4!} + \dots,$$
(53)

where the function v_G in Eq. (53) is u_G^* , u_G^{*u} , $\frac{\partial^2 u_G^*}{\partial x^2}$, $\frac{\partial^2 u_G^{*v}}{\partial x^2}$, $\frac{\partial^3 u_G^*}{\partial x^3}$, $\frac{\partial^4 u_G^*}{\partial x^3}$, and $\frac{\partial^4 u_G^{*v}}{\partial x^4}$. Inserting Eqs. (10)-(13), (53) into Eq. (48) we get the following Taylor series of the local truncation error in space for OLTEM:



$$e = b_{1}u_{2}^{*} + b_{2}u_{2}^{**} + h\left[b_{3}\frac{\partial u_{2}^{*}}{\partial x} + b_{4}\frac{\partial u_{2}^{**}}{\partial x}\right]$$

$$+ h^{2}\left[b_{5}\frac{\partial^{2}u_{2}^{*}}{\partial x^{2}} + b_{6}\frac{\partial^{2}u_{2}^{**}}{\partial x^{2}}\right]$$

$$+ h^{3}\left[b_{7}\frac{\partial^{3}u_{2}^{*}}{\partial x^{3}} + b_{8}\frac{\partial^{3}u_{2}^{**}}{\partial x^{3}}\right]$$

$$+ h^{4}\left[b_{9}\frac{\partial^{4}u_{2}^{*}}{\partial x^{4}} + b_{10}\frac{\partial^{4}u_{2}^{**}}{\partial x^{4}}\right]$$

$$+ h^{5}\left[b_{11}\frac{\partial^{5}u_{2}^{*}}{\partial x^{5}} + b_{12}\frac{\partial^{5}u_{2}^{**}}{\partial x^{5}}\right]$$

$$+ h^{6}\left[b_{13}\frac{\partial^{6}u_{2}^{*}}{\partial x^{6}} + b_{14}\frac{\partial^{6}u_{2}^{**}}{\partial x^{6}}\right] + O(h^{7}),$$

$$(54)$$

where the coefficients b_p (p = 1, 2, ...) are expressed in terms of the coefficients m_i , k_i , q_j (i = 1, 2, 3 and j = 1, 2, ..., 5) and the distance ξ . The coefficients b_p (p = 1, 2, ...) in Eq. (54) are different from those in Eq. (51) and have simpler expressions. However, if we zero the first 10 coefficients $b_p = 0$ (p = 1, 2, ..., 10) in Eq. (54) for the smallest power of h with the condition $k_2 = 1$ (see the Remark 1), then we get the same stencil coefficients as those given by Eq. (52).

It is also interesting to mention that if we do not use the last three interface conditions in Eq. (44) (i.e., if we assume that $q_3 = q_4 = q_5 = 0$) then we have just the 8 unknown coefficients m_l , k_l , q_j (l = 1, 2, 3 and j = 1, 2). In this case, we can zero the 7 coefficients $b_p = 0$ (p = 1, 2, ..., 6, 8) in Eq. (51) for the smallest power of h and we get only the third order of the local truncation error in Eq. (51), i.e, the use of the last three interface conditions in Eq. (44) allows us to improve the local truncation error in Eq. (51) by two orders.

3 OLTEM for Time-Dependent PDEs in the 2-D and 3-D Cases: Scalar Wave and Heat Equations, a System of Elastodynamics Equations

Here, we will shortly review OLTEM for the scalar wave and heat equations with constant, variable and discontinuous coefficients as well as for the elastodynamics equations with constant and discontinuous coefficients in the 2-D and 3-D cases.

3.1 Scalar Wave and Heat Equations

3.1.1 Homogeneous Materials

The corresponding PDEs with constant coefficients in domain Ω can written down as:

$$\frac{\partial^2 u}{\partial t^2} - c^2 \nabla^2 u = f. \tag{55}$$

for wave propagation in an isotropic homogeneous medium as well as

$$\frac{\partial u}{\partial t} - a\nabla^2 u = f. \tag{56}$$

for heat propagation in an isotropic homogeneous medium. Equations (55)-(56) can be uniformly written down in domain Ω as:

$$\frac{\partial^n u}{\partial t^n} - \bar{c} \nabla^2 u = f, \tag{57}$$

where n=2 and $\bar{c}=c^2$ (c is the wave velocity) for the wave equation as well as n=1 and $\bar{c}=a$ (a is the thermal diffusivity) for the heat equation. The Dirichlet boundary conditions

$$u = g(\mathbf{x}, t) \tag{58}$$

on the boundary Γ^u and with the Neumann boundary conditions

$$n_x \frac{\partial u}{\partial x} + n_y \frac{\partial u}{\partial y} + n_z \frac{\partial u}{\partial z} = \bar{g}(\mathbf{x}, t)$$
 (59)

on the boundary Γ^s are applied where the entire boundary Γ is $\Gamma = \Gamma^s U \Gamma^u$ and n_x , n_y , n_z are the x-, y- and z-components of the outward unit normal vector, g and \bar{g} are the given functions. In Eqs. (55)-(56), c is the wave velocity, a is the thermal diffusivity, f(x,t) is the loading (source) term, u is the field variable. The standard initial conditions should be also given in domain Ω . For OLTEM derived below, we consider semi-discrete equations without the time discretization. After the derivation of the coefficients of the semidiscrete equations, any existing time-integration method can be used for the time integration of the semidiscrete equations. The initial conditions used for the time integration of the semidiscrete equations are similar to those for other numerical methods (e.g., for FEM).

The detailed derivation of OLTEM is presented in our papers [1, 22, 23] in the 2-D and 3-D cases on regular domains and in our papers [25, 27, 28] in the 2-D and 3-D cases on irregular domains. Below we present the summary of the results.

The compact stencil equation for OLTEM for the scalar wave and heat equations in the 2-D and 3-D cases can be uniformly given for each internal grid point as follows:



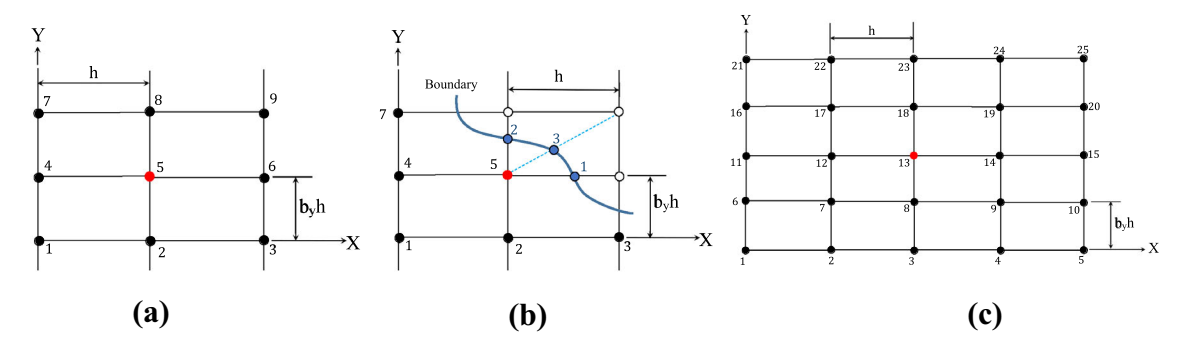


Fig. 3 The spatial locations of the grid (black) and boundary (blue) points for the $3 \times 3 = 9$ -point regular (a) and cut (b) stencils (similar to those for linear finite elements) as well as for the $5 \times 5 = 25$ -point regular (c) stencils (similar to those for quadratic finite elements) in

the 2-D case. The irregular boundary in (b) cuts the regular stencil and leads to the inclusion of the boundary points into the derivations. These stencils are given for the central grid (red) point 5 (a, b) and 13 (c)

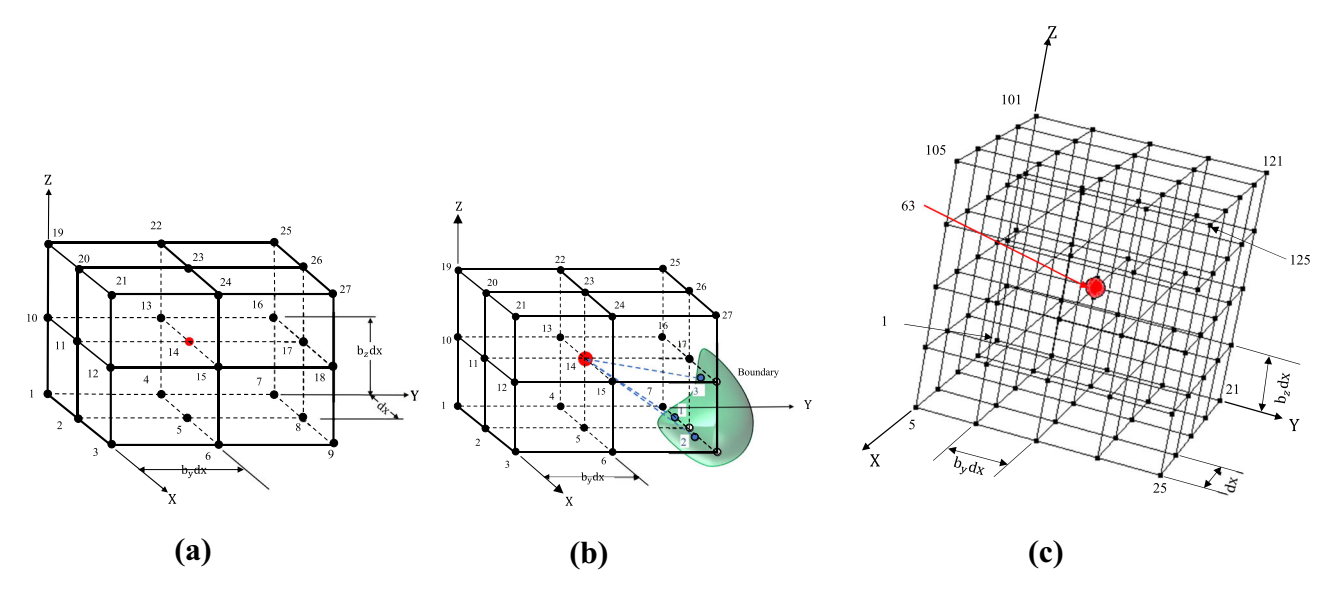


Fig. 4 The spatial locations of the grid (black) and boundary (blue) points for the $3 \times 3 \times 3 = 27$ -point regular (a) and cut (b) stencils (similar to those for linear finite elements) as well as for the $5 \times 5 \times 5 = 125$ -point regular (c) stencils (similar to those for

$$\sum_{i=1}^{L} \left[h^2 m_i \frac{d^n u_i^{num}}{dt^n} + k_i u_i^{num} \right] = \bar{f}, \tag{60}$$

where u_i^{num} and $\frac{d^n u_i^{num}}{dt^n}$ are the numerical solution for function u and its time derivative at the grid points, m_i , k_i are the unknown coefficients to be determined, $\bar{f}(t)$ is the discretized loading (source) term; L is the number of the grid points included into the stencil equation, n=2 for the wave equation and n=1 for the heat equation, h is the mesh size along the x- axis. The location of the grid and boundary points for some compact stencils in the 2-D and 3-D cases is shown in Figs. 3 and 4.

The local truncation errors e for the stencil equations given by Eq. (60) can obtained by the replacement of the numerical value of function u_i^{num} in Eq. (60) by the exact value u_i at the grid points i (i = 1, 2, ..., L) as well as by the

quadratic finite elements) in the 3-D case. The irregular boundary in (**b**) cuts the regular stencil and leads to the inclusion of the boundary points into the derivations. These stencils are given for the central grid (red) point 14 (**a**, **b**) and 63 (**c**)

addition of the boundary conditions at a small number $N_B = M_1 + M_2$ of the selected boundary points as the constraints with some unknown coefficients (Lagrange multipliers) $q_{m,i}$ ($m = 1, 2, 3, 4, i = 1, 2, ..., N_B$) as follows (the 3-D case):

$$e = \sum_{i=1}^{L} \left[h^{2} m_{i} \frac{d^{n} u_{i}}{dt^{n}} + k_{i} u_{i} \right] - \bar{f}$$

$$+ \sum_{i=1}^{M_{1}} \left[h^{2} q_{1,i} \left(\frac{d^{n} g_{i}}{dt^{n}} - \frac{d^{n} u_{B,i}}{dt^{n}} \right) + q_{2,i} (g_{i} - u_{B,i}) \right]$$

$$+ \sum_{i=1}^{M_{2}} \left[h^{3} q_{3,i} \left(\frac{d^{n} \bar{g}}{dt^{n}} - n_{x,i} \frac{\partial^{n+1} u_{B,i}}{\partial t^{n} \partial x} + n_{y,i} \frac{\partial^{n+1} u_{B,i}}{\partial t^{n} \partial y} + n_{z,i} \frac{\partial^{n+1} u_{B,i}}{\partial t^{n} \partial z} \right)$$

$$+ h q_{4,i} \left(\bar{g}_{i} - n_{x,i} \frac{\partial u_{B,i}}{\partial x} + n_{y,i} \frac{\partial u_{B,i}}{\partial y} + n_{z,i} \frac{\partial u_{B,i}}{\partial z} \right) \right]$$

$$(61)$$



where M_1 and M_2 are the numbers of the selected boundary points with the Dirichlet and Neumann boundary conditions, respectively; the expressions after $q_{2,i}$ and $q_{4,i}$ are the Dirichlet and Neumann boundary conditions given by Eqs. (58) and (59) at the selected boundary points, the expressions after $q_{1,i}$ and $q_{3,i}$ are the time derivatives of the boundary conditions at the selected boundary points. Therefore, the expressions after the term \bar{f} in Eq. (61) are zero and do not affect the value of the local truncation error e.

Remark 3 We should mention that the imposition of the Dirichlet and Neumann boundary conditions for OLTEM in our published papers is different from that given by Eq. (61) (nevertheless, the final expressions and equations are the same). The the imposition of the boundary conditions in Eq. (61) as the constraints allows us to uniformly implement the Dirichlet and Neumann boundary conditions as well as the interface conditions for heterogeneous materials (see Sects. 2.6, 3.2.2, 4.1.2, 4.3.2).

Using the partial differential equation, Eq. (55), the time derivatives of the exact solution at the grid and boundary points in Eq. (61) can be replaced by the spatial derivatives as well the discretized load \bar{f} can be defined similar to those in Sects. 2.2 and 2.5. Then, it follows from Eq. (61) that

$$e = \sum_{i=1}^{L} \left[h^{2} \bar{c} m_{i} \left(\frac{\partial^{2} u_{i}}{\partial x^{2}} \right) + \frac{\partial^{2} u_{i}}{\partial y^{2}} + \frac{\partial^{2} u_{i}}{\partial z^{2}} \right) + k_{i} u_{i} \right]$$

$$- \sum_{i=1}^{M_{1}} \left[h^{2} q_{1,i} \bar{c} \left(\frac{\partial^{2} u_{B,i}}{\partial x^{2}} \right) + q_{2,i} u_{B,i} \right]$$

$$+ \frac{\partial^{2} u_{B,i}}{\partial y^{2}} + \frac{\partial^{2} u_{B,i}}{\partial z^{2}} \right) + q_{2,i} u_{B,i} \right]$$

$$- \sum_{i=1}^{M_{2}} h q_{4,i} \left(n_{x,i} \frac{\partial u_{B,i}}{\partial x} \right)$$

$$+ n_{y,i} \frac{\partial u_{B,i}}{\partial y} + n_{z,i} \frac{\partial u_{B,i}}{\partial z} \right)$$

$$- \sum_{i=1}^{M_{2}} h^{3} \bar{c} q_{3,i} \left[n_{x,i} \left(\frac{\partial^{3} u_{B,i}}{\partial x^{3}} \right) \right]$$

$$+ \frac{\partial^{3} u_{B,i}}{\partial x \partial y^{2}} + \frac{\partial^{3} u_{B,i}}{\partial x \partial z^{2}} \right)$$

$$+ n_{y,i} \left(\frac{\partial^{3} u_{B,i}}{\partial y \partial x^{2}} + \frac{\partial^{3} u_{B,i}}{\partial y \partial x^{2}} + \frac{\partial^{3} u_{B,i}}{\partial y \partial z^{2}} \right)$$

$$+ n_{z,i} \left(\frac{\partial^{3} u_{B,i}}{\partial z \partial y^{2}} + \frac{\partial^{3} u_{B,i}}{\partial z \partial y^{2}} + \frac{\partial^{3} u_{B,i}}{\partial z \partial y^{2}} \right)$$

$$+ n_{z,i} \left(\frac{\partial^{3} u_{B,i}}{\partial z \partial x^{2}} + \frac{\partial^{3} u_{B,i}}{\partial z \partial y^{2}} + \frac{\partial^{3} u_{B,i}}{\partial z \partial y^{2}} \right)$$

$$+ n_{z,i} \left(\frac{\partial^{3} u_{B,i}}{\partial z \partial x^{2}} + \frac{\partial^{3} u_{B,i}}{\partial z \partial y^{2}} + \frac{\partial^{3} u_{B,i}}{\partial z \partial y^{2}} \right)$$

and

$$\bar{f} = \left\{ h^2 \sum_{i=1}^{L_2} m_i f_i - h^2 \sum_{i=1}^{M_1} q_{1,i} f_{B,i} \right. \\
- h^3 \sum_{i=1}^{M_2} q_{3,i} (n_{x,i} \frac{\partial f_{B,i}}{\partial x} \\
+ n_{y,i} \frac{\partial f_{B,i}}{\partial y} + n_{z,i} \frac{\partial f_{B,i}}{\partial z}) \right\}$$

$$+ \left\{ \sum_{i=1}^{M_1} (h^2 q_{1,i} \frac{d^n g_i}{dt^n} + q_{2,i} g_i) \right\} \\
+ \left\{ \sum_{i=1}^{M_2} (h^3 q_{3,i} \frac{d^n \bar{g}}{dt^n} + h q_{4,i} \bar{g}_i) \right\}, \tag{63}$$

where $\bar{c} = c^2$ and n = 2 for the wave equation as well as $\bar{c} = a$ and n = 1 for the heat equation. In Eq. (63), the expression in the first curly brackets corresponds to the contribution due to the body forces, the expression in the second curly brackets corresponds to the contribution due to the Dirichlet boundary conditions (if the boundary with the Dirichlet boundary conditions intersects the corresponding cell), the expression in the third curly brackets corresponds to the contribution due to the Neumann boundary conditions (if the boundary with the Neumann boundary conditions intersects the corresponding cell).

Let us describe the coordinates of the grid and boundary points used in Eqs. (60–63) with respect to the stencil central grid point with the coordinates x_c , y_c , z_c as follow:

$$x_i = x_c + r_{x,i}h, y_i = y_c + r_{y,i}b_yh,$$

 $z_i = z_c + r_{z,i}b_zh,$ (64)

for the grid points, and

$$x_{B,i} = x_c + d_{x,i}h, y_{B,i} = y_c + d_{y,i}b_yh, z_{B,i} = z_c + d_{z,i}b_zh, (65)$$

for the boundary points where $r_{x,i}$, $r_{y,i}$, $r_{z,i}$ and $d_{x,i}$, $d_{y,i}$, $d_{z,i}$ are the coefficients describing the location of the grid points and the boundary points, b_y and b_z are the aspect ratios of Cartesian meshes along the y- and z-axes; see Fig. 4.

In order to represent the local truncation error e as a Taylor series, let us expand the exact solution and its spatial derivatives at the grid and boundary points into a Taylor series at small $h \ll 1$ in the vicinity of the stencil central grid point x_c , y_c , z_c as follows:



$$w_{i} = w_{c} + \frac{\partial w_{c}}{\partial x} [d_{x,j}h] + \frac{\partial w_{c}}{\partial y} [d_{y,j}b_{y}h]$$

$$+ \frac{\partial w_{c}}{\partial z} [d_{z,j}b_{z}h] + \frac{\partial^{2}w_{c}}{\partial x^{2}} \frac{[d_{x,j}h]^{2}}{2!}$$

$$+ \frac{\partial^{2}w_{c}}{\partial y^{2}} \frac{[d_{y,j}b_{y}h]^{2}}{2!} + \frac{\partial^{2}w_{c}}{\partial z^{2}} \frac{[d_{z,j}b_{z}h]^{2}}{2!}$$

$$+ 2 \frac{\partial^{2}w_{c}}{\partial x \partial y} \frac{[(d_{x,j}h)[d_{y,j}b_{y}h]}{2!} + ..., ,$$

$$(66)$$

where the function w_i is u_i , $\frac{\partial^2 u_i}{\partial x^2}$, $\frac{\partial^2 u_i}{\partial y^2}$, $\frac{\partial^2 u_i}{\partial z^2}$ (i = 1, 2, ..., L), $u_{B,i}$, $\frac{\partial^2 u_{B,i}}{\partial x^2}$, $\frac{\partial^2 u_{B,i}}{\partial y^2}$, $\frac{\partial^2 u_{B,i}}{\partial z^2}$ $(i = 1, 2, ..., M_1)$ and $\frac{\partial u_{B,i}}{\partial x}$, $\frac{\partial u_{B,i}}{\partial y}$, $\frac{\partial u_{B,i}}{\partial z}$, $\frac{\partial^3 u_{B,i}}{\partial z^3}$ $(i = 1, 2, ..., M_2)$; for the regular grid points the coefficients $d_{x,i}$, $d_{y,i}$, $d_{z,i}$ in Eq. (66) should be replaced by the coefficients $r_{x,i}$, $r_{y,i}$, $r_{z,i}$; see Eqs. (64)-(65). Using Eq. (66), a Taylor series of the local truncation error in Eq. (62) for the 27-point stencils (see Fig. 4a,b) can be represented as:

$$e = \bar{c} \{b_{1}u_{14} + h[b_{2}\frac{\partial u_{14}}{\partial x} + b_{3}\frac{\partial u_{14}}{\partial y} + b_{4}\frac{\partial u_{14}}{\partial z}]$$

$$+ h^{2}[b_{5}\frac{\partial^{2}u_{14}}{\partial x^{2}} + b_{6}\frac{\partial^{2}u_{14}}{\partial x\partial y} + b_{7}\frac{\partial^{2}u_{14}}{\partial x\partial z}$$

$$+ b_{8}\frac{\partial^{2}u_{14}}{\partial y^{2}} + b_{9}\frac{\partial^{2}u_{14}}{\partial y\partial z} + b_{10}\frac{\partial^{2}u_{14}}{\partial z^{2}}]$$

$$+ h^{3}[b_{11}\frac{\partial^{3}u_{14}}{\partial x^{3}} + b_{12}\frac{\partial^{3}u_{14}}{\partial x^{2}\partial y} + b_{13}\frac{\partial^{3}u_{14}}{\partial x^{2}\partial z}$$

$$+ b_{14}\frac{\partial^{3}u_{14}}{\partial x\partial y^{2}} + b_{15}\frac{\partial^{3}u_{14}}{\partial x\partial y\partial z} + b_{16}\frac{\partial^{3}u_{14}}{\partial x\partial z^{2}}$$

$$+ b_{17}\frac{\partial^{3}u_{14}}{\partial y^{3}} + b_{18}\frac{\partial^{3}u_{14}}{\partial y^{2}\partial z} + b_{19}\frac{\partial^{3}u_{14}}{\partial y\partial z^{2}}$$

$$+ b_{20}\frac{\partial^{3}u_{14}}{\partial z^{3}}]$$

$$+ h^{4}[b_{21}\frac{\partial^{4}u_{14}}{\partial x^{4}} + \dots + b_{35}\frac{\partial^{4}u_{14}}{\partial z^{4}}]$$

$$+ h^{5}[b_{36}\frac{\partial^{5}u_{14}}{\partial x^{5}} + \dots + b_{56}\frac{\partial^{5}u_{14}}{\partial z^{5}}]$$

$$+ h^{6}[b_{57}\frac{\partial^{6}u_{14}}{\partial x^{6}} + \dots + b_{84}\frac{\partial^{6}u_{14}}{\partial z^{6}}]$$

$$+ h^{7}[b_{85}\frac{\partial^{7}u_{14}}{\partial x^{7}} + \dots + b_{120}\frac{\partial^{7}u_{14}}{\partial z^{7}}] + h^{8}[b_{121}\frac{\partial^{8}u_{14}}{\partial x^{8}}$$

$$+ \dots + b_{165}\frac{\partial^{8}u_{14}}{\partial x^{8}}] + \dots \},$$

where the coefficients b_p ($p=1,2,\ldots$) are expressed as a linear combination of the coefficients m_i , k_i , $q_{1,i}$, $q_{2,i}$, $q_{3,i}$ and $q_{4,i}$ used in Eqs. (60)-(63); see our papers [25, 27, 28] on OLTEM with 2-D and 3-D irregular domains. We should mention that the explicit expression for the coefficients b_p can be first calculated just for one internal and one

boundary point with the general expression for the location of these points given Eqs. (64)-(65). Then, we should consider the summation over all internal and boundary points. For example, the first five coefficients b_p in Eq. (67) have the following form:

$$b_{1} = \sum_{i=1}^{L} k_{i} + \sum_{j=1}^{M_{1}} q_{2,j}, b_{2}$$

$$= \sum_{i=1}^{L} k_{i} r_{x,i} + \sum_{j=1}^{M_{1}} q_{2,j} d_{x,j} + \sum_{l=1}^{M_{2}} q_{4,l} n_{x,l}, b_{3}$$

$$= \sum_{i=1}^{L} b_{y} k_{i} r_{y,i} + \sum_{j=1}^{M_{1}} b_{y} q_{2,j} d_{y,j} + \sum_{l=1}^{M_{2}} q_{4,l} n_{y,l}, b_{4}$$

$$= \sum_{i=1}^{L} b_{z} k_{i} r_{z,i} + \sum_{j=1}^{M_{1}} b_{z} q_{2,j} d_{z,j} + \sum_{l=1}^{M_{2}} q_{4,l} n_{z,l}, b_{5}$$

$$= \sum_{l=1}^{L} \left(\bar{c} m_{l} + \frac{1}{2} k_{i} r_{x,l}^{2} \right) + \sum_{j=1}^{M_{1}} \left(\bar{c} q_{1,j} + \frac{1}{2} q_{2,j} d_{x,j}^{2} \right)$$

$$+ \sum_{l=1}^{M_{2}} q_{4,l} n_{x,l} d_{x,l}.$$

$$(68)$$

Below we will shortly present the procedure for the formation of the local system of linear algebraic equations for the calculation of the stencil coefficients using Eq. (67). OLTEM with the 27-point stencils for the 3-D wave (heat) equation described in our paper [28] is considered. In our papers [27, 28] we suggested a very simple procedure for the selection of the boundary points for cut stencils for the wave (heat) equation. For example if any grid point of the regular stencil is located outside the actual physical domain then we joint this point with the central grid point of the stencil. The intersection of this line with the boundary determines the boundary point included into the cut stencils. This means that the total number of the grid and boundary points included into the cut stencil is 27 $(L + M_1 + M_2 = 27)$; see [27, 28]. For some simple stencils (no boundary points or just few boundary points), the expressions for coefficients b_p (p = 1, 2, ...) can be simplified and some results can be analytically obtained. For example, for the stencil with just one boundary point with the Neumann boundary conditions, we do not have the correct solution if we zero the first 35 coefficients $b_p = 0$ for p = 1, 2, ..., 35 (however, we can do this for the boundary points with the Dirichlet boundary conditions). Therefore, in order to improve the order of the local truncation error in Eq. (67) for the cut stencils with the boundary points with the Neumann boundary conditions, we will zero the first 20 coefficients b_p in Eq. (67) up to the third order with respect to h, i.e,

$$b_p = 0, \quad p = 1, 2, \dots, 20.$$
 (69)

Then, in order to have a sufficient number of linearly independent equations for the calculation of the stencil



coefficients m_i , k_i , $q_{1,i}$, $q_{2,i}$, $q_{3,i}$ and $q_{4,i}$, we use the least square method for the minimization of coefficients b_p related to the fourth and higher orders of the local truncation error with the following residual R:

$$R = \sum_{p=21}^{35} b_p^2 + h_1 \sum_{p=36}^{56} b_p^2 + h_2 \sum_{p=57}^{84} b_p^2 + h_3 \sum_{p=85}^{120} b_p^2 + h_4 \sum_{p=121}^{165} b_p^2,$$

$$(70)$$

where h_i (i = 1, 2, 3, 4) are the weighting factors to be selected (e.g., the numerical experiments show that $h_i = 1$ (i = 1, 2, 3, 4) yields accurate results). In order to minimize the residual R with the constraints given by Eq. (69), we can form a new residual \bar{R} with the Lagrange multipliers λ_p :

$$\bar{R} = \sum_{p=1}^{20} \lambda_p b_p + \sum_{p=21}^{35} b_p^2 + h_1 \sum_{p=36}^{56} b_p^2 + h_2 \sum_{p=57}^{84} b_p^2 + h_3 \sum_{p=85}^{120} b_p^2 + h_4 \sum_{p=121}^{165} b_p^2.$$
(71)

The residual \bar{R} is a quadratic function of coefficients m_i , k_i , $q_{1,j}$, $q_{2,j}$, $q_{3,l}$ and $q_{4,l}$ and a linear function of the Lagrange multipliers λ_p , i.e, $\bar{R} = \bar{R}(m_i, k_i, q_{1,j}, q_{2,j}, q_{3,l}, q_{4,l}, \lambda_p)$. In order minimize the residual $\bar{R} = \bar{R}(m_i, k_i, q_{1,j}, q_{2,j}, q_{3,l}, q_{4,l}, \lambda_p)$, the following equations based on the least square method for the residual \bar{R} can be written down:

$$\frac{\partial \bar{R}}{\partial m_{i}} = 0, \qquad \frac{\partial \bar{R}}{\partial k_{i}} = 0,
\frac{\partial \bar{R}}{\partial q_{1,j}} = 0, \qquad \frac{\partial \bar{R}}{\partial q_{2,j}} = 0,
\frac{\partial \bar{R}}{\partial q_{3,l}} = 0, \qquad \frac{\partial \bar{R}}{\partial q_{4,l}} = 0,
i = 1, 2, ..., L, \qquad j = 1, 2, ..., M_{1}, \qquad l = 1, 2, ..., M_{2},$$
(72)

$$\frac{\partial \bar{R}}{\partial \lambda_p} = 0, \qquad p = 1, 2, \dots, 20, \tag{73}$$

where equation $\frac{\partial \bar{R}}{\partial k_{14}} = 0$ should be replaced by $k_{14} = 1$, the grid point 14 is the central point of the 27-point stencil; see Remark 1. Equations (72) and (73) form a system of 74 linear algebraic equations with respect to 54 unknown coefficients m_i , k_i , $q_{1,j}$, $q_{2,j}$, $q_{3,l}$ and $q_{4,l}$ (i = 1, 2, ..., L, $j = 1, 2, ..., M_1$ and $l = 1, 2, ..., M_2$, $L + M_1 + M_2 = 27$) and 20 Lagrange multipliers λ_p (p = 1, 2, ..., 20). Solving these linear algebraic equations numerically, we can find the coefficients m_i , k_i , $q_{1,j}$, $q_{2,j}$, $q_{3,l}$ and $q_{4,l}$ (i = 1, 2, ..., L,

 $j = 1, 2, ..., M_1$ and $l = 1, 2, ..., M_2$) for the 27-point regular and cut stencils.

OLTEM with the 27-point stencils provides the fourth order of accuracy for the Dirichlet boundary conditions (see our paper [27]) and the third order of accuracy for the Neumann boundary conditions (see our paper [28]). Linear finite elements with similar 27-point stencils provides just the second order of accuracy. Moreover, due to the minimization of the leading fourth order terms of the local truncation error in Eq. (71), at the same numbers of degrees of freedom OLTEM vields more accurate results than those obtained by high-order finite elements (up to the fourth order) with much wider stencils; see the numerical examples in our papers [27, 28]. We should also mention that as shown in our paper [23], OLTEM in the 2-D case with high order $(2p+1) \times (2p+1)$ -point stencils (p=2,3) provides the 4p + 2 and 2p + 2 order of the local truncation error with the non-diagonal and diagonal mass matrices on regular domains with conforming Cartesian meshes (similar to the 1-D case in Sects. 2.3 and 2.4).

3.1.1.1 Diagonal Mass Matrix It is interesting to note that similar to the calculation of the diagonal mass matrix in the 1-D case (see Sects. 2.4), a very simple formula can be obtained for the calculation of the diagonal mass matrix in the multidimensional case. Let us find the coefficient b_p for the smallest power of h in Eq. (67) that includes the diagonal term m_d of the mass matrix (all other m_i coefficients in the stencil equation, Eq. (60), are zero). For example, we can select the coefficient b_5 in Eq. (68). Assuming that the order of the local truncation error in Eq. (67) is at least greater than two and equating the coefficient b_5 to zero $b_5 = 0$, we will get the following expression for the diagonal term of the mass matrix:

$$m_{d} = -\frac{1}{\bar{c}} \sum_{i=1}^{L} \frac{1}{2} k_{i} r_{x,i}^{2} - \sum_{j=1}^{M_{1}} (\bar{c} q_{1,j} + \frac{1}{2} q_{2,j} d_{x,j}^{2})$$

$$- \sum_{l=1}^{M_{2}} q_{4,l} n_{x,l} d_{x,l}.$$

$$(74)$$

If the internal grid point is located far from the boundary, then the stencil equation for this grid point is not affected by the boundary conditions ($M_1 = M_2 = 0$). In this case Eq. (74) reduces to a very simple formula for the diagonal mass matrix in terms of the coefficients of the stiffness matrix:

$$m_d = -\frac{1}{\bar{c}} \sum_{i=1}^{L} \frac{1}{2} k_i r_{x,i}^2. \tag{75}$$

We should mention that this formula can be used for the calculation of the diagonal mass matrix for any numerical method with the stencil equation given by Eq. (60) (e.g.,



for linear and high-order finite elements) on Cartesian meshes as well as on unstructured meshes (the coefficients $r_{x,i}$ should be correspondingly defined for unstructured meshes; see Eq. (64)). In contrast to many known ad-hoc techniques for the calculation of the diagonal mass matrix (e.g., the 'row summation' technique) that manipulates with the coefficients of the non-diagonal mass matrix, the coefficients of the stiffness matrix are used in the new approach. For example, the coefficients of the finite element stiffness matrix should be used for the finite element diagonal mass matrix.

3.1.2 Inhomogeneous Materials

Currently, we have developed OLTEM for inhomogeneous materials in the 2-D case; see our paper [33]. The corresponding PDEs with the variable coefficients in domain Ω can written down as:

$$\frac{\partial^2 u}{\partial t^2} - \left[\frac{\partial}{\partial x} \left(c_x^2(x, y) \frac{\partial u}{\partial x} \right) + \frac{\partial}{\partial y} \left(c_y^2(x, y) \frac{\partial u}{\partial y} \right) \right] = f. \tag{76}$$

for wave propagation in an anisotropic inhomogeneous medium as well as

$$\frac{\partial u}{\partial t} - \left[\frac{\partial}{\partial x} \left(a_x(x, y) \frac{\partial u}{\partial x} \right) + \frac{\partial}{\partial y} \left(a_y(x, y) \frac{\partial u}{\partial y} \right) \right] = f. \tag{77}$$

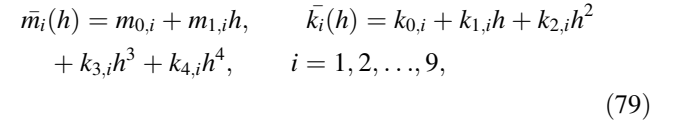
for heat propagation in an anisotropic inhomogeneous medium with the Dirichlet boundary conditions. In Eqs. (76)-(77), c_x and c_y are the wave velocity along the x- and y-axes ($c_x = c_y$ for isotropic materials), a_x and a_x are the thermal diffusivity along the x- and y-axes ($a_x = a_y$ for isotropic materials), f(x, t) is the loading (source) term, u is the field variable.

The detailed derivation of OLTEM with 9-point stencils in the 2-D case on irregular domains with the Dirichlet boundary conditions is presented in our paper [33]. Below we present the summary of the results.

The compact stencil equation for OLTEM for the scalar wave and heat equations in the 2-D and 3-D cases can be uniformly given for each internal grid point as follows:

$$\sum_{i=1}^{L} \left[h^2 \bar{m_i}(h) \frac{d^n u_i^{num}}{dt^n} + \bar{k_i}(h) u_i^{num} \right] = \bar{f}, \tag{78}$$

for the grid point located far from the boundary. In contrast to our approach presented in [25, 27] for the wave (heat) equation with the constant coefficients (see also the previous Sect. 3.1.1), now we assume that the coefficients $\bar{m}_i(h)$ and $\bar{k}_i(h)$ depend on the mesh size h and for the 9-point stencils they will be expressed in terms of polynomial functions of h as follows:



where $m_{l,i}$, $k_{i,i}$ (l = 0, 1, j = 0, 1, 2, 3, 4, i = 1, 2, ..., 9) are unknown coefficients. This polynomial representation of $\bar{m}_i(h)$ and $\bar{k}_i(h)$ can be considered as a Taylor series of functions $\bar{m}_i(h)$ and $\bar{k}_i(h)$ at small h. We should mention that for the solution of the global system, we use the 9point stencil equation, Eq. (78) with L=9 and the 18 stencil coefficients $\bar{m}_i(h)$ and $\bar{k}_i(h)$ (i = 1, 2, ..., 9) similar to Eq. (60) with the 9-point stencils for the PDE with the constant coefficients in presented Sect. 3.1.1. However, in order to calculate these 18 stencil coefficients at a given h, we introduce $9 \times 7 = 63$ unknown coefficients $m_{l,i}$, $k_{i,i}$ (l = 0, 1, j = 0, 1, 2, 3, 4, i = 1, 2, ..., 9) that can be defined from the minimization of the local truncation error. Similar to the previous Sect. 3.1.1, we can show that a Taylor series of the local truncation error e for the 9-point stencil equation, Eq. (78) with L = 9 and the central grid point 5 (see Fig. 3a), can be represented as follows:

$$e = \bar{c} \left\{ b_{1}u_{5} + h \left[b_{2} \frac{\partial u_{5}}{\partial x} + b_{3} \frac{\partial u_{5}}{\partial y} + b_{4}u_{5} \right] \right.$$

$$+ h^{2} \left[b_{5} \frac{\partial^{2}u_{5}}{\partial x^{2}} + b_{6} \frac{\partial^{2}u_{5}}{\partial x \partial y} + b_{7} \frac{\partial u_{5}}{\partial x} + b_{8} \frac{\partial^{2}u_{5}}{\partial y^{2}} + b_{9} \frac{\partial u_{5}}{\partial y} + b_{10}u_{5} \right]$$

$$+ h^{3} \left[b_{11} \frac{\partial^{3}u_{5}}{\partial x^{3}} + \dots + b_{20}u_{5} \right] + h^{4} \left[b_{21} \frac{\partial^{4}u_{5}}{\partial x^{4}} + \dots + b_{35}u_{5} \right]$$

$$+ h^{5} \left[b_{36} \frac{\partial^{5}u_{5}}{\partial x^{5}} + \dots + b_{56}u_{5} \right] + h^{6} \left[b_{57} \frac{\partial^{6}u_{5}}{\partial x^{6}} + \dots + b_{84}u_{5} \right]$$

$$+ h^{7} \left[b_{85} \frac{\partial^{7}u_{5}}{\partial x^{7}} + \dots + b_{120}u_{5} \right] + h^{8} \left[b_{121} \frac{\partial^{8}u_{5}}{\partial x^{8}} + \dots + b_{165}u_{5} \right]$$

$$+ \dots \right\},$$
(80)

where the coefficients b_p (p = 1, 2, ...) are expressed in terms of the coefficients $m_{l,i}$, $k_{i,i}$ (l = 0, 1, j = 0, 1, 2, 3, 4, i = 1, 2, ..., 9; see our paper [33]. We should mention that by the use of the wave (heat) partial differential equation, Eqs. (76) - (77), the time derivatives in Eq. (80) for the local truncation error are excluded. By zeroing the coefficients b_p for the smallest orders of h and using the least square method for the coefficients b_p for higher orders of h(similar to the procedure in Sect. 3.1.1), we can form a local system of algebraic equations for the calculation of the unknown coefficients $m_{l,i}$, $k_{i,i}$ (l = 0, 1, j = 0, 1, 2, 3, 4, i = 1, 2, ..., 9). As shown in our paper [33], OLTEM with the 9-point stencils on irregular domains with the Dirichlet boundary conditions provides the fourth order of accuracy of global solutions (similar to OLTEM for the homogeneous materials and the Dirichlet boundary conditions in the previous Sect. 3.1.1)). Moreover, due to



minimization of the leading terms of the local truncation error, at the same numbers of degrees of freedom OLTEM on irregular domains yields more accurate results than those obtained by high-order finite elements (up to the third order) with much wider stencils; see the numerical examples in our paper [33].

3.1.3 Heterogeneous Materials with Interfaces

Wave propagation in a composite domain $\Omega = \bigcup \Omega_l$ $(l = 1, 2, ..., \overline{N}$ where \overline{N} is the total number of subdomains) is described by the following scalar wave equation in each subdomain Ω_l :

$$\frac{\partial^2 u_l}{\partial t^2} - c_l^2 \nabla^2 u_l = f_l. \tag{81}$$

Similarly, the heat equation in each subdomain Ω_l can be written as:

$$\frac{\partial u_l}{\partial t} - a_l \nabla^2 u_l = f_l. \tag{82}$$

For each subdomain Ω_l we use the following notations in Eqs. (81)-(82): c_l is the wave velocity, a_l is the thermal diffusivity, $f_l(\mathbf{x}, t)$ is the loading (source) term, u_l is the field variable.

At the interface G (G is a curve in the 2-D case and a surface in the 3-D case) between any two subdomains, the following interface conditions are applied:

$$u_{G}^{*} - u_{G}^{**} = \delta_{1}, \qquad e_{*} \left(n_{x} \frac{\partial u_{G}^{*}}{\partial x} + n_{y} \frac{\partial u_{G}^{*}}{\partial y} + n_{z} \frac{\partial u_{G}^{*}}{\partial z} \right) - e_{**} \left(n_{x} \frac{\partial u_{G}^{**}}{\partial x} + n_{y} \frac{\partial u_{G}^{**}}{\partial y} + n_{z} \frac{\partial u_{G}^{**}}{\partial z} \right) = \delta_{2},$$
(83)

where $\delta_1(x, y, z, t) \mid_{(x,y,z) \in G}$ and $\delta_2(x, y, z, t) \mid_{(x,y,z) \in G}$ are the given jumps for the function and the flux, n_x , n_y and n_z are the x-, y- and z-components of the normal vector at the interface, e_* and e_{**} are the corresponding material

constants, the symbols * and ** correspond to the quantities on the opposite sides from the interface for the corresponding subdomains Ω_l . For zero jumps $\delta_1(x,y,z,t)=\delta_2(x,y,z,t)=0$, the functions u_l are continuous across the interfaces but can have the discontinuous spatial derivatives across the interfaces. The functions f_l can be discontinuous across the interfaces.

Similar to Eq. (42) in the 1-D case, the compact stencil equation of OLTEM for the scalar wave and heat equations in the 2-D and 3-D cases can be uniformly given for each internal grid point as follows:

$$h^{2} \sum_{p=1}^{L} m_{p} \left[a_{p} \frac{d^{n} u_{p}^{*,num}}{dt^{n}} + (1 - a_{p}) \right] \frac{d^{n} u_{p}^{**,num}}{dt^{n}}$$

$$+ \sum_{p=1}^{L} k_{p} \left[a_{p} u_{p}^{*,num} + (1 - a_{p}) u_{p}^{**,num} \right]$$

$$= \bar{f},$$
(84)

for the grid point located far from the boundary. Here, the coefficients $a_p = 1$ if the grid point p belongs to material * and $a_p = 0$ if the grid point p belongs to another material ** (i.e., only one variable $u_p^{*,num}$ or $u_p^{**,num}$ ($p = 1, 2, \ldots, L$) is included into Eq. (84) for each grid point. As can be seen, the stencil equation, Eq. (84), includes the same number of the stencil coefficients m_p and k_p ($p = 1, 2, \ldots, L$) as that for the homogeneous case, Eq. (60). The derivation of OLTEM for heterogeneous materials in the 2-D and 3-D cases includes the use of the interface conditions at a small number N_G of interface points along a part of the interface located within the corresponding compact cell; see Figs. 5 and 6.

To describe the coordinates of the selected N_G points on the interface with respect to the stencil central grid point, we introduce $3N_G$ coefficients $\bar{d}_{x,p}$, $\bar{d}_{y,p}$ and $\bar{d}_{z,p}$ $(p=1,2,\ldots,N_G)$ in the 3-D case as follows (see also Eqs. (64) - (65) for the internal and boundary points):

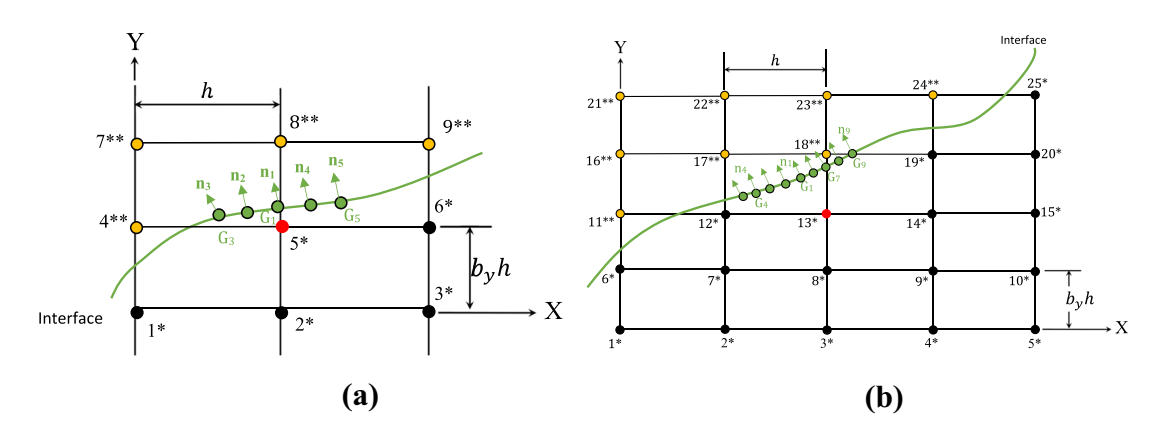


Fig. 5 The spatial locations of the grid and interface points for the 9-point (a) and 25-point (b) stencils (similar to those for linear and quadratic finite elements, respectively) for heterogeneous materials with irregular interfaces in the 2-D case



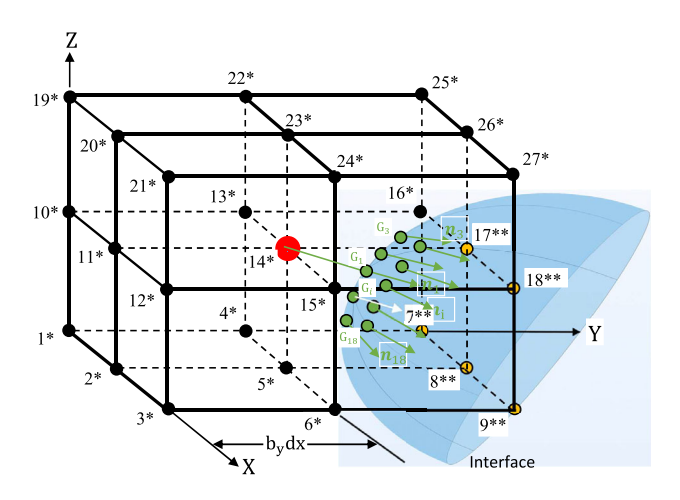


Fig. 6 The spatial locations of the grid and interface points for the 27-point stencils (similar to those for linear finite elements) for heterogeneous materials with irregular interfaces in the 3-D case

$$x_{G,j} = x_c + \bar{d}_{x,j}h, y_{G,j} = y_c + \bar{d}_{y,j}b_yh, z_{G,j} = z_c + \bar{d}_{z,j}b_zh, j = 1, 2, ..., N_G.$$
(85)

Below we will shortly present OLTEM for the 2-D case with 9-point stencils developed in our paper [34]. Similar to the 1-D case in Sect. 2.6, we will add the interface conditions at a small number of the interface points (we use 5 interface points) to the local truncation error of the stencil equation, Eq. (84), as the constraints:

$$e = h^{2} \sum_{p=1}^{9} m_{p} \left[a_{p} \frac{d^{n} u_{p}^{*}}{dt^{n}} + (1 - a_{p}) \frac{d^{n} u_{p}^{**}}{dt^{n}} \right]$$

$$+ \sum_{p=1}^{9} k_{p} \left[a_{p} u_{p}^{*} + (1 - a_{p}) u_{p}^{**} \right] - \bar{f}$$

$$+ \left\{ \sum_{j=1}^{5} q_{1,j} (u_{G,j}^{*} - u_{G,j}^{**} - \delta_{1,j}) \right.$$

$$+ \sum_{j=1}^{5} h q_{2,j} \left[e_{*} \left(n_{x,j} \frac{\partial u_{G,j}^{*}}{\partial x} + n_{y,j} \frac{\partial u_{G,j}^{**}}{\partial y} \right) \right.$$

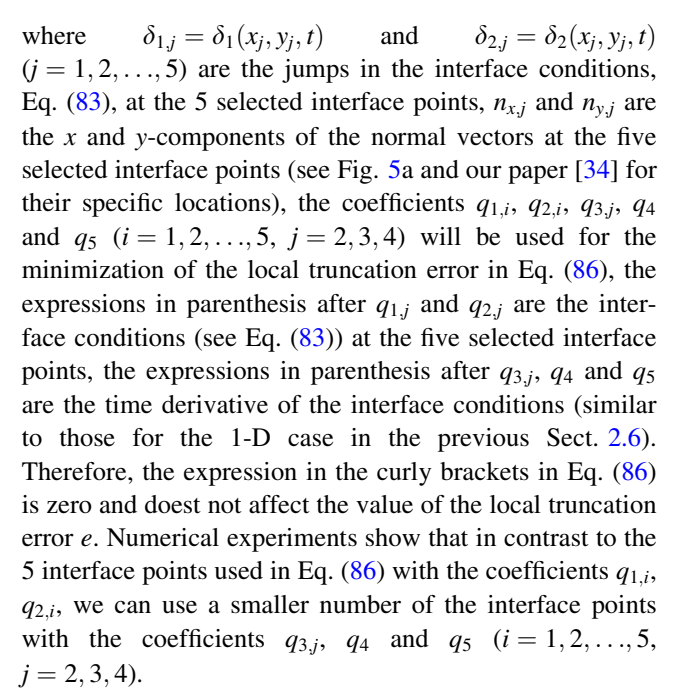
$$- e_{**} \left(n_{x,j} \frac{\partial u_{G,j}^{**}}{\partial x} + n_{y,j} \frac{\partial u_{G,j}^{**}}{\partial y} \right) - \delta_{2,j} \right] + \sum_{j=2}^{4} h^{2} q_{3,j}$$

$$\left(\frac{\partial^{n} u_{G,j}^{*}}{\partial t^{n}} - \frac{\partial^{n} u_{G,j}^{**}}{\partial t^{n}} - \frac{\partial^{n} \delta_{1,j}}{\partial t^{n}} \right)$$

$$+ h^{3} q_{4} \left[e_{*} \left(n_{x,3} \frac{\partial^{n+1} u_{G,3}^{**}}{\partial t^{n} \partial x} + n_{y,3} \frac{\partial^{n+1} u_{G,3}^{**}}{\partial t^{n} \partial y} \right) - \frac{\partial^{n} \delta_{2,3}}{\partial t^{n}} \right]$$

$$- e_{**} \left(n_{x,3} \frac{\partial^{n+1} u_{G,3}^{**}}{\partial t^{n} \partial x} + n_{y,3} \frac{\partial^{n+1} u_{G,3}^{**}}{\partial t^{n} \partial y} \right) - \frac{\partial^{n} \delta_{2,3}}{\partial t^{n}} \right]$$

$$+ h^{4} q_{5} \left(\frac{\partial^{2n} u_{G,3}^{*}}{\partial t^{2n}} - \frac{\partial^{2n} u_{G,3}^{**}}{\partial t^{2n}} - \frac{\partial^{2n} \delta_{1,3}}{\partial t^{2n}} \right) \right\},$$



Similar to the previous Section 3.1.1, we can show that a Taylor series of the local truncation error e for the 9-point stencil equation, Eq. (86), can be represented as follows:

$$e = b_{1}u_{5}^{*} + b_{2}u_{5}^{**} + h\left(b_{3}\frac{\partial u_{5}^{*}}{\partial x} + b_{4}\frac{\partial u_{5}^{**}}{\partial x} + b_{5}\frac{\partial u_{5}^{*}}{\partial y} + b_{6}\frac{\partial u_{5}^{**}}{\partial y}\right)$$

$$+ h^{2}\left(b_{7}\frac{\partial^{2}u_{5}^{*}}{\partial x^{2}} + b_{8}\frac{\partial^{2}u_{5}^{**}}{\partial x^{2}} + b_{9}\frac{\partial^{2}u_{5}^{*}}{\partial x\partial y} + b_{10}\frac{\partial^{2}u_{5}^{**}}{\partial x\partial y}\right)$$

$$+ b_{11}\frac{\partial^{2}u_{5}^{*}}{\partial y^{2}} + b_{12}\frac{\partial^{2}u_{5}^{**}}{\partial y^{2}}\right)$$

$$+ h^{3}\left(b_{13}\frac{\partial^{3}u_{5}^{*}}{\partial x^{3}} + b_{14}\frac{\partial^{3}u_{5}^{**}}{\partial x^{3}} + b_{15}\frac{\partial^{3}u_{5}^{*}}{\partial x^{2}\partial y} + +b_{16}\frac{\partial^{3}u_{5}^{**}}{\partial x^{2}\partial y}\right)$$

$$+ b_{17}\frac{\partial^{3}u_{5}^{*}}{\partial x\partial y^{2}} + b_{18}\frac{\partial^{3}u_{5}^{**}}{\partial x\partial y^{2}} + b_{19}\frac{\partial^{3}u_{5}^{*}}{\partial y^{3}} + b_{20}\frac{\partial^{3}u_{5}^{**}}{\partial y^{3}}\right)$$

$$+ h^{4}\left(b_{21}\frac{\partial^{4}u_{5}^{*}}{\partial x^{4}} + \dots + b_{30}\frac{\partial^{4}u_{5}^{**}}{\partial y^{4}}\right)$$

$$+ h^{5}\left(b_{31}\frac{\partial^{5}u_{5}^{*}}{\partial x^{5}} + \dots + b_{42}\frac{\partial^{5}u_{5}^{**}}{\partial y^{5}}\right)$$

$$+ h^{6}\left(b_{43}\frac{\partial^{6}u_{5}^{*}}{\partial x^{6}} + \dots + b_{56}\frac{\partial^{6}u_{5}^{**}}{\partial y^{6}}\right) + \dots,$$

$$(87)$$

where the coefficients b_p (p=1,2,...,56) are expressed in terms of the coefficients m_i , k_i , $q_{1,j}$, $q_{2,j}$, $q_{3,l}$, q_4 and q_5 (i=1,2,...,9, j=1,2,3,4,5, l=2,3,4,); see our paper [34] for the details. We should mention that by the use of the wave (heat) equation, Eqs. (81, 82), the time derivatives in the local truncation error in Eq. (87) are excluded. By zeroing the coefficients b_p for the smallest orders of h and using the least square method for the coefficients b_p for



higher orders of h (similar to the procedure in Sect. 3.1.1), we can form a local system of algebraic equations for the calculation of the unknown coefficients m_i , k_i , $q_{1,j}$, $q_{2,j}$, $q_{3,l}$, q_4 and q_5 ($i=1,2,\ldots,9$, j=1,2,3,4,5, l=2,3,4). As shown in our paper [34], OLTEM with the 9-point stencils and irregular interfaces provides the third order of accuracy of global solutions (similar to OLTEM for the homogeneous materials in the previous Sect. 3.1.1). Moreover, due to the minimization of the leading terms of the local truncation error, at the same numbers of degrees of freedom OLTEM with irregular interfaces yields more accurate results than those obtained by high-order finite elements (up to the third order) with much wider stencils; see the numerical examples in our paper [34].

3.2 Elastodynamics Equations

Currently, we have developed OLTEM for the elastodynamics equations in the 2-D case; see our papers [24, 32, 38]).

3.2.1 Homogeneous Materials

The corresponding 2-D elastodynamics PDEs with constant coefficients in domain Ω can written down as:

$$\rho \frac{\partial^{2} u}{\partial t^{2}} = \mu \nabla^{2} u + (\mu + \lambda) \left(\frac{\partial^{2} u}{\partial x^{2}} + \frac{\partial^{2} v}{\partial x \partial y} \right) + f_{x},$$

$$\rho \frac{\partial^{2} v}{\partial t^{2}} = \mu \nabla^{2} v + (\mu + \lambda) \left(\frac{\partial^{2} v}{\partial y^{2}} + \frac{\partial^{2} u}{\partial x \partial y} \right) + f_{y},$$
(88)

with the Dirichlet boundary conditions

$$u = g_1(\mathbf{x}, t), \qquad v = g_2(\mathbf{x}, t) \tag{89}$$

on the boundary Γ^u and with the Neumann boundary conditions

$$t_{x} = n_{x} \left[(\lambda + 2\mu) \frac{\partial u}{\partial x} + \lambda \frac{\partial v}{\partial y} \right] + n_{y} \mu \left(\frac{\partial u}{\partial y} + \frac{\partial v}{\partial x} \right) = \bar{g}_{1}(\mathbf{x}, t),$$

$$t_{y} = n_{y} \left[(\lambda + 2\mu) \frac{\partial v}{\partial y} + \lambda \frac{\partial u}{\partial x} \right] + n_{x} \mu \left(\frac{\partial u}{\partial y} + \frac{\partial v}{\partial x} \right) = \bar{g}_{2}(\mathbf{x}, t),$$
(90)

on the boundary Γ^s where the entire boundary Γ is $\Gamma = \Gamma^s U \Gamma^u$. In Eqs. (88)-(90), u = u(x, y, t) and v =

v(x, y, t) are the x- and y-components of the displacement vector, $f_x = f_x(x, y, t)$ and $f_y = f_y(x, y, t)$ are the x- and y-components of the body forces, t_x and t_y are the x- and y-components of the tractive forces, n_x , n_y are the x- and y-components of the outward unit normal vector, g_i and \bar{g}_i (i=1,2) are the given functions, t is the time, ρ is the density, μ and λ are the Lamé coefficients that can be also expressed in terms of Young's modulus E and Poisson's ratio v as $\mu = \frac{E}{2(1+v)}$ and $\lambda = \frac{Ev}{(1+v)(1-2v)}$.

The detailed derivation of OLTEM in the 2-D case is presented in our paper [24] on regular domains and in our paper [32] on irregular domains. Below we present the summary of the results.

According to OLTEM we assume the following general form of two stencil equations for each grid point after the space discretization of Eq. (88) with a rectangular Cartesian mesh:

$$h^{2} \left(\sum_{i=1}^{L} m_{j,i} \frac{\partial^{2} u_{i}^{num}}{\partial t^{2}} + \sum_{i=1}^{L} m_{j,i} \frac{\partial^{2} v_{i}^{num}}{\partial t^{2}} \right) + \sum_{i=1}^{L} k_{j,i} u_{i}^{num} + \sum_{i=1}^{L} k_{\bar{j},i} v_{i}^{num} = \bar{f_{j}}, \qquad j = 1, 2,$$

$$(91)$$

where u_i^{num} , v_i^{num} , $\frac{\partial^2 u_i^{num}}{\partial t^2}$ and $\frac{\partial^2 v_i^{num}}{\partial t^2}$ are the numerical solution for the displacements u, v and their second time derivatives at the i-th grid point, $m_{j,i}$, $\bar{m}_{j,i}$, $k_{j,i}$, $\bar{k}_{j,i}$ are the unknown stencil coefficients to be determined, L is the number of the grid points included into the stencil equation, h is the mesh size, \bar{f}_j are the components of the discretized loading term.

The local truncation errors e_j for the stencil equations given by Eq. (91) can obtained by the replacement of the numerical values of the displacements u_i^{num} , v_i^{num} in Eq. (91) by the exact values u_i , v_i at the grid points i ($i=1,2,\ldots,L$) as well as by the addition of the boundary conditions at a small number $N_B=M_1+M_2$ of the selected boundary points with some unknown coefficients (Lagrange multipliers) $q_{m,i}$ and $\bar{q}_{m,i}$ (m=1,2,3,4, $i=1,2,\ldots,N_B$) as follows:



$$\begin{split} e_{j} &= h^{2} \left(\sum_{i=1}^{L} m_{j,i} \frac{\partial^{2} u_{i}}{\partial t^{2}} + \sum_{i=1}^{L} \bar{m}_{j,i} \frac{\partial^{2} v_{i}}{\partial t^{2}} \right) \\ &+ \sum_{i=1}^{L} k_{j,i} u_{i} + \sum_{i=1}^{L} \bar{k}_{j,i} v_{i} - \bar{f}_{j} \\ &+ h^{2} \left[\sum_{i=1}^{M_{1}} q_{1,i} \left(\frac{d^{n} g_{1,i}}{dt^{n}} - \frac{d^{n} u_{B,i}}{dt^{n}} \right) + \sum_{i=1}^{M_{1}} \bar{q}_{1,i} \left(\frac{d^{n} g_{2,i}}{dt^{n}} - \frac{d^{n} v_{B,i}}{dt^{n}} \right) \right] \\ &+ \sum_{i=1}^{M_{1}} q_{2,i} (g_{1,i} - u_{B,i}) + \sum_{i=1}^{M_{1}} \bar{q}_{2,i} (g_{2,i} - v_{B,i}) \\ &+ h^{3} \left[\sum_{i=1}^{M_{2}} q_{3,i} \left(\frac{d^{n} \bar{g}_{1,i}}{dt^{n}} - \frac{d^{n} t_{x,B,i}}{dt^{n}} \right) \right] \\ &+ \sum_{i=1}^{M_{2}} \bar{q}_{3,i} \left(\frac{d^{n} \bar{g}_{2,i}}{dt^{n}} - \frac{d^{n} t_{y,B,i}}{dt^{n}} \right) \right] \\ &+ h \left[\sum_{i=1}^{M_{2}} q_{4,i} (\bar{g}_{1,i} - t_{x,B,i}) + \sum_{i=1}^{M_{2}} \bar{q}_{4,i} (\bar{g}_{2,i} - t_{y,B,i}) \right], \end{split}$$

$$(92)$$

where M_1 and M_2 are the numbers of the selected boundary points with the Dirichlet and Neumann boundary conditions, respectively; $g_{1,i}$, $g_{2,i}$ and $\bar{g}_{1,i}$, $\bar{g}_{2,i}$ are the known values of the Dirichlet and Neumann boundary conditions at the selected boundary points (see Eqs. (89) and (90)), the expressions after $q_{2,i}$, $\bar{q}_{2,i}$ and $q_{4,i}$, $\bar{q}_{4,i}$ are the boundary conditions at the selected boundary points given by Eqs. (89) and (90), the expressions after $q_{1,i}$, $\bar{q}_{1,i}$, and $q_{3,i}$, $\bar{q}_{3,i}$ are the time derivatives of the boundary conditions at the selected boundary points. Therefore, the expressions after the term \bar{f}_j in Eq. (92) are zero and do not affect the value of the local truncation error e_i .

The stencil equations, Eq. (91), written for all internal grid points form the global system of ordinary differential equations that can be also presented in the matrix form. In this case, the coefficients $m_{j,i}$, $\bar{m}_{j,i}$ form the mass matrix while the coefficients $k_{j,i}$, $\bar{k}_{j,i}$ form the stiffness matrix. In contrast to the stencils for the scalar wave equation given by Eq. (60) in Sect. 3.1.1, the stencil equations for elastodynamics include two unknown functions u and v as well as the Neumann boundary conditions for elastodynamics in Eq. (92) have a more complicated expression; see Eq. (90).

Using the procedure similar to that for the wave (heat) equation in Sect. 3.1.1, we can: a) replace the time derivatives in Eq. (92) by the spatial derivatives with the help of the elastodynamics equations (see Eq. (88)), b) find the discretized loading term $\bar{f_j}$ in terms of the body forces $f_{x,i}$, $f_{y,i}$ at the grid points and the known Dirichlet and Neumann boundary conditions $g_{1,i}$, $g_{2,i}$ and $\bar{g}_{1,i}$, $\bar{g}_{2,i}$ at the selected boundary points, and c) express the local

truncation error e_j (j = 1, 2) in Eq. (92) as a Taylor series as follows:

$$e_{j} = b_{j,1}u_{5} + b_{j,2}v_{5} + h(b_{j,3}\frac{\partial u_{5}}{\partial x} + b_{j,4}\frac{\partial u_{5}}{\partial y} + b_{j,5}\frac{\partial v_{5}}{\partial x} + b_{j,6}\frac{\partial v_{5}}{\partial y})$$

$$+ h^{2}(b_{j,7}\frac{\partial^{2}u_{5}}{\partial x^{2}} + b_{j,8}\frac{\partial^{2}u_{5}}{\partial x\partial y} + b_{j,9}\frac{\partial^{2}u_{5}}{\partial y^{2}}$$

$$+ b_{j,10}\frac{\partial^{2}v_{5}}{\partial x^{2}} + b_{j,11}\frac{\partial^{2}v_{5}}{\partial x\partial y} + b_{j,12}\frac{\partial^{2}v_{5}}{\partial y^{2}})$$

$$+ h^{3}(b_{j,13}\frac{\partial^{3}u_{5}}{\partial x^{3}} + b_{j,14}\frac{\partial^{3}u_{5}}{\partial x^{2}\partial y} + b_{j,15}\frac{\partial^{3}u_{5}}{\partial x\partial y^{2}} + b_{j,16}\frac{\partial^{3}u_{5}}{\partial y^{3}}$$

$$+ b_{j,17}\frac{\partial^{3}v_{5}}{\partial x^{3}} + b_{j,18}\frac{\partial^{3}v_{5}}{\partial x^{2}\partial y} + b_{j,19}\frac{\partial^{3}v_{5}}{\partial x\partial y^{2}} + b_{j,20}\frac{\partial^{3}v_{5}}{\partial y^{3}})$$

$$+ h^{4}(b_{j,21}\frac{\partial^{4}u_{5}}{\partial x^{4}} + \dots + b_{j,30}\frac{\partial^{4}v_{5}}{\partial y^{4}}) + h^{5}(b_{j,31}\frac{\partial^{5}u_{5}}{\partial x^{5}} + \dots$$

$$+ b_{j,42}\frac{\partial^{5}v_{5}}{\partial y^{5}}) + h^{6}(b_{j,43}\frac{\partial^{6}u_{5}}{\partial x^{6}} + \dots + b_{j,56}\frac{\partial^{6}v_{5}}{\partial y^{6}}) + \dots$$

$$(93)$$

with j = 1 and j = 2 for the first and second stencils and with the coefficients $b_{i,i}$ expressed as a linear combination of the coefficients $m_{j,i}$, $\bar{m}_{j,i}$, $k_{j,i}$, $\bar{k}_{j,i}$ and $\bar{q}_{1,i}$, $q_{1,i}$, $\bar{q}_{2,i}$, $q_{2,i}$, $\bar{q}_{3,i}, q_{3,i}, \bar{q}_{4,i}, q_{4,i}$ used in Eqs. (91)-(92); see our paper [32]. We should mention that the explicit expression for the coefficients $b_{i,i}$ can be first calculated just for one internal and one boundary points with the general expression for the location of these points given by Eqs. (64-65). Then, we should consider the summation of these expressions over all internal and boundary points (similar to Eq. (68) in Sect. 3.1.1). We should mention that by the use of the elastodynamics equations, Eq. (88), the time derivatives for the local truncation error in Eq. (93) are excluded. By zeroing the coefficients $b_{i,i}$ for the smallest orders of h and using the least square method for the coefficients $b_{i,i}$ for higher orders of h (similar to the procedure in Sect. 3.1.1), we can form a local system of algebraic equations for the calculation of the unknown coefficients $m_{i,i}$, $\bar{m}_{i,i}$, $k_{i,i}$, $\bar{k}_{i,i}$ and $\bar{q}_{1,i}$, $q_{1,i}$, $\bar{q}_{2,i}$, $q_{2,i}$, $\bar{q}_{3,i}$, $q_{3,i}$, $\bar{q}_{4,i}$, $q_{4,i}$. As shown in our paper [32], OLTEM with the 9-point stencils and irregular boundaries provides the second order of accuracy of global solutions (similar to linear finite elements with the 9-point stencils). However, due to the minimization of the leading terms of the local truncation error, at the same numbers of degrees of freedom OLTEM on irregular domains yields more accurate results than those obtained by linear and high-order finite elements (up to the third order) with much wider stencils; see the numerical examples in our paper [32]. We should also mention that as shown in our paper [24], OLTEM in the 2-D case with wider $5 \times 5 = 25$ -point



stencils provides the 8-th and 6-th orders of the local truncation errors with the non-diagonal and diagonal mass matrices on regular domains with conforming Cartesian meshes, i.e for elastodynamics the optimal accuracy for the $5 \times 5 = 25$ -point stencils is two orders lower than that for the scalar wave equation on similar stencils; see Sect. 3.1.1.

3.2.2 Heterogeneous Materials

The 2-D elastodynamics equations in a composite domain $\Omega = \cup \Omega_l$ ($l = 1, 2, ..., \overline{N}$ where \overline{N} is the total number of subdomains) can be written down in each subdomain Ω_l as follows:

$$\mu_{l}\nabla^{2}u_{l} + (\mu_{l} + \lambda_{l})\left(\frac{\partial^{2}u_{l}}{\partial x^{2}} + \frac{\partial^{2}v_{l}}{\partial x\partial y}\right) + f_{x}^{l} = \rho_{l}\frac{\partial^{2}u_{l}}{\partial t^{2}},$$

$$\mu_{l}\nabla^{2}v_{l} + (\mu_{l} + \lambda_{l})\left(\frac{\partial^{2}v_{l}}{\partial y^{2}} + \frac{\partial^{2}u_{l}}{\partial x\partial y}\right) + f_{y}^{l} = \rho_{l}\frac{\partial^{2}v_{l}}{\partial t^{2}},$$
(94)

where $u_l = u_l(x,y,t)$ and $v_l = v_l(x,y,t)$ are the x- and y-components of the displacement vector, $f_x^l = f_x^l(x,y,t)$ and $f_y^l = f_y^l(x,y,t)$ are the x- and y-components of the body forces that can be discontinuous across interfaces. We also assume that the functions u_l and f_l are sufficiently smooth in each subdomain Ω_l . At the interface G between any two subdomains, the following interface conditions are applied:

$$u_G^* - u_G^{**} = \delta_1, \qquad v_G^* - v_G^{**} = \bar{\delta}_1,$$
 (95)

$$t_{x,G}^* - t_{x,G}^{**} = \delta_2, \qquad t_{y,G}^* - t_{y,G}^{**} = \bar{\delta}_2,$$
 (96)

where $\delta_1(x,y,t)|_{(x,y)\in G}$, $\bar{\delta}_1(x,y,t)|_{(x,y)\in G}$ and $\delta_2(x,y,t)|_{(x,y)\in G}$, $\bar{\delta}_2(x,y,t)|_{(x,y)\in G}$ are the given jumps in the displacements and in the tractive forces across the interface, the symbols * and ** correspond to the quantities on the opposite sides from the interface for the corresponding subdomains Ω_l . The x- and y-components of the tractive forces $t_{x,G}$ and $t_{y,G}$ can be expressed in terms of the displacements using Eq. (90) where symbol *(**) in Eq. (90) should be used for the displacements and Lame coefficients for material *(**).

The detailed derivation of OLTEM with the 9-point stencils for heterogeneous materials with irregular interfaces in the 2-D case is given in our paper [38] for the cases with the non-diagonal and diagonal mass matrices. Below we present the summary of the results.

Similar to the homogeneous materials in the previous section 3.2.1 (see also Eq. (91)), for heterogeneous materials with an interface we assume the following general form of two stencil equations for each grid point after the space discretization of Eq. (94) with a rectangular Cartesian mesh:

$$h^{2} \left\{ \sum_{p=1}^{L} m_{j,p} \left[a_{p} \frac{\hat{o}^{2} u_{p}^{*}}{\hat{o}t^{2}} + (1 - a_{p}) \frac{d^{2} u_{p}^{**,num}}{dt^{2}} \right] + \sum_{p=1}^{L} \bar{m}_{j,p} \left[a_{p} \frac{d^{2} v_{p}^{*,num}}{dt^{2}} + (1 - a_{p}) \frac{d^{2} v_{p}^{**,num}}{dt^{2}} \right] \right\} + \sum_{p=1}^{L} k_{j,p} \left[a_{p} u_{p}^{*,num} + (1 - a_{p}) u_{p}^{**,num} \right] + \sum_{p=1}^{L} \bar{k}_{j,p} \left[a_{p} v_{p}^{*,num} + (1 - a_{p}) v_{p}^{**,num} \right] = \bar{f_{j}}, \qquad j = 1, 2,$$

$$(97)$$

where the coefficients $a_p = 1$ if the grid point p belongs to material * and $a_p = 0$ if the grid point p belongs to another material ** (i.e., only two variables $u_p^{*,num}$, $v_p^{*,num}$ or $u_p^{**,num}$, $v_p^{**,num}$ are included into Eq. (97) for each grid point, e.g., see Fig. 5a with $a_1 = a_2 = a_3 = a_5 = a_6 = 1$ and $a_4 = a_7 = a_8 = a_9 = 0$). As can be seen, the stencil equations, Eq. (97), for heterogeneous materials include the same number of the stencil coefficients $m_{j,p}$, $\bar{m}_{j,p}$, $k_{j,p}$ and $\bar{k}_{j,p}$ (p = 1, 2, ..., L) as that for the homogeneous materials, Eq. (91).

The local truncation error e_j for the stencil equations, Eq. (97), can be obtained by the replacement of the numerical solution for $u^{*,num}$, $v^{*,num}$, $u^{**,num}$, $v^{**,num}$ in Eq. (97) by the exact solution u^* , v^* , u^{**} , v^{**} and by the addition of the interface conditions, Eqs. (95)-(96), at a small number N_G of the selected interface point to the obtained expression as the constraints (see the previous Sect. 3.1.3 for the wave equation):

$$\begin{split} e_{j} &= h^{2} \left\{ \sum_{p=1}^{L} m_{j,p} \left[a_{p} \frac{\partial^{2} u_{p}^{*}}{\partial t^{2}} + (1 - a_{p}) \frac{\partial^{2} u_{p}^{**}}{\partial t^{2}} \right] \right. \\ &+ \sum_{p=1}^{L} \bar{m}_{j,p} \left[a_{p} \frac{\partial^{2} v_{p}^{*}}{\partial t^{2}} + (1 - a_{p}) \frac{\partial^{2} v_{p}^{**}}{\partial t^{2}} \right] \right\} \\ &+ \sum_{p=1}^{L} k_{j,p} \left[a_{p} u_{p}^{*} + (1 - a_{p}) u_{p}^{**} \right] + \sum_{p=1}^{L} \bar{k}_{j,p} \left[a_{p} v_{p}^{*} + (1 - a_{p}) v_{p}^{**} \right] - \bar{f}_{j} \\ &+ \left[\sum_{l=1}^{N_{G}} q_{1,l} (u_{G,l}^{*} - u_{G,l}^{**} - \delta_{1,l}) + \sum_{l=1}^{N_{G}} q_{2,l} (v_{G,l}^{*} - v_{G,l}^{***} - \bar{\delta}_{1,l}) \right. \\ &+ \sum_{l=1}^{N_{G}} h q_{3,l} (t_{x(G,l)}^{*} - t_{x(G,l)}^{**} - \delta_{2,l}) + \sum_{l=1}^{N_{G}} h q_{4,l} (t_{y(G,l)}^{*} - t_{y(G,l)}^{**} - \bar{\delta}_{2,l}) \right], \ j = 1, 2, \end{split}$$

where the additional unknown stencil coefficients $q_{1,l}$, $q_{2,l}$, $q_{3,l}$, $q_{4,l}$ ($l=1,2,\ldots,N_G$) are related to the interface conditions (see Eq. (98)) and should be determined from the minimization of the local truncation error. As shown in our paper [38], $N_G = 5$ uniformly spaced interface points can be used for the 9-point stencils. In contrast to the scalar wave equation in Sect. 3.1.3, for the 9-point stencil (L=9) we do not use the time derivatives of the interface conditions in Eq. (98) (the optimal second order of accuracy of OLTEM can be reached without these additional interface



conditions; they may be needed for higher accuracy with wider L > 9 stencils).

Using the elastodynamics equations for each grid point, we can exclude the time derivatives from the expression for the local truncation error in Eq. (98) as well as find the expression for the discretized load $\bar{f_i}$:

$$\begin{split} e_{j} &= h^{2} \{ \sum_{p=1}^{L} m_{j,p} [a_{p} \frac{\mu_{*}}{\rho_{*}} (\frac{\partial^{2} u_{p}^{*}}{\partial x^{2}} + \frac{\partial^{2} u_{p}^{*}}{\partial y^{2}}) \\ &+ \frac{(\mu_{*} + \lambda_{*})}{\rho_{*}} (\frac{\partial^{2} u_{p}^{*}}{\partial x^{2}} + \frac{\partial^{2} v_{p}^{*}}{\partial x \partial y}) \\ &+ (1 - a_{p}) \frac{\mu_{**}}{\rho_{**}} (\frac{\partial^{2} u_{p}^{**}}{\partial x^{2}} + \frac{\partial^{2} u_{p}^{**}}{\partial y^{2}}) \\ &+ \frac{(\mu_{**} + \lambda_{**})}{\rho_{**}} (\frac{\partial^{2} u_{p}^{**}}{\partial x^{2}} + \frac{\partial^{2} v_{p}^{*}}{\partial x \partial y})] \\ &+ \sum_{p=1}^{L} \bar{m}_{j,p} [a_{p} \frac{\mu_{*}}{\rho_{*}} (\frac{\partial^{2} v_{p}^{*}}{\partial x^{2}} + \frac{\partial^{2} v_{p}^{*}}{\partial x^{2}}) \\ &+ \frac{(\mu_{*} + \lambda_{*})}{\rho_{*}} (\frac{\partial^{2} v_{p}^{*}}{\partial y^{2}} + \frac{\partial^{2} u_{p}^{*}}{\partial x \partial y}) \\ &+ (1 - a_{p}) \frac{\mu_{**}}{\rho_{**}} (\frac{\partial^{2} v_{p}^{*}}{\partial x^{2}} + \frac{\partial^{2} v_{p}^{*}}{\partial x \partial y}) \\ &+ \frac{(\mu_{**} + \lambda_{**})}{\rho_{**}} (\frac{\partial^{2} v_{p}^{*}}{\partial x^{2}} + \frac{\partial^{2} v_{p}^{*}}{\partial x \partial y})] \} \\ &+ \sum_{p=1}^{L} k_{j,p} [a_{p} u_{p}^{*} + (1 - a_{p}) u_{p}^{**}] \\ &+ \sum_{p=1}^{L} k_{j,p} [a_{p} v_{p}^{*} + (1 - a_{p}) v_{p}^{**}] \\ &+ \left[\sum_{l=1}^{N_{G}} q_{1,l} (u_{G,l}^{*} - u_{G,l}^{**}) + \sum_{l=1}^{N_{G}} q_{2,l} (v_{G,l}^{*} - v_{G,l}^{**}) \\ &+ \sum_{l=1}^{N_{G}} hq_{3,l} (t_{\chi(G,l)}^{*} - t_{\chi(G,l)}^{**}) + \sum_{l=1}^{N_{G}} hq_{4,l} (t_{\gamma(G,l)}^{*} - t_{\gamma(G,l)}^{**}) \right], \end{split}$$

and

$$\begin{split} \bar{f_{j}} &= h^{2} \left\{ \sum_{p=1}^{L} m_{j,p} \left[a_{p} \frac{1}{\rho_{*}} f_{x,p}^{*} + (1 - a_{p}) \frac{1}{\rho_{**}} f_{x,p}^{**} \right] \right. \\ &+ \sum_{p=1}^{L} \bar{m_{j,p}} \left[a_{p} \frac{1}{\rho_{*}} f_{y,p}^{*} + (1 - a_{p}) \frac{1}{\rho_{**}} f_{y,p}^{**} \right] \right\} \\ &- \sum_{l=1}^{N_{G}} \left(q_{1,l} \delta_{1,l} + q_{2,l} \bar{\delta}_{1,l} + h q_{3,l} \delta_{2,l} + h q_{4,l} \bar{\delta}_{2,l} \right), \qquad j = 1, 2, \end{split}$$

$$(100)$$

where the last expression in the parenthesis in Eq. (100) corresponds to the contribution due to the non-zero jump conditions in Eqs. (95) and (96). Expanding the values of

the exact solutions for the displacements u and v at the grid and interface points in Eq. (99) into a Taylor series in the vicinity of the central grid point with the coordinates x_c and y_c (e.g., c = 5 for the 9-point stencils), a Taylor series of the local truncation error e_j in Eq. (99) can be represented as follows:

$$\begin{split} e_{j} &= b_{j,1} u_{c}^{*} + b_{j,2} u_{c}^{**} + b_{j,3} v_{c}^{*} + b_{j,4} v_{c}^{**} + h(b_{j,5} \frac{\partial u_{c}^{*}}{\partial x} \\ &+ b_{j,6} \frac{\partial u_{c}^{**}}{\partial x} + b_{j,7} \frac{\partial v_{c}^{*}}{\partial x} + b_{j,8} \frac{\partial v_{c}^{**}}{\partial x} + b_{j,9} \frac{\partial u_{c}^{*}}{\partial y} + b_{10} \frac{\partial u_{c}^{**}}{\partial y} \\ &+ b_{j,11} \frac{\partial v_{c}^{*}}{\partial y} + b_{j,12} \frac{\partial v_{c}^{**}}{\partial y} + b_{j,12} \frac{\partial^{2} u_{c}^{*}}{\partial x^{2}} + b_{j,14} \frac{\partial^{2} u_{c}^{**}}{\partial x^{2}} \\ &+ b_{j,15} \frac{\partial^{2} v_{c}^{*}}{\partial x^{2}} + b_{j,16} \frac{\partial^{2} v_{c}^{**}}{\partial x^{2}} + b_{j,17} \frac{\partial^{2} u_{c}^{*}}{\partial x^{2}} + b_{j,18} \frac{\partial^{2} u_{c}^{**}}{\partial x^{2}} \\ &+ b_{j,19} \frac{\partial^{2} v_{c}^{*}}{\partial x^{2}} + b_{j,20} \frac{\partial^{2} v_{c}^{**}}{\partial x^{2}} + b_{j,21} \frac{\partial^{2} u_{c}^{*}}{\partial y^{2}} + b_{j,22} \frac{\partial^{2} u_{c}^{**}}{\partial x^{3}} \\ &+ b_{j,23} \frac{\partial^{2} v_{c}^{*}}{\partial y^{2}} + b_{j,24} \frac{\partial^{2} v_{c}^{**}}{\partial y^{2}} + h^{3} (b_{j,25} \frac{\partial^{3} u_{c}^{*}}{\partial x^{3}} + b_{j,26} \frac{\partial^{3} u_{c}^{**}}{\partial x^{3}} \\ &+ b_{j,27} \frac{\partial^{3} v_{c}^{*}}{\partial x^{3}} + b_{j,28} \frac{\partial^{3} v_{c}^{**}}{\partial x^{3}} + b_{j,29} \frac{\partial^{3} u_{c}^{*}}{\partial x^{2}\partial y} + b_{j,30} \frac{\partial^{3} u_{c}^{**}}{\partial x^{2}\partial y} \\ &+ b_{j,31} \frac{\partial^{3} v_{c}^{*}}{\partial x^{2}\partial y} + b_{j,32} \frac{\partial^{3} v_{c}^{**}}{\partial x^{2}\partial y} + b_{j,33} \frac{\partial^{3} u_{c}^{*}}{\partial x^{2}\partial y} + b_{j,34} \frac{\partial^{3} u_{c}^{**}}{\partial x^{2}\partial y} \\ &+ b_{j,35} \frac{\partial^{3} v_{c}^{*}}{\partial x^{2}\partial y^{2}} + b_{j,36} \frac{\partial^{3} v_{c}^{**}}{\partial x^{2}\partial y} + b_{j,37} \frac{\partial^{3} u_{c}^{*}}{\partial y^{3}} + b_{j,38} \frac{\partial^{3} u_{c}^{**}}{\partial y^{3}} \\ &+ b_{j,39} \frac{\partial^{3} v_{c}^{*}}{\partial y^{3}} + b_{j,40} \frac{\partial^{3} v_{c}^{**}}{\partial y^{3}} \right) \\ &+ h^{4} \left(b_{j,41} \frac{\partial^{4} u_{c}^{*}}{\partial x^{4}} + \dots + b_{j,60} \frac{\partial^{4} v_{c}^{**}}{\partial y^{4}} \right) \\ &+ h^{5} \left(b_{j,61} \frac{\partial^{5} u_{c}^{*}}{\partial x^{5}} + \dots + b_{j,84} \frac{\partial^{5} v_{c}^{**}}{\partial y^{5}} \right) \\ &+ h^{6} \left(b_{j,85} \frac{\partial^{6} u_{c}^{*}}{\partial x^{6}} + \dots + b_{j,112} \frac{\partial^{6} u_{c}^{**}}{\partial y^{6}} \right) + \dots, \quad j = 1, 2 \\ j = 1, 2, \end{split}$$

where the coefficients $b_{j,p}$ (j=1,2,p=1,2,...,112) can be expressed as a linear combination of the coefficients $m_{j,i}$, $\bar{m}_{j,i}$, $k_{j,i}$, $\bar{k}_{j,i}$ (i=1,2,...,L) and $q_{1,l}$, $q_{2,l}$, $q_{3,l}$, $q_{4,l}$ $(l=1,2,...,N_G)$. By zeroing the coefficients $b_{j,i}$ for the smallest orders of h and using the least square method for the coefficients $b_{j,i}$ for higher orders of h (similar to the procedure in Sect. 3.1.1), we can form a local system of algebraic equations for the calculation of the unknown coefficients $m_{j,i}$, $\bar{m}_{j,i}$, $k_{j,i}$, $\bar{k}_{j,i}$ (i=1,2,...,L) and $q_{1,l}$, $q_{2,l}$, $q_{3,l}$, $q_{4,l}$ $(l=1,2,...,N_G)$. As shown in our paper [38], OLTEM with the 9-point stencils and irregular interfaces provides the second order of accuracy of global solutions (similar linear finite elements with 9-point stencils). However, due to the minimization of the leading terms of the local truncation error, at the same numbers of degrees



of freedom, OLTEM for heterogeneous materials with irregular interfaces yields more accurate results than those obtained by linear and high-order finite elements (up to the third order) with much wider stencils; see the numerical examples in our paper [38].

4 OLTEM for Time Independent PDEs: Poisson, Helmholtz, Elasticity Equations

The development of OLTEM for time-independent PDEs is different from that for the time-dependent PDEs considered in the previous Sections. First of all, the stencil equations for OLTEM are assumed to be ordinary differential equations for the time-dependent PDEs and algebraic equations for time-independent PDEs. For the time-dependent PDEs, we exclude the time derivatives in the expression for the local truncation error using the original PDEs at the grid, boundary and interface points before considering a Taylor series expansion of the local truncation error. For the time-independent PDEs, the local truncation error is first expressed as an algebraic equation without the spatial derivatives. Therefore, in order to use the time-independent PDEs we first expand the local truncation error in a Taylor series and then we use the original PDEs in order to express one spatial derivative in terms of other spatial derivatives in the expression for the Taylor series of the local truncation error. The derivations of OLTEM for the time-independent Poisson equation will be presented in more detail in the next Section. For other time-independent PDEs we will use similarity with derivations for the Poisson equation and will refer to our papers for more details.

4.1 Poisson Equation

4.1.1 Homogeneous Materials

The Poisson equation in domain Ω can be written down as:

$$\nabla^2 u = f, \tag{102}$$

with the Dirichlet boundary conditions

$$u = g(\mathbf{x}) \tag{103}$$

on the boundary Γ^u and with the Neumann boundary conditions

$$n_x \frac{\partial u}{\partial x} + n_y \frac{\partial u}{\partial y} + n_z \frac{\partial u}{\partial z} = \bar{g}(\mathbf{x})$$
 (104)

on the boundary Γ^s where u is the field variable, $f(\mathbf{x},t)$ is the source term, the entire boundary Γ is $\Gamma = \Gamma^s U \Gamma^u$ and n_x , n_y , n_z are the x-, y- and z-components of the outward unit normal vector, g and \bar{g} are the given functions.

The detailed derivation of OLTEM for the Poisson equation is presented in our papers [1, 22, 23] in the 2-D and 3-D cases on regular domains and in our papers [25, 27, 28] in the 2-D and 3-D cases on irregular domains. Below we present the summary of the results.

The compact stencil equation for OLTEM for the Poisson equation in the 2-D and 3-D cases can be given for each internal grid point as follows:

$$\sum_{i=1}^{L} k_i u_i^{num} = \bar{f}, \tag{105}$$

where u_i^{num} are the numerical solution for function u at the grid points, k_i are the unknown stencil coefficients to be determined, \bar{f} is the discretized source term; L is the number of the grid points included into the stencil equation.

The local truncation errors e for the stencil equations given by Eq. (105) can obtained by the replacement of the numerical value of function u_i^{num} in Eq. (105) by the exact value u_i at the grid points i (i = 1, 2, ..., L) as well as by the addition of the boundary conditions at a small number $N_B = M_1 + M_2$ of the selected boundary points with some unknown coefficients (Lagrange multipliers) $q_{1,i}$ and $q_{2,i}$, $i = 1, 2, ..., N_B$) as the constraints:

$$e = \sum_{i=1}^{L} k_{i} u_{i} - \bar{f} + \sum_{i=1}^{M_{1}} q_{1,i} (g_{i} - u_{B,i}) + \sum_{i=1}^{M_{2}} h q_{2,i} \left(\bar{g}_{i} - n_{x,i} \frac{\partial u_{B,i}}{\partial x} + n_{y,i} \frac{\partial u_{B,i}}{\partial y} + n_{z,i} \frac{\partial u_{B,i}}{\partial z} \right),$$
(106)

where M_1 and M_2 are the numbers of the selected boundary points with the Dirichlet and Neumann boundary conditions, respectively; the expressions after $q_{1,i}$ and $q_{2,i}$ are the boundary conditions at the selected boundary points given by Eqs. (103) and (104). Therefore, the expressions after the term \bar{f} in Eq. (106) are zero and do not affect the value of the local truncation error e.

In order to represent the local truncation errors e given by Eq. (106) as a Taylor series, let us expand the exact solution and its spatial derivatives at the grid and boundary points into a Taylor series at small $h \ll 1$ in the vicinity of the central grid point with the coordinates x_c , y_c , z_c using Eqs. (64–66). In this case we will obtain the expression given by Eq. (67) with $\bar{c}=1$ and the coefficients b_p ($p=1,2,\ldots$) expressed as a linear combination of the coefficients k_i and $q_{1,i},q_{2,i}$ used in Eqs. (105)-(106); see our papers [25, 27, 28] in the 2-D and 3-D cases on irregular domains. We should mention that the explicit expression for the coefficients b_p can be first calculated just for one internal and one boundary point with the general expression for the location of these points given Eqs. (64)-(65). Then, we should consider the summation



over all internal and boundary points similar to those expressions given by Eq. (68).

The exact solution u_c to the Poisson equation, Eq. (102), at the central grid point with the coordinates $x = x_c$, $y = y_c$ and $z = z_c$ meets the following equations:

$$\frac{\partial^2 u_c}{\partial x^2} = -\left(\frac{\partial^2 u_c}{\partial y^2} + \frac{\partial^2 u_c}{\partial z^2}\right) + f_c,\tag{107}$$

$$\frac{\partial^{(2+i+j+k)} u_c}{\partial x^{2+i} \partial y^j \partial z^k} = -\left(\frac{\partial^{(2+i+j+k)} u_c}{\partial x^i \partial y^{(j+2)} \partial z^k} + \frac{\partial^{(2+i+j+k)} u_c}{\partial x^i \partial y^j \partial z^{(k+2)}}\right) + \frac{\partial^{(i+j+k)} f_c}{\partial x^i \partial y^j \partial z^k}$$
(108)

with i,j,k = 0,1,2,3,4,... Here, Eq. (108) is directly obtained by the differentiation of Eq. (107) with respect to x, y and z. Using Eqs. (107) and (108), we can exclude the second and higher order partial derivatives of x in Eq. (67), and the local truncation error in space e can be written down as:

$$e = b_{1}u_{c} + h\left[b_{2}\frac{\partial u_{c}}{\partial z} + b_{3}\frac{\partial u_{c}}{\partial y} + b_{4}\frac{\partial u_{c}}{\partial x}\right] + h^{2}\left[b_{5}\frac{\partial^{2}u_{c}}{\partial z^{2}}\right]$$

$$+ b_{6}\frac{\partial^{2}u_{c}}{\partial y\partial z} + b_{7}\frac{\partial^{2}u_{c}}{\partial y^{2}} + b_{8}\frac{\partial^{2}u_{c}}{\partial x\partial z} + b_{9}\frac{\partial^{2}u_{c}}{\partial x\partial y}$$

$$+ h^{3}\left[b_{10}\frac{\partial^{3}u_{c}}{\partial z^{3}} + b_{11}\frac{\partial^{3}u_{c}}{\partial y\partial z^{2}} + b_{12}\frac{\partial^{3}u_{c}}{\partial y^{2}\partial z}\right]$$

$$+ b_{13}\frac{\partial^{3}u_{c}}{\partial y^{3}} + b_{14}\frac{\partial^{3}u_{c}}{\partial x\partial z^{2}} + b_{15}\frac{\partial^{3}u_{c}}{\partial x\partial y\partial z} + b_{16}\frac{\partial^{3}u_{c}}{\partial x\partial y^{2}}$$

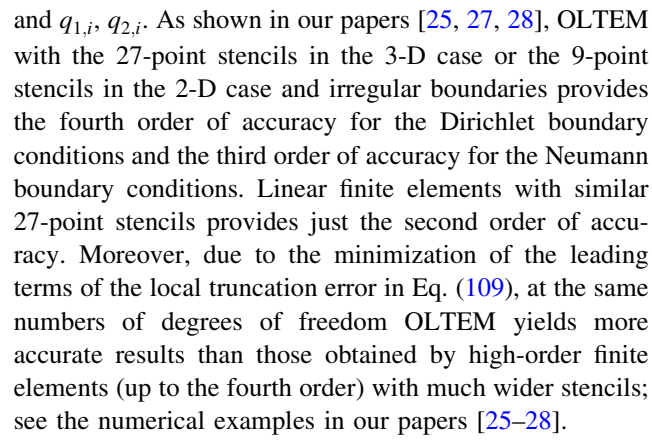
$$+ h^{4}\left[b_{17}\frac{\partial^{4}u_{c}}{\partial z^{4}} + \dots + b_{25}\frac{\partial^{4}u_{c}}{\partial x\partial y^{3}}\right] + h^{5}\left[b_{26}\frac{\partial^{5}u_{c}}{\partial z^{5}} + \dots + b_{36}\frac{\partial^{5}u_{c}}{\partial x\partial y^{4}}\right]$$

$$+ h^{6}\left[b_{37}\frac{\partial^{6}u_{c}}{\partial z^{6}} + \dots + b_{49}\frac{\partial^{6}u_{c}}{\partial x\partial y^{5}}\right] + \dots,$$

$$(109)$$

where the coefficients b_p (p = 1, 2, ...) are expressed in terms of the coefficients k_i and $q_{1,i}$, $q_{2,i}$; see our papers [1, 22, 23, 25, 27, 28]. Due to Eqs. (107)-(108), there are no second and higher order partial derivatives of x in Eq. (109). We should also mention that substituting Eqs. (107)-(108) into Eq. (67), the discretized source term \bar{f} in Eq. (105) can be calculated as the addition of the terms due to the Dirichlet and Neumann boundary conditions at the selected boundary points $\sum_{i=1}^{M_1} q_{1,i}g_i + \sum_{i=1}^{M_2} hq_{2,i}\bar{g}_i$ plus a Taylor series of non-zero source term f in the Poisson equation, Eq. (102);see our papers [1, 22, 23, 25, 27, 28] for the details.

By zeroing the coefficients b_p for the smallest orders of h and using the least square method for the coefficients b_p for higher orders of h (similar to the procedure in Sect. 3.1.1), we can form a local system of algebraic equations for the calculation of the unknown coefficients k_i



We should also mention that for the Poisson equation on regular domains, OLTEM with conforming Cartesian meshes provides a higher accuracy on square meshes than that on rectangular meshes. For example, OLTEM with the 27-point stencils in the 3-D case or the 9-point stencils in the 2-D case yields the 6-th and 4-th orders of accuracy on uniform square (with the same mesh aspect ratios along the Cartesian axes) and rectangular meshes, respectively (see our papers [22, 25]). OLTEM with wider $5 \times 5 = 25$ -point stencils in the 2-D case (similar to the stencils for quadratic finite elements) provides 18-th and 14-th orders of accuracy on uniform square (with the same mesh aspect ratios along the Cartesian axes) and rectangular meshes, respectively (see our paper [1]).

4.1.2 Heterogeneous Materials

The Poisson equation in a composite domain $\Omega = \cup \Omega_l$ $(l=1,2,\ldots,\bar{N})$ where \bar{N} is the total number of subdomains) can be written down in each subdomain Ω_l as follows:

$$e_I \nabla^2 u_I = f_I, \tag{110}$$

where e_l is a constant in each subdomain Ω_l and can be discontinuous across the interfaces between subdomains Ω_l $(l=1,2,\ldots,\bar{N}), f_l(x)$ is the source term that can be also discontinuous across the interfaces between subdomains Ω_l , u_l is the field variable. We also assume that the functions u_l and f_l are sufficiently smooth in each subdomain Ω_l . At the interface G between any two subdomains, the following interface conditions are applied:

$$u_{G}^{*} - u_{G}^{**} = \delta_{1}, \qquad e_{*} \left(n_{x} \frac{\partial u_{G}^{*}}{\partial x} + n_{y} \frac{\partial u_{G}^{*}}{\partial y} + n_{z} \frac{\partial u_{G}^{*}}{\partial z} \right)$$

$$- e_{**} \left(n_{x} \frac{\partial u_{G}^{**}}{\partial x} + n_{y} \frac{\partial u_{G}^{**}}{\partial y} + n_{z} \frac{\partial u_{G}^{**}}{\partial z} \right) = \delta_{2},$$

$$(111)$$

where $\delta_1(x, y, z)$ and $\delta_2(x, y, z)$ are the given jumps for the function and for the flux across the interface, n_x , n_y and n_z



are the x-, y- and z-components of the normal vector at the interface, e_* (e_{**}) is the corresponding material constant, the symbols * and ** correspond to the quantities on the opposite sides from the interface for the corresponding subdomains Ω_l . For zero jumps $\delta_1 = \delta_2 = 0$ the functions u_l are continuous across the interfaces but can have the discontinuous spatial derivatives across the interfaces.

The detailed derivation of OLTEM for heterogeneous materials with irregular interfaces in the 2-D and 3-D cases is presented in our papers [35, 36]. Below we present the summary of the results.

Similar to the stencil given by Eq. (84) for the wave (heat) equation, the compact OLTEM stencil equation for the 2-D and 3-D Poisson equation for each internal grid point located far from the boundary can be given as follows:

$$\sum_{p=1}^{L} k_p [a_p u_p^{*,num} + (1 - a_p) u_p^{**,num}] = \bar{f},$$
 (112)

where the coefficients $a_p = 1$ if the grid point p belongs to material * and $a_p = 0$ if the grid point p belongs to another material ** (i.e., only one variable $u_p^{*,num}$ or $u_p^{**,num}$ or $u_p^{**,num}$ (i = 1, 2, ..., L) is included into Eq. (112) for each grid point. As can be seen, the stencil equation, Eq. (112), includes the same number of the stencil coefficients k_p (p = 1, 2, ..., L) as that for the homogeneous case, Eq. (105). The derivation of OLTEM for heterogeneous materials in the 2-D and 3-D cases includes the use of the interface conditions at a small number N_G of interface points along a part of the interface located within the corresponding compact cell. The coordinates of the selected N_G points on the interface (see Fig. 6) are described with respect to the stencil central grid point by Eq. (85).

One of the ideas of the new approach is to include the interface conditions for the exact solution at a small number N_G of the interface points in the expression for the local truncation error of Eq. (112) as the constraints:

$$e = \sum_{p=1}^{L} k_{p} [a_{p} u_{p}^{*} + (1 - a_{p}) u_{p}^{**}] - \bar{f}$$

$$+ \{ \sum_{j=1}^{N_{G}} q_{1,j} (u_{G,j}^{*} - u_{G,j}^{**} - \delta_{1})$$

$$+ \sum_{j=1}^{N_{G}} h q_{2,j} [e_{*} (n_{x,j} \frac{\partial u_{G,j}^{*}}{\partial x} + n_{y,j} \frac{\partial u_{G,j}^{*}}{\partial y} + n_{z,j}$$

$$\frac{\partial u_{G,j}^{**}}{\partial z}) - e_{**} (n_{x,j} \frac{\partial u_{G,j}^{**}}{\partial x} + n_{y,j}$$

$$\frac{\partial u_{G,j}^{**}}{\partial y} + n_{z,j} \frac{\partial u_{G,j}^{**}}{\partial z}) - \delta_{2}] \},$$

$$(113)$$

where $n_{x,j}$, $n_{y,j}$ and $n_{z,j}$ are the x-, y-, and z-components of the normal vectors at the N_G selected interface points (e.g., see Fig. 6), the coefficients $q_{1,j}$ and $q_{2,j}$ ($j=1,2,\ldots,N_G$) are unknown and are used for the minimization of the local truncation error in Eq. (113), the expressions in parenthesis after $q_{1,j}$ and $q_{2,j}$ are the interface conditions at the N_G selected interface points. Therefore, the expression in the curly brackets in Eq. (113) is zero (see Eq. (111)) and does not affect the value of the local truncation error e. The addition of the interface conditions at N_G points in Eq. (113) with the unknown coefficients $q_{1,j}$, $q_{2,j}$ ($j=1,2,\ldots,N_G$) allows us to couple functions u_p^* and u_p^{**} as well as to get a high accuracy of the proposed method for general geometry of interfaces; see below.

In order to represent the local truncation error e as a Taylor series, let us expand the exact solution at the grid and selected interface points in Eq. (113) into a Taylor series at small $h \ll 1$ in the vicinity of the central grid point with the coordinates $x = x_c$, $y = y_c$ and $z = z_c$ using Eq. (66). The exact solution u_p^* and u_p^{**} to the Poisson equations, Eq. (110), at the central grid point $x = x_c$, $y = y_c$ and $z = z_c$ meets the following equations:

$$\frac{\partial^{2} u_{c}^{*}}{\partial x^{2}} = -\frac{\partial^{2} u_{c}^{*}}{\partial y^{2}} - \frac{\partial^{2} u_{c}^{*}}{\partial z^{2}} + \frac{1}{e_{*}} f^{*},
\frac{\partial^{2} u_{c}^{**}}{\partial x^{2}} = -\frac{\partial^{2} u_{c}^{**}}{\partial y^{2}} - \frac{\partial^{2} u_{c}^{**}}{\partial z^{2}} + \frac{1}{e_{**}} f^{**},
\frac{\partial^{(i+j+t+2)} u_{c}^{*}}{\partial z^{t} \partial y^{i} \partial x^{(2+j)}}
= -\frac{\partial^{(i+j+t+2)} u_{c}^{*}}{\partial z^{t} \partial y^{(i+2)} \partial x^{j}} - \frac{\partial^{(i+j+t+2)} u_{c}^{*}}{\partial z^{(t+2)} \partial y^{i} \partial x^{j}}
+ \frac{1}{e_{*}} \frac{\partial^{(i+j+t)} f^{*}}{\partial z^{t} \partial y^{i} \partial x^{j}},
\frac{\partial^{(i+j+t+2)} u_{c}^{**}}{\partial z^{t} \partial y^{i} \partial x^{(2+j)}} = -\frac{\partial^{(i+j+t+2)} u_{c}^{**}}{\partial z^{t} \partial y^{(i+2)} \partial x^{j}}
- \frac{\partial^{(i+j+t+2)} u_{c}^{**}}{\partial z^{(t+2)} \partial y^{i} \partial x^{j}} + \frac{1}{e_{**}} \frac{\partial^{(i+j+t)} f^{**}}{\partial z^{t} \partial y^{i} \partial x^{j}}$$
(114)

with i,j,t=0,1,2,3,4,... Equation (115) is obtained by the differentiation of Eq. (114) with respect to x, y and z. Inserting Eqs. (66), (114), (115) into Eq. (113) we get the discretized source term \bar{f} (see our papers [35, 36]) as well as the following local truncation error in space e:

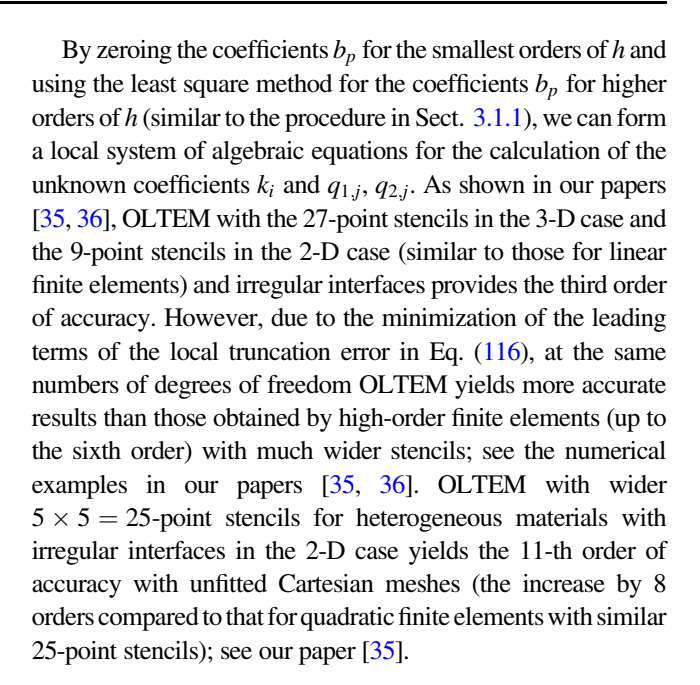


$$e = b_1 u_c^* + b_2 u_c^{**} + h(b_3 \frac{\partial u_c^*}{\partial z} + b_4 \frac{\partial u_c^{**}}{\partial z} + b_5 \frac{\partial u_c^*}{\partial y} + b_6 \frac{\partial u_c^{**}}{\partial x})$$

$$+ b_5 \frac{\partial u_c^*}{\partial x} + b_8 \frac{\partial u_c^{**}}{\partial x})$$

$$+ b^7 (b_9 \frac{\partial^2 u_c^*}{\partial z^2} + b_{10} \frac{\partial^2 u_c^{**}}{\partial z \partial y^2} + b_{11} \frac{\partial^3 u_c^*}{\partial z \partial y^2} + b_{12} \frac{\partial^3 u_c^{**}}{\partial z \partial y^2} + b_{13} \frac{\partial^2 u_c^*}{\partial z \partial x^2} + b_{16} \frac{\partial^3 u_c^{**}}{\partial z \partial x^2} + b_{17} \frac{\partial^3 u_c^*}{\partial x \partial y} + b_{18} \frac{\partial^3 u_c^{**}}{\partial z \partial x^2} + b_{19} \frac{\partial^3 u_c^{**}}{\partial z^2 \partial y} + b_{19} \frac{\partial^3 u_c^{**}}{\partial z \partial y \partial x} + b_{19} \frac{\partial^3 u_c^{**}}{\partial z \partial y \partial x} + b_{19} \frac{\partial^3 u_c^{**}}{\partial z \partial y \partial x} + b_{19} \frac{\partial^3 u_c^{**}}{\partial z \partial y \partial x} + b_{19} \frac{\partial^3 u_c^{**}}{\partial z \partial y \partial x} + b_{19} \frac{\partial^3 u_c^{**}}{\partial z \partial y \partial x} + b_{19} \frac{\partial^3 u_c^{**}}{\partial z \partial y \partial x} + b_{19} \frac{\partial^3 u_c^{**}}{\partial z \partial y \partial x} + b_{19} \frac{\partial^3 u_c^{**}}{\partial z \partial y \partial x} + b_{19} \frac{\partial^3 u_c^{**}}{\partial z \partial y \partial x} + b_{19} \frac{\partial^3 u_c^{**}}{\partial z \partial y \partial x} + b_{19} \frac{\partial^3 u_c^{**}}{\partial z \partial y \partial x} + b_{19} \frac{\partial^3 u_c^{**}}{\partial z \partial y \partial x} + b_{19} \frac{\partial^3 u_c^{**}}{\partial z \partial y \partial x} + b_{19} \frac{\partial^3 u_c^{**}}{\partial z \partial y \partial x} + b_{19} \frac{\partial^3 u_c^{**}}{\partial z \partial y \partial x} + b_{19} \frac{\partial^3 u_c^{**}}{\partial z \partial y \partial x} + b_{19} \frac{\partial^3 u_c^{**}}{\partial z \partial y \partial x} + b_{19} \frac{\partial^3 u_c^{**}}{\partial z \partial y \partial x} + b_{19} \frac{\partial^3 u_c^{**}}{\partial z \partial y \partial x} + b_{19} \frac{\partial^3 u_c^{**}}{\partial z \partial y \partial x} + b_{19} \frac{\partial^3 u_c^{**}}{\partial z \partial y \partial x} + b_{19} \frac{\partial^3 u_c^{**}}{\partial z \partial y \partial x} + b_{19} \frac{\partial^3 u_c^{**}}{\partial z \partial y \partial x$$

where the coefficients b_p (p = 1, 2, ...) are expressed in terms of the coefficients k_i and $q_{1,j}$, $q_{2,j}$ (i = 1, 2, ..., L, $j = 1, 2, ..., N_G$). We should mention that the expression for the local truncation error, Eq. (116), includes only the first order derivatives with respect to x (the higher order derivatives with respect to x are excluded with the help of Eqs. (114) - (115)).



4.2 Helmholtz Equation

The Helmholtz equation as well as its simple modification called the screened Poisson equation on an irregular domain Ω can be written down as:

$$\nabla^2 u + \alpha \beta^2 u = f, \tag{117}$$

where $\alpha = 1$ for the Helmholtz equation, $\alpha = -1$ for the screened Poisson equation, β is the wave number for the Helmholtz equation, f(x, y, z) is the loading term, u(x, y, z) is the field variable. The Dirichlet boundary conditions u = g(x) (118)

on the boundary Γ^u and the Neumann boundary conditions

$$n_x \frac{\partial u}{\partial x} + n_y \frac{\partial u}{\partial y} + n_z \frac{\partial u}{\partial z} = \bar{g}(\mathbf{x})$$
 (119)

on the boundary Γ^s are applied where the entire boundary Γ is $\Gamma = \Gamma^s U \Gamma^u$. These boundary conditions given by Eqs. (118) and (119) are similar to those for the Poisson equation; see Eqs. (103) and (104).

The detailed derivation of OLTEM for the Helmholtz equation is presented in our papers [29, 30] in the 2-D and 3-D cases on irregular domains. Below we present the summary of the results.

The compact stencil equation for OLTEM in the 2-D and 3-D cases can be uniformly given for each internal grid point as follows:

$$\sum_{i=1}^{L} (\alpha \beta^2 h^2 m_i u_i^{num} + k_i u_i^{num}) = \bar{f},$$
 (120)

where m_i , k_i are the unknown stencil coefficients to be determined. It is interesting to mention that the left-hand



side of Eq. (120) can be written in terms of one stencil coefficient $\bar{k_i}(h)$ as follows:

$$\sum_{i=1}^{L} (\alpha \beta^2 h^2 m_i u_i^{num} + k_i u_i^{num}) = \sum_{i=1}^{L} \bar{k_i}(h) u_i^{num}, \qquad (121)$$

with

$$\bar{k_i}(h) = (\alpha \beta^2 h^2 m_i + k_i), \tag{122}$$

where $\bar{k_i}(h)$ is a polynomial function of the mesh size h (similar to the stencil coefficients for inhomogeneous materials in Sect. 3.1.2).

The local truncation errors e for the stencil equation, Eq. (120), can obtained by the replacement of the numerical value of function u_i^{num} in Eq. (120) by the exact value u_i at the grid points i (i = 1, 2, ..., L) as well as by the addition of the boundary conditions at a small number $N_B = M_1 + M_2$ of the selected boundary points with some unknown coefficients (Lagrange multipliers) $q_{1,i}$, $q_{2,i}$, $q_{3,i}$ and $q_{4,i}$, $i = 1, 2, ..., N_B$) as the constraints:

$$e = \sum_{i=1}^{L} [(\alpha \beta^{2} h^{2} m_{i} + k_{i}) u_{i}] - \bar{f} + \sum_{i=1}^{M_{1}} [(\alpha \beta^{2} h^{2} q_{1,i} + q_{2,i}) (g_{i} - u_{B,i})]$$

$$+ \sum_{i=1}^{M_{2}} \{ (\alpha \beta^{2} h^{3} q_{3,i} + h q_{4,i}) [\bar{g}_{i} - (n_{x,i} \frac{\partial u_{B,i}}{\partial x} + n_{y,i} \frac{\partial u_{B,i}}{\partial y} + n_{z,i} \frac{\partial u_{B,i}}{\partial z})] \}$$

$$(123)$$

where M_1 and M_2 are the numbers of the selected boundary points with the Dirichlet and Neumann boundary conditions, respectively; the expressions after $q_{2,i}$ and $q_{4,i}$ are the boundary conditions at the selected boundary points given by Eqs. (118) and (119). Therefore, the expressions after the term f in Eq. (123) are zero and do not affect the value of the local truncation error e. Similar to the Poisson equation in the previous Sect. 4.1.1, we expand the exact solution and its spatial derivatives at the grid and boundary points into a Taylor series at small $h \ll 1$ in the vicinity of the central grid point with the coordinates x_c , y_c , z_c using Eqs. (64)-(66). The exact solution u_c to Eqs. (117) at the stencil central grid point with the coordinates $x = x_c$, $y = y_c$ and $z = z_c$ meets the following equations:

$$\frac{\partial^2 u_c}{\partial x^2} = -\frac{\partial^2 u_c}{\partial y^2} - \frac{\partial^2 u_c}{\partial z^2} - \alpha \beta^2 u_c + f_c, \tag{124}$$

$$\frac{\partial^{(i+j+k+2)} u_c}{\partial x^{i+2} \partial y^j \partial z^k} = -\frac{\partial^{(i+j+k+2)} u_c}{\partial x^i \partial y^{j+2} \partial z^k}
-\frac{\partial^{(i+j+k+2)} u_c}{\partial x^i \partial y^j \partial z^{k+2}} - \alpha \beta^2 \frac{\partial^{(i+j+k)} u_c}{\partial x^i \partial y^j \partial z^k} + \frac{\partial^{(i+j+k)} f_c}{\partial x^i \partial y^j \partial z^k}$$
(125)

with $i,j,k = 0, 1, 2, 3, 4, \dots$ Here, Eq. (125) is directly obtained by the differentiation of Eq. (124) with respect to x, y and z. Similar to the derivation of a Taylor series of the local truncation error e for the Poisson equation in the

previous Sect. 4.1.1, a Taylor series of the local truncation error e for the Helmholtz equation can be obtained in the following form:

$$e = b_{1}u_{c} + h \left[b_{2} \frac{\partial u_{c}}{\partial x} + b_{3} \frac{\partial u_{c}}{\partial y} + b_{4} \frac{\partial u_{c}}{\partial z} \right]$$

$$+ h^{2} \left[b_{5} \frac{\partial^{2} u_{c}}{\partial x \partial y} + b_{6} \frac{\partial^{2} u_{c}}{\partial x \partial z} + b_{7} \frac{\partial^{2} u_{c}}{\partial y^{2}} \right]$$

$$+ h^{3} \left[b_{11} \frac{\partial^{3} u_{c}}{\partial x \partial y^{2}} + b_{12} \frac{\partial^{3} u_{c}}{\partial x \partial y \partial z} \right]$$

$$+ h^{3} \left[b_{11} \frac{\partial^{3} u_{c}}{\partial x \partial y^{2}} + b_{12} \frac{\partial^{3} u_{c}}{\partial x \partial y \partial z} \right]$$

$$+ h^{3} \left[b_{11} \frac{\partial^{3} u_{c}}{\partial x \partial y^{2}} + b_{12} \frac{\partial^{3} u_{c}}{\partial x \partial y \partial z} \right]$$

$$+ b_{13} \frac{\partial^{3} u_{c}}{\partial x \partial y^{2}} + b_{14} \frac{\partial^{3} u_{c}}{\partial y^{3}} + b_{15} \frac{\partial^{3} u_{c}}{\partial y^{2} \partial z}$$

$$+ b_{16} \frac{\partial^{3} u_{c}}{\partial y \partial z^{2}} + b_{17} \frac{\partial^{3} u_{c}}{\partial z^{3}} + b_{18} \alpha \beta^{2} \frac{\partial u_{c}}{\partial x}$$

$$+ b_{19} \alpha \beta^{2} \frac{\partial u_{c}}{\partial y} + b_{20} \alpha \beta^{2} \frac{\partial u_{c}}{\partial z} \right]$$

$$+ h^{4} \left[b_{21} \frac{\partial^{4} u_{c}}{\partial x \partial y^{3}} + b_{22} \frac{\partial^{4} u_{c}}{\partial x \partial y^{2} \partial z} \right]$$

$$+ b_{23} \frac{\partial^{4} u_{c}}{\partial x \partial y \partial z^{2}} + b_{24} \frac{\partial^{4} u_{c}}{\partial x \partial z^{3}}$$

$$+ b_{25} \frac{\partial^{4} u_{c}}{\partial y^{4}} + b_{26} \frac{\partial^{4} u_{c}}{\partial y^{3} \partial z}$$

$$+ b_{27} \frac{\partial^{4} u_{c}}{\partial y^{2} \partial z^{2}} + b_{28} \frac{\partial^{4} u_{c}}{\partial y \partial z^{3}}$$

$$+ b_{29} \frac{\partial^{4} u_{c}}{\partial z^{4}}$$

$$+ b_{30} \alpha \beta^{2} \frac{\partial^{2} u_{c}}{\partial x^{2}} + b_{31} \alpha \beta^{2} \frac{\partial^{2} u_{c}}{\partial x \partial z}$$

$$+ b_{32} \alpha \beta^{2} \frac{\partial^{2} u_{c}}{\partial z^{2}} + b_{33} \alpha \beta^{2} \frac{\partial^{2} u_{c}}{\partial y \partial z}$$

$$+ b_{35} \beta^{4} u_{c} \right] + h^{5} \left[b_{36} \frac{\partial^{5} u_{c}}{\partial x \partial y^{4}} + \cdots$$

$$+ b_{56} \beta^{4} \frac{\partial^{5} u_{c}}{\partial z} \right]$$

$$+ h^{6} \left[b_{57} \frac{\partial^{6} u_{c}}{\partial x \partial y^{5}} + \cdots + b_{84} \alpha^{3} \beta^{6} u_{c} \right]$$

$$+ h^{7} \left[b_{85} \frac{\partial^{7} u_{c}}{\partial x \partial y^{5}} + \cdots + b_{120} \alpha^{3} \beta^{6} \frac{\partial u_{c}}{\partial z} \right]$$

$$+ h^{8} \left[b_{121} \frac{\partial^{8} u_{c}}{\partial x \partial y^{5}} + \cdots + b_{165} \beta^{8} u_{c} \right] + O(h^{9}),$$

where the coefficients b_p (p = 1, 2, 165) are expressed as a linear combination of the coefficients m_i , k_i , $q_{1,i}$, $q_{2,i}$, $q_{3,i}$ and $q_{4,i}$ used in Eqs. (120) and (123); see our papers [29, 30] for the 2-D and 3-D cases on irregular domains. Here we should mention that the expression for the local



truncation error, Eq. (126), includes the first-order derivatives with respect to x only (the higher order derivatives with respect to x are excluded with the help of Eqs. (124) - (125)).

By zeroing the coefficients b_p for the smallest orders of h and using the least square method for the coefficients b_p for higher orders of h (similar to the procedure in Sect. 3.1.1), we can form a local system of algebraic equations for the calculation of the unknown coefficients m_i , k_i , $q_{1,i}$, $q_{2,i}$, $q_{3,i}$ and $q_{4,i}$. As shown in our papers [29, 30], OLTEM with the 27-point stencils in the 3-D case (the 9-point stencils in the 2-D case) and irregular boundaries provides the fourth order of accuracy for the Dirichlet boundary conditions and the third order of accuracy for the Neumann boundary conditions. Linear finite elements with similar 27-point stencils provides just the second order of accuracy. Moreover, due to the minimization of the leading terms of the local truncation error in Eq. (126), at the same numbers of degrees of freedom OLTEM yields more accurate results than those obtained by high-order finite elements (up to the fourth order) with much wider stencils; see the numerical examples in our papers [29, 30].

4.3 Elasticity Equations

Currently, we have developed OLTEM for the elastostatics equations in the 2-D case; see our papers [2, 3, 31, 37]).

4.3.1 Homogeneous Materials

The corresponding 2-D elastostatics PDEs with constant coefficients in domain Ω can written down as:

$$\mu \nabla^2 u + (\mu + \lambda) \left(\frac{\partial^2 u}{\partial x^2} + \frac{\partial^2 v}{\partial x \partial y} \right) + f_x = 0,$$

$$\mu \nabla^2 v + (\mu + \lambda) \left(\frac{\partial^2 v}{\partial y^2} + \frac{\partial^2 u}{\partial x \partial y} \right) + f_y = 0,$$
(127)

with the Dirichlet boundary conditions

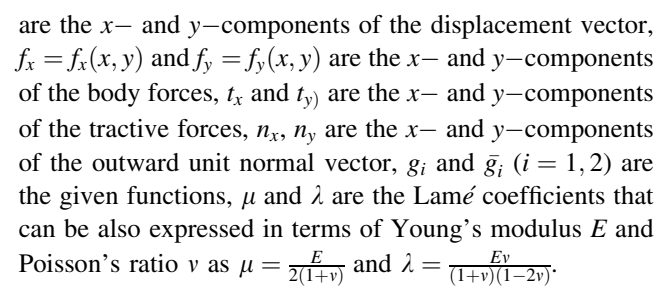
$$u = g_1(\mathbf{x}), \qquad v = g_2(\mathbf{x}) \tag{128}$$

on the boundary Γ^u and with the Neumann boundary conditions

$$t_{x} = n_{x} \left[(\lambda + 2\mu) \frac{\partial u}{\partial x} + \lambda \frac{\partial v}{\partial y} \right] + n_{y} \mu \left(\frac{\partial u}{\partial y} + \frac{\partial v}{\partial x} \right) = \bar{g}_{1}(\mathbf{x}),$$

$$t_{y} = n_{y} \left[(\lambda + 2\mu) \frac{\partial v}{\partial y} + \lambda \frac{\partial u}{\partial x} \right] + n_{x} \mu \left(\frac{\partial u}{\partial y} + \frac{\partial v}{\partial x} \right) = \bar{g}_{2}(\mathbf{x}),$$
(129)

on the boundary Γ^s where the entire boundary Γ is $\Gamma = \Gamma^s U \Gamma^u$. In Eqs. (127–129), u = u(x, y) and v = v(x, y)



The detailed derivation of OLTEM for the elastostatics equations is presented in our paper [2] in the 2-D case on regular domains and in our paper [31] in the 2-D case on irregular domains. Below we present the summary of the results.

According to OLTEM we assume the following general form of two stencil equations for each grid point after the space discretization of Eq. (127) with a rectangular Cartesian mesh:

$$\sum_{i=1}^{L} k_{j,i} u_i^{num} + \sum_{i=1}^{L} \bar{k}_{j,i} v_i^{num}$$

$$= \bar{f}_j, \qquad j = 1, 2,$$
(130)

where u_i^{num} , v_i^{num} are the numerical solution for the displacements u, v at the i-th grid point, $k_{j,i}$, $\bar{k_{j,i}}$ are the unknown stencil coefficients to be determined, L is the number of the grid points included into the stencil equation, $\bar{f_i}$ are the components of the discretized loading term.

The local truncation errors e_j for the stencil equations given by Eq. (130) can obtained by the replacement of the numerical values of the displacements u_i^{num} , v_i^{num} in Eq. (130) by the exact values u_i , v_i at the grid points i (i = 1, 2, ..., L) as well as by the addition of the boundary conditions at a small number $N_B = M_1 + M_2$ of the selected boundary points with some unknown coefficients (Lagrange multipliers) $q_{m,i}$ and $\bar{q}_{m,i}$ (m = 1, 2, ..., l) as the constraints:

$$e_{j} = \sum_{i=1}^{L} k_{j,i} u_{i} + \sum_{i=1}^{L} \bar{k}_{j,i} v_{i}$$

$$-\bar{f}_{j} + \sum_{i=1}^{M_{1}} q_{1,i} (g_{1,i} - u_{B,i}) + \sum_{i=1}^{M_{1}} \bar{q}_{1,i} (g_{2,i} - v_{B,i})$$

$$+ h \left[\sum_{i=1}^{M_{2}} q_{2,i} (\bar{g}_{1,i} - t_{x,B,i}) + \sum_{i=1}^{M_{2}} \bar{q}_{2,i} (\bar{g}_{2,i} - t_{y,B,i}) \right],$$

$$(131)$$

where M_1 and M_2 are the numbers of the selected boundary points with the Dirichlet and Neumann boundary conditions, respectively; the expressions after $q_{1,i}$, $\bar{q}_{1,i}$ and $q_{2,i}$, $\bar{q}_{2,i}$ are the Dirichlet and Neumann boundary conditions at the selected boundary points given by Eqs. (128) and



(129)). Therefore, the expressions after the term f_j in Eq. (131) are zero and do not affect the value of the local truncation error e_j . Similar to the Poisson equation in the previous Sect. 4.1.1, we expand the exact solution for the displacements and their spatial derivatives at the grid and boundary points into a Taylor series at small $h \ll 1$ in the vicinity of the central grid point with the coordinates x_c , y_c using Eqs. (64)-(66). The exact solution for the displacements u_c and v_c of the elasticity equations, Eq. (127), at the stencil central grid point with the coordinates $x = x_c$ and $y = y_c$ satisfies the following equations:

$$\frac{\partial^{2} u_{c}}{\partial x^{2}} = -\left[\frac{\mu}{(2\mu + \lambda)} \frac{\partial^{2} u_{c}}{\partial y^{2}} + \frac{(\mu + \lambda)}{(2\mu + \lambda)} \frac{\partial^{2} v_{c}}{\partial x \partial y} + \frac{1}{(2\mu + \lambda)} f_{c,x}\right],$$
(132)
$$\frac{\partial^{2} v_{c}}{\partial x^{2}} = -\left[\frac{(2\mu + \lambda)}{\mu} \frac{\partial^{2} v_{c}}{\partial y^{2}} + \frac{(\mu + \lambda)}{\mu} \frac{\partial^{2} u_{c}}{\partial x \partial y} + \frac{1}{\mu} f_{c,y}\right],$$
(133)
$$\frac{\partial^{(2+i+j)} u_{c}}{\partial x^{(2+i)} \partial y^{j}} = -\left[\frac{\mu}{(2\mu + \lambda)} \frac{\partial^{(2+i+j)} u_{c}}{\partial x^{i} \partial y^{(2+j)}} + \frac{(\mu + \lambda)}{(2\mu + \lambda)} \frac{\partial^{(2+i+j)} v_{c}}{\partial x^{(i+1)} \partial y^{(j+1)}} + \frac{1}{(2\mu + \lambda)} \frac{\partial^{(i+j)} f_{c,x}}{\partial x^{i} \partial y^{j}}\right],$$
(134)
$$\frac{\partial^{(2+i+j)} v_{c}}{\partial x^{(2+i)} \partial y^{j}} = -\left[\frac{(2\mu + \lambda)}{\mu} \frac{\partial^{(2+i+j)} v_{c}}{\partial x^{i} \partial y^{(2+j)}} + \frac{(\mu + \lambda)}{\mu} \frac{\partial^{(2+i+j)} u_{c}}{\partial x^{(i+1)} \partial y^{(j+1)}} + \frac{1}{\mu} \frac{\partial^{(i+j)} f_{c,y}}{\partial x^{i} \partial y^{j}}\right],$$

with i,j=0,1,2,3,4,... as well as $f_{c,x}=f_x(x_c,y_c)$ and $f_{c,y}=f_y(x_c,y_c)$. We should mention that Eqs. (132) and (133) directly follow from the elasticity equations, Eq. (127), while Eqs. (134) and (135) are obtained by the differentiation of Eqs. (132) and (133) with respect to $\frac{\partial^i}{\partial x^i}$ and $\frac{\partial^j}{\partial y^i}$.

Remark 4 In Eqs. (132) and (133), we have expressed the second x derivatives in terms of the second y derivatives and the second mixed derivatives. However, we can similarly express the second y derivatives in terms of the second x derivatives and the second mixed derivatives. This latter case (with the corresponding modifications of Eqs. (134) and (135)) will be used for the calculation of the local truncation error and the stencil coefficients for the second stencil equation; see below.

Similar to the derivation of a Taylor series of the local truncation error e for the Poisson equation in the previous Sect. 4.1.1, a Taylor series of the local truncation error e_1 for the first stencil (j = 1) for the elasticity equations can be obtained in the following form:

$$e_{1} = \left(b_{1,1}u_{c} + b_{1,2}v_{c}\right) + h\left(b_{1,3}\frac{\partial u_{c}}{\partial x}\right) + b_{1,4}\frac{\partial v_{c}}{\partial x} + b_{1,5}\frac{\partial u_{c}}{\partial y} + b_{1,6}\frac{\partial v_{c}}{\partial y}\right) + h^{2}\left(b_{1,7}\frac{\partial^{2}u_{c}}{\partial x\partial y} + b_{1,8}\right) + h^{2}\left(b_{1,7}\frac{\partial^{2}u_{c}}{\partial x\partial y} + b_{1,8}\right) + h^{2}\left(b_{1,1}\frac{\partial^{2}u_{c}}{\partial y^{2}}\right) + h^{3}\left(b_{1,11}\frac{\partial^{3}u_{c}}{\partial x\partial y^{2}}\right) + h^{3}\left(b_{1,11}\frac{\partial^{3}u_{c}}{\partial x\partial y^{2}}\right) + h^{3}\left(b_{1,11}\frac{\partial^{3}u_{c}}{\partial y^{3}}\right) + h^{4}\left(b_{1,15}\frac{\partial^{4}u_{c}}{\partial x\partial y^{3}}\right) + h^{4}\left(b_{1,15}\frac{\partial^{4}u_{c}}{\partial x\partial y^{3}}\right) + h^{4}\left(b_{1,15}\frac{\partial^{4}u_{c}}{\partial x\partial y^{3}}\right) + h^{5}\left(b_{1,19}\frac{\partial^{5}u_{c}}{\partial x\partial y^{4}}\right) + h^{5}\left(b_{1,19}\frac{\partial^{5}u_{c}}{\partial x\partial y^{4}}\right) + h^{5}\left(b_{1,19}\frac{\partial^{5}u_{c}}{\partial x\partial y^{4}}\right) + h^{5}\left(b_{1,23}\frac{\partial^{5}u_{c}}{\partial x\partial y^{5}}\right) + h^{6}\left(b_{1,23}\frac{\partial^{6}u_{c}}{\partial x\partial y^{5}}\right) + h^{6}\left(b_{1,23}\frac{\partial^{6}u_{c}}{\partial x\partial y^{5}}\right) + h^{6}\left(b_{1,23}\frac{\partial^{6}u_{c}}{\partial x\partial y^{5}}\right) + h^{1,24}\left(\frac{\partial^{6}v_{c}}{\partial x\partial y^{5}}\right) + h^{1,25}\left(\frac{\partial^{6}u_{c}}{\partial x\partial y^{5}}\right) + h^{1,26}\left(\frac{\partial^{6}v_{c}}{\partial x\partial y^{5}}\right) + h^{1,25}\left(\frac{\partial^{6}u_{c}}{\partial x\partial y^{5}}\right) + h^{1,26}\left(\frac{\partial^{6}v_{c}}{\partial x\partial y^{5}}\right) + h^{1,26}\left(\frac{$$

where the coefficients $b_{1,p}$ $(p=1,2,\ldots)$ are expressed as a linear combination of the coefficients $k_{1,i}$, $\bar{k}_{1,i}$, $q_{1,i}$, $\bar{q}_{1,i}$, $q_{2,i}$ and $\bar{q}_{2,i}$ used in Eqs. (130) and (131); see our paper [31]. Here we should mention that the expression for the local truncation error, Eq. (136), includes only the first-order derivatives with respect to x (the higher order derivatives with respect to x are excluded with the help of the elasticity equations, Eqs. (132)-(135)). A similar expression can be derived for the local truncation error e_2 for the second stencil; see also Remark 4.

By zeroing the coefficients $b_{j,i}$ for the smallest orders of h and using the least square method for the coefficients $b_{j,i}$ for higher orders of h (similar to the procedure in Sect. 3.1.1), we can form a local system of algebraic equations for the calculation of the unknown coefficients



 $k_{i,i}$, $\bar{k}_{i,i}$ and $q_{1,i}$, $\bar{q}_{1,i}$, $q_{2,i}$, $\bar{q}_{2,i}$. As shown in our paper [31], OLTEM with the 9-point stencils and irregular boundaries provides the second order of accuracy for global solutions (similar to linear finite elements with the 9-point stencils). However, due to the minimization of the leading terms of the local truncation error, at the same numbers of degrees of freedom OLTEM on irregular domains yields more accurate results than those obtained by linear and highorder finite elements (up to the third order) with much wider stencils; see the numerical examples in our paper [31]. We should also mention that as shown in our paper [2], OLTEM with wider $5 \times 5 = 25$ -point stencils in the 2-D case provides the 10-th order of accuracy on regular domains with conforming Cartesian meshes, i.e for elastostatics the optimal accuracy for the $5 \times 5 = 25$ -point stencils is 7 orders higher than that for quadratic finite elements with similar stencils.

4.3.2 Heterogeneous Materials

The 2-D elastostatics equations in a composite domain $\Omega = \bigcup \Omega_l$ $(l = 1, 2, ..., \overline{N}$ where \overline{N} is the total number of subdomains) can be written down in each subdomain Ω_l as follows:

$$\mu_{l}\nabla^{2}u_{l} + (\mu_{l} + \lambda_{l})\left(\frac{\partial^{2}u_{l}}{\partial x^{2}} + \frac{\partial^{2}v_{l}}{\partial x\partial y}\right) + f_{x}^{l} = 0,$$

$$\mu_{l}\nabla^{2}v_{l} + (\mu_{l} + \lambda_{l})\left(\frac{\partial^{2}v_{l}}{\partial y^{2}} + \frac{\partial^{2}u_{l}}{\partial x\partial y}\right) + f_{y}^{l} = 0,$$
(137)

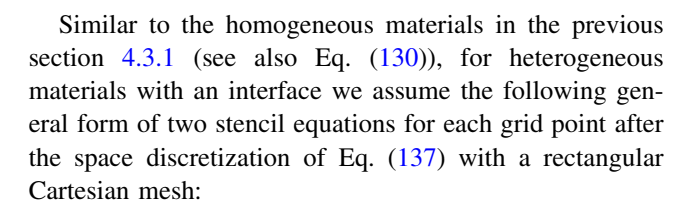
where $u_l = u_l(x, y)$ and $v_l = v_l(x, y)$ are the x- and y-components of the displacement vector, $f_x^l = f_x^l(x, y)$ and $f_y^l = f_y^l(x, y)$ are the x- and y-components of the body forces that can be discontinuous across interfaces. We also assume that the functions u_l and f_l are sufficiently smooth in each subdomain Ω_l . At the interface G between any two subdomains, the following interface conditions are applied:

$$u_G^* - u_G^{**} = \delta_1, \qquad v_G^* - v_G^{**} = \bar{\delta}_1,$$
 (138)

$$t_{x,G}^* - t_{x,G}^{**} = \delta_2, \qquad t_{y,G}^* - t_{y,G}^{**} = \bar{\delta}_2,$$
 (139)

where $\delta_1(x,y)\mid_{(x,y)\in G}$, $\bar{\delta}_1(x,y)\mid_{(x,y)\in G}$ and $\delta_2(x,y)\mid_{(x,y)\in G}$, $\bar{\delta}_2(x,y)\mid_{(x,y)\in G}$ are the given jumps in the displacements and in the tractive forces across the interface, the symbols * and ** correspond to the quantities on the opposite sides from the interface for the corresponding subdomains Ω_l . The x- and y-components of the tractive forces $t_{x,G}$ and $t_{y,G}$ can be expressed in terms of the displacements by Eq. (90).

The detailed derivation of OLTEM for heterogeneous materials with irregular interfaces in the 2-D case is presented in our papers [3, 37]. Below we present the summary of the results.



$$\sum_{p=1}^{L} k_{j,p} \left[a_{p} u_{p}^{*,num} + (1 - a_{p}) u_{p}^{**,num} \right]$$

$$+ \sum_{p=1}^{L} \bar{k_{j,p}} \left[a_{p} v_{p}^{*,num} + (1 - a_{p}) v_{p}^{**,num} \right] = \bar{f_{j}}, \qquad j = 1, 2,$$

$$(140)$$

where the coefficients $a_p = 1$ if the grid point p belongs to material * and $a_p = 0$ if the grid point p belongs to another material ** (i.e., only two variables $u_p^{*,num}$, $v_p^{*,num}$ or $u_p^{**,num}$, $v_p^{**,num}$ are included into Eq. (140) for each grid point, e.g., see Fig. 5a with $a_1 = a_2 = a_3 = a_5 = a_6 = 1$ and $a_4 = a_7 = a_8 = a_9 = 0$). As can be seen, the stencil equations, Eq. (140), for heterogeneous materials include the same number of the stencil coefficients $k_{j,p}$ and $\bar{k}_{j,p}$ (p = 1, 2, ..., L) as that for the homogeneous materials, Eq. (130).

The local truncation error e_j for the stencil equations, Eq. (140), can be obtained by the replacement of the numerical solution for $u^{*,num}$, $v^{*,num}$, $u^{**,num}$, $v^{**,num}$ in Eq. (140) by the exact solution u^* , v^* , u^{**} , v^{**} and by the addition of the interface conditions, Eqs. (138)-(139), at a small number N_G of the selected interface point to the obtained expression as the constraints (see the previous Sect. 4.1.2 for the Poisson equation):

$$\begin{split} e_{j} &= \sum_{p=1}^{L} k_{j,p} \left[a_{p} u_{p}^{*} + (1-a_{p}) u_{p}^{**} \right] + \sum_{p=1}^{L} \bar{k}_{j,p} \left[a_{p} v_{p}^{*} + (1-a_{p}) v_{p}^{**} \right] - \bar{f_{j}} \\ &+ \left[\sum_{m=1}^{N_{G}} q_{1,m} (u_{G,m}^{*} - u_{G,m}^{**} - \delta_{1}) + \sum_{m=1}^{N_{G}} \bar{q}_{1,m} (v_{G,m}^{*} - v_{G,m}^{**} - \bar{\delta}_{1}) \right. \\ &+ \sum_{m=1}^{N_{G}} h q_{2,m} \left(t_{x(G,m)}^{*} - t_{x(G,m)}^{**} - \delta_{2} \right) + \sum_{m=1}^{N_{G}} h \bar{q}_{2,m} \left(t_{y(G,m)}^{*} - t_{y(G,m)}^{**} - \bar{\delta}_{2} \right) \right], \qquad j = 1, 2, \end{split}$$

where the additional unknown coefficients $q_{1,m}$, $\bar{q}_{1,m}$, $q_{2,m}$, $\bar{q}_{2,m}$ ($m=1,2,\ldots,N_G$) are related to the interface conditions (see Eqs. (138)-(139)) and should be determined from the minimization of the local truncation error. As shown in our paper [38], $N_G=5$ uniformly spaced interface points can be used with the 9-point stencils.

Similar to the derivation of a Taylor series of the local truncation error e for the Poisson equation in the previous Sect. 4.1.2, a Taylor series of the local truncation error e_1 for the first stencil (j=1) for the elasticity equations can be obtained in the following form:



$$\begin{split} e_1 &= b_{1,1} u_c^* + b_{1,2} v_c^* + b_{1,3} u_c^{**} + b_{1,4} v_c^{**} \\ &+ h \left(b_{1,5} \frac{\partial u_c^*}{\partial x} + b_{1,6} \frac{\partial v_c^*}{\partial x} + b_{1,7} \frac{\partial u_c^{**}}{\partial x} + b_{1,8} \frac{\partial v_c^{**}}{\partial x} \right. \\ &+ b_{1,9} \frac{\partial u_c^*}{\partial y} + b_{1,10} \frac{\partial v_c^*}{\partial y} + b_{1,11} \frac{\partial u_c^{**}}{\partial y} + b_{1,12} \frac{\partial v_c^{**}}{\partial y} \right) \\ &+ h^2 \left(b_{1,13} \frac{\partial^2 u_c^*}{\partial x \partial y} + b_{1,14} \frac{\partial^2 v_c^*}{\partial x \partial y} + b_{1,15} \frac{\partial^2 u_c^{**}}{\partial x \partial y} \right. \\ &+ b_{1,16} \frac{\partial^2 v_c^{**}}{\partial x \partial y} + b_{1,17} \frac{\partial^2 u_c^*}{\partial y^2} + b_{1,18} \frac{\partial^2 v_c^*}{\partial y^2} + b_{1,19} \frac{\partial^2 u_c^{**}}{\partial y^2} + b_{1,20} \frac{\partial^2 v_c^{**}}{\partial y^2} \right) \\ &+ h^3 \left(b_{1,21} \frac{\partial^3 u_c^*}{\partial x \partial y^2} + \dots + b_{1,28} \frac{\partial^3 v_c^{**}}{\partial y^3} \right) \\ &+ h^4 \left(b_{1,29} \frac{\partial^4 u_c^*}{\partial x \partial y^3} + \dots + b_{1,36} \frac{\partial^4 v_c^{**}}{\partial y^4} \right) \\ &+ h^5 \left(b_{1,37} \frac{\partial^5 u_c^*}{\partial x \partial y^3} + \dots + b_{1,44} \frac{\partial^5 v_c^{**}}{\partial y^5} \right) \\ &+ h^6 \left(b_{1,45} \frac{\partial^6 u_c^*}{\partial x \partial y^5} + \dots + b_{1,52} \frac{\partial^6 v_c^{***}}{\partial y^6} \right) \\ &+ h^7 \left(b_{1,53} \frac{\partial^7 u_c^*}{\partial x \partial y^5} + \dots + b_{1,60} \frac{\partial^7 v_c^{**}}{\partial y^7} \right) \\ &+ h^8 \left(b_{1,61} \frac{\partial^8 u_c^*}{\partial x \partial y^7} + \dots + b_{1,68} \frac{\partial^8 v_c^{**}}{\partial y^8} \right) \\ &+ h^9 \left(b_{1,69} \frac{\partial^9 u_c^*}{\partial x \partial y^8} + \dots + b_{1,76} \frac{\partial^9 v_c^{**}}{\partial y^9} \right) \\ &+ h^{10} \left(b_{1,77} \frac{\partial^{10} u_c^*}{\partial x \partial y^9} + \dots + b_{1,84} \frac{\partial^{10} v_c^{**}}{\partial y^{10}} \right) \\ &+ h^{11} \left(b_{1,85} \frac{\partial^{11} u_c^*}{\partial x \partial y^{10}} + \dots + b_{1,92} \frac{\partial^{11} v_c^{**}}{\partial y^{11}} \right) \\ &+ h^{12} \left(b_{1,93} \frac{\partial^{12} u_c^*}{\partial x \partial y^{11}} + \dots + b_{1,100} \frac{\partial^{12} v_c^{**}}{\partial y^{12}} \right) + O(h^{13}) \end{split}$$

where the coefficients b_p (p=1,2,...) are expressed as a linear combination of the coefficients k_i , $\bar{k}_{1,i}$, $q_{1,i}$, $\bar{q}_{1,i}$, $q_{2,i}$ and $\bar{q}_{2,i}$ used in Eqs. (140) and (141); see our papers [3, 37] for the 2-D case with irregular interfaces. Here we should mention that the expression for the local truncation error, Eq. (142), includes only the first-order derivatives with respect to x (the higher order derivatives with respect to x are excluded with the help of the elasticity equations, Eq. (137).

By zeroing the coefficients $b_{j,i}$ for the smallest orders of h and using the least square method for the coefficients $b_{j,i}$ for higher orders of h (similar to the procedure in Sect. 3.1.1), we can form a local system of algebraic equations for the calculation of the unknown coefficients $k_{j,i}$, $\bar{k}_{j,i}$ and $q_{1,i}$, $\bar{q}_{1,i}$, $q_{2,i}$, $\bar{q}_{2,i}$. As shown in our paper [37], OLTEM with the 9-point stencils and irregular interfaces provides the second order of accuracy of global solutions (similar to linear finite elements with the 9-point stencils). However, due to the minimization of the leading terms of the local truncation error, at the same numbers of degrees of freedom OLTEM on irregular domains yields more accurate results than those obtained by linear and high-

order finite elements (up to the third order) with much wider stencils; see the numerical examples in our paper [37]. We should also mention that as shown in our paper [3], OLTEM in the 2-D case with wider $5 \times 5 = 25$ -point stencils provides the 10-th order of accuracy for heterogeneous materials with irregular interfaces and unfitted Cartesian meshes, i.e for the elastostatics the optimal accuracy OLTEM with the $5 \times 5 = 25$ -point stencils is 7 orders higher than that for quadratic finite elements with similar stencils.

5 OLTEM for Post-processing

For the analysis of engineering problems the calculation of the spatial derivatives of primary functions are necessary in many applications, e.g., fluxes for heat transfer problems or stresses for solid mechanics. Therefore, after the calculation of the numerical solution for the primary functions, many computer codes include special post-processing procedures for the calculation of the spatial derivatives of the numerical solution for the primary functions. Here we show in detail the application of OLTEM and PDEs to the calculation of the spatial derivatives at the grid points for the 3-D Poisson equation as well as to briefly introduce the calculation of stresses for the time-independent and timedependent elasticity equations. The cases of heterogeneous materials with irregular interfaces will be considered. The application of PDEs for post-processing significantly increases the accuracy of the numerical results for the spatial derivatives.

5.1 3-D Poisson Equation for Heterogeneous Materials with Irregular Interfaces

Here we consider the calculation of the spatial derivatives $\frac{\partial u^{num}}{\partial x}$, $\frac{\partial u^{num}}{\partial y}$ and $\frac{\partial u^{num}}{\partial z}$ at the grid points for the 3-D Poisson equation with interfaces; see the previous Sect. 4.1.2 as well as our paper [36]. Because the calculations of these three derivatives are similar then we show the procedure for the calculation of $\frac{\partial u^{num}}{\partial x}$.

The compact stencil for the calculation of $\frac{\partial u^{num}}{\partial x}$ at the stencil central point with the coordinates x_c , y_c and z_c (see Fig. 6 with the central point c = 14) can be selected similar to Eq. (112) as follows:

$$-\left[a_{c}\frac{\partial u_{c}^{*,num}}{\partial x} + (1 - a_{c})\frac{\partial u_{c}^{**,num}}{\partial x}\right]h$$

$$+\sum_{p=1}^{L}k_{p}\left[a_{p}u_{p}^{*,num} + (1 - a_{p})u_{p}^{**,num}\right] = \bar{f},$$
(143)

where L = 27 for the 27-point stencils (see Fig. 6), the



explanation of the coefficients a_i (i = 1, 2, ..., L) is given in Sect. 4.1.2. The local truncation error e for Eq. (143) can be obtained by the replacement of the numerical solution $u_p^{*,num}$ and $u_p^{**,num}$ in Eq. (143) by the exact solution u_p^* and u_p^{**} :

$$e = -\left[a_{c}\frac{\partial u_{c}^{*}}{\partial x} + (1 - a_{c})\frac{\partial u_{c}^{**}}{\partial x}\right]h$$

$$+ \sum_{p=1}^{L} k_{p}\left[a_{p}u_{p}^{*} + (1 - a_{p})u_{p}^{**}\right] - \bar{f}.$$
(144)

Similar to Eq. (113) in Sect. 4.1.2, we include the interface conditions for the exact solution at the same small number N_G of the interface points in the expression for the local truncation error in Eq. (144) as the constraints:

$$e = -\left[a_{c} \frac{\partial u_{c}^{*}}{\partial x} + (1 - a_{c}) \frac{\partial u_{c}^{**}}{\partial x}\right] h$$

$$+ \sum_{p=1}^{L} k_{p} \left[a_{p} u_{p}^{*} + (1 - a_{p}) u_{p}^{**}\right]$$

$$- \bar{f} + \left\{\sum_{j=1}^{N_{G}} q_{1,j} (u_{G,j}^{*} - u_{G,j}^{**} - \delta_{1})\right\}$$

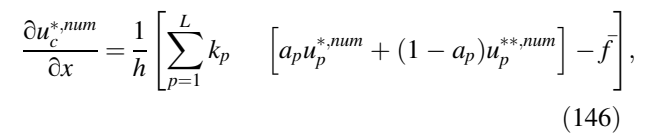
$$+ \sum_{j=1}^{N_{G}} h q_{2,j} \left[e_{*} (n_{x,j} \frac{\partial u_{G,j}^{*}}{\partial x} + n_{y,j} \frac{\partial u_{G,j}^{*}}{\partial y} + n_{z,j} \frac{\partial u_{G,j}^{*}}{\partial z} + n_{y,j} \frac{\partial u_{G,j}^{**}}{\partial x} + n_{y,j} \frac{\partial u_{G,j}^{**}}{\partial y} + n_{z,j} \frac{\partial u_{G,j}^{**}}{\partial z} - \delta_{2}\right],$$

$$(145)$$

see the corresponding explanations in Sect. 4.1.2. Similar to Sect. 4.1.2, the coefficients k_i and $q_{1,j}$, $q_{2,j}$ ($i=1,2,\ldots,L$, $j=1,2,\ldots,N_G$) are calculated by the minimization of the local truncation error e given by Eq. (145); see our paper [36] for the 27-point stencils for the details.

To summarize, for the calculation of the derivative $\frac{\partial u^{num}}{\partial x}$ using OLTEM with the compact stencils, we should follow the following procedure:

- Calculate the stencil coefficients k_i and $q_{1,j}$, $q_{2,j}$ $(i = 1, 2, ..., L, j = 1, 2, ..., N_G)$ for each internal grid point (similar to those in Sect. 4.1.2) for homogeneous (without interfaces) and heterogeneous (with interfaces) materials by the minimization of the local truncation error, Eq. (145).
- Using these stencil coefficients, calculate the right-hand side \bar{f} in Eq. (143) for each internal grid point (similar to \bar{f} in Sect. 4.1.2); see our paper [36] for the 27-point stencils for the details.
- Calculate the derivative $\frac{\partial u^{num}}{\partial x}$ from Eq. (143) for each internal grid point as follow:



if the stencil central grid point belongs to material $*(a_c = 1)$ and

$$\frac{\partial u_c^{**,num}}{\partial x} = \frac{1}{h} \left[\sum_{p=1}^{L} k_p \left[a_p u_p^{*,num} + (1 - a_p) u_p^{**,num} \right] - \bar{f} \right], \tag{147}$$

if the stencil central grid point belongs to material ** $(a_c = 0)$.

The calculation of the derivatives $\frac{\partial u^{num}}{\partial y}$ and $\frac{\partial u^{num}}{\partial z}$ can be done similar to the calculation of the derivative $\frac{\partial u^{num}}{\partial x}$ as described above.

Remark 5. If any regular stencil is cut by the boundary then for post-processing the local truncation error of the cut stencil should also include the corresponding boundary conditions, e.g., see Eq. (106).

It is interesting to note that for homogeneous materials the post-processing procedure described above can be also used for the calculation of the spatial derivatives without the application of the partial differential equation as in other post-processing techniques (e.g., see [40–42] for finite and isogeometric elements). Let us assume that we can calculate the derivative $\frac{\partial u^{num}}{\partial x}$ at the internal grid point in terms of the values of the function u^{num} at the neighboring grid points using the following compact stencil:

$$-h\frac{\partial u_c^{num}}{\partial x} + \sum_{p=1}^L k_p u_p^{num} = 0$$
 (148)

with the following local truncation error e:

$$e = -h\frac{\partial u_c}{\partial x} - \sum_{p=1}^{L} k_p u_p. \tag{149}$$

Repeating the procedure described in Sect. 4.1.1 without the use of Eqs. (124) and (125) and zeroing the corresponding coefficients b_p in the Taylor series of the local truncation error e for Eq. (149), we can calculate the maximum possible order of the local truncation error, Eq. (149), without the application of the Poisson equation. In our paper [36] we showed that the use of the Poisson equation for the calculation of the coefficients k_p in Eq. (148) for the 3-D 27-point stencils with L=27 increases the accuracy in the calculation of $\frac{\partial u^{mum}}{\partial x}$ by two orders compared to the calculations without the use of the Poisson equations. It can be also shown that the use of the Poisson equation for the calculation of the coefficients k_p in Eq. (148) for the 3-D 125-point stencils with L=125



increases the accuracy in the calculation of $\frac{\partial u^{num}}{\partial x}$ by 6 orders compared to the calculations without the use of the Poisson equation.

To summarize, the proposed post-processing procedure provides the optimal accuracy of the spatial derivatives of primary functions calculated at the grid points with the help of compact stencils. It can be developed with or without the use of PDEs. However, the use of PDEs significantly improves the accuracy of the spatial derivatives for the given stencils. Despite the fact that we have applied the proposed post-processing technique to the stencils defined on Cartesian meshes, it can be also used for non-uniform meshes with the corresponding coefficients $r_{x,p}$, $r_{y,p}$, $r_{z,p}$ used in Eq. (64) (similar to OLTEM developed in our papers [25, 27, 28] for irregular boundaries). Finally, the post-processing procedure developed can be independently used with any known numerical technique (e.g., with finite elements).

5.2 The Stencils and the Local Truncation Errors Used for the Calculation of $\frac{\partial u}{\partial x}$ for the Time-Independent Elasticity Equations for Heterogeneous Materials with Irregular Interfaces

Similar to the previous Sect. 5.1, here we will discuss the calculation of the spatial derivative $\frac{\partial u^{num}}{\partial x}$ of the u displacement for the elastostatics equations. The calculation of the other spatial derivatives for other displacement components can be similarly done. Then, the stresses can be calculated using Hooke's law.

For simplicity, below we consider the compact stencil for heterogeneous materials with interfaces in the 2-D case that can be written similar to that in basic computations (see Eq. (140) in the previous Sect. 4.3.2) as follows:

$$-\left[a_{c}\frac{\partial u_{c}^{*,num}}{\partial x} + (1 - a_{c})\frac{\partial u_{c}^{**,num}}{\partial x}\right]h$$

$$+\sum_{p=1}^{L}k_{p}\left[a_{p}u_{p}^{*,num} + (1 - a_{p})u_{p}^{**,num}\right]$$

$$+\sum_{p=1}^{L}\bar{k_{p}}\left[a_{p}v_{p}^{*,num} + (1 - a_{p})v_{p}^{**,num}\right] = \bar{f},$$
(150)

with the following local truncation error e:

$$e = -\left[a_{c}\frac{\partial u_{c}^{*}}{\partial x} + (1 - a_{c})\frac{\partial u_{c}^{**}}{\partial x}\right]h$$

$$+ \sum_{p=1}^{L} k_{p}\left[a_{p}u_{p}^{*} + (1 - a_{p})u_{p}^{**}\right]$$

$$+ \sum_{p=1}^{L} \bar{k_{p}}\left[a_{p}v_{p}^{*} + (1 - a_{p})v_{p}^{**}\right] - \bar{f}$$

$$+ \sum_{m=1}^{N_{G}} q_{1,m}(u_{G,m}^{*} - u_{G,m}^{**} - \delta_{1})$$

$$+ \sum_{m=1}^{N_{G}} \bar{q}_{1,m}(v_{G,m}^{*} - v_{G,m}^{**} - \bar{\delta}_{1})$$

$$+ \sum_{m=1}^{N_{G}} hq_{2,m}\left(t_{x,(G,m)}^{*} - t_{x,(G,m)}^{**} - \delta_{2}\right)$$

$$+ \sum_{m=1}^{N_{G}} h\bar{q}_{2,m}\left(t_{y,(G,m)}^{*} - t_{y,(G,m)}^{**} - \bar{\delta}_{2}\right),$$
(151)

see also Eq. (141) and the corresponding explanations in Sect. 4.3.2. Similar to Sect. 4.3.2, the coefficients k_p , $\bar{k_p}$ and $q_{1,j}$, $\bar{q}_{1,j}$, $q_{2,j}$, $\bar{q}_{2,j}$ $(p=1,2,\ldots,L,j=1,2,\ldots,N_G)$ are calculated by the minimization of the local truncation error e given by Eq. (151); see our paper [3] for the 25-point stencils for the details. It is interesting to note that in contrast to the known post-processing procedures for the elasticity equations (e.g., used with finite elements), the calculation of $\frac{\partial u^{mum}}{\partial x}$ includes not only the numerical solution for the displacement u but also for the displacement v; see Eq. (150).

The proposed post-processing procedure provides a very high order of accuracy for the stresses. For example, the numerical results in our paper [3] show the 10-th order of accuracy of stresses for OLTEM with the 25-point stencils used in basic computations and for post-processing.

5.3 The Stencils and the Local Truncation Errors Used for the Calculation of $\frac{\partial u}{\partial x}$ for the Time-Dependent Elasticity Equations for Heterogeneous Materials with Irregular Interfaces

The 2-D compact stencil for the calculation of $\frac{\partial u^{num}}{\partial x}$ at the stencil central grid point with the coordinates x_c and y_c (see Fig. 5) can be selected similar to Eq. (97) as follows:



$$-\left[a_{c}\frac{\partial u_{c}^{*,num}}{\partial x}+(1-a_{c})\frac{\partial u_{c}^{**,num}}{\partial x}\right]h$$

$$+h^{2}\left\{\sum_{p=1}^{L}m_{p}\left[a_{p}\frac{d^{2}u_{p}^{*,num}}{dt^{2}}+(1-a_{p})\frac{d^{2}u_{p}^{**,num}}{dt^{2}}\right]\right\}$$

$$+\sum_{p=1}^{L}\bar{m}_{p}\left[a_{p}\frac{d^{2}v_{p}^{*,num}}{dt^{2}}+(1-a_{p})\frac{d^{2}v_{p}^{**,num}}{dt^{2}}\right]$$

$$+\sum_{p=1}^{L}k_{p}\left[a_{p}u_{p}^{*,num}+(1-a_{p})u_{p}^{**,num}\right]$$

$$+\sum_{p=1}^{L}\bar{k}_{p}\left[a_{p}v_{p}^{*,num}+(1-a_{p})v_{p}^{**,num}\right]=\bar{f},$$
(152)

where $a_c=1$ if the stencil central grid point belongs to material * and $a_c=0$ if the stencil central grid point belongs to material **. We should mention that in contrast to the known post-processing procedures (e.g., used with finite elements), in the proposed approach the calculation of the spatial derivative $\frac{\partial u}{\partial x}$ depends not only on the displacement u but also on the displacement v as well as their second order time derivatives $\frac{\partial^2 u}{\partial t^2}$ and $\frac{\partial^2 v}{\partial t^2}$. The local truncation error e for Eq. (152) can be obtained by the replacement of the numerical solution $u_p^{*,num}$, $u_p^{**,num}$, $v_p^{*,num}$ and $v_p^{**,num}$ in Eq. (152) by the exact solutions u_p^{*} , u_p^{**} , v_p^{*} and v_p^{**} :

$$e = -\left[a_{c}\frac{\partial u_{c}^{*}}{\partial x} + (1 - a_{c})\frac{\partial u_{c}^{**}}{\partial x}\right]h$$

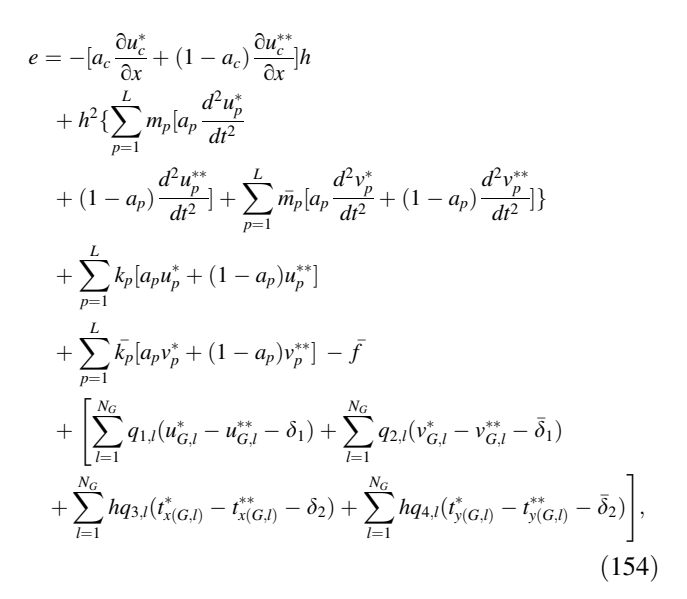
$$+ h^{2}\left\{\sum_{p=1}^{L} m_{p}\left[a_{p}\frac{d^{2}u_{p}^{*}}{dt^{2}} + (1 - a_{p})\frac{d^{2}u_{p}^{**}}{dt^{2}}\right]\right\}$$

$$+ \sum_{p=1}^{L} \bar{m}_{p}\left[a_{p}\frac{d^{2}v_{p}^{*}}{dt^{2}} + (1 - a_{p})\frac{d^{2}v_{p}^{**}}{dt^{2}}\right]$$

$$+ \sum_{p=1}^{L} k_{p}\left[a_{p}u_{p}^{*} + (1 - a_{p})u_{p}^{**}\right]$$

$$+ \sum_{p=1}^{L} \bar{k}_{p}\left[a_{p}v_{p}^{*} + (1 - a_{p})v_{p}^{**}\right] - \bar{f}.$$
(153)

We should note that in Eq. (153) we do not use index 'j' for the local truncation error e and for the stencil coefficients m_i , \bar{m}_i , k_i , $\bar{k_i}$ ($i=1,2,\ldots,9$) because for the calculation of $\frac{\partial u^{mum}}{\partial x}$ we consider just one stencil equation for the grid point. Similar to Eq. (98) in Sect. 3.2.2, we will include the interface conditions for the exact solution at the same small number N_G of the interface points into the expression for the local truncation error in Eq. (153) as follows:



see the corresponding explanations in Sect. 3.2.2.

Remark 6. If any regular stencil is cut by the boundary then for post-processing the local truncation error of the cut stencil should also include the corresponding boundary conditions, e.g., see Eq. (92).

Remark 7. The described post-processing procedure can be equally applied to OLTEM with the diagonal mass matrix. Because post-processing does not include the solution of the global system of algebraic equations, the stencil with all non-zero m_p coefficients in Eq. (152) can be used for post-processing the results obtained in basic computations with the diagonal mass matrix; see our paper [38] for the details.

It is interesting to note that for homogeneous materials the post-processing procedure described above can be also used for the calculation of the spatial derivatives without the application of the partial differential equation as in other post-processing techniques (e.g., see [40–42] for finite and isogeometric elements). Let us assume that we can calculate the derivative $\frac{\partial u^{num}}{\partial x}$ at the internal grid point in terms of the values of the displacement u^{num} at the neighboring grid points with the following stencil:

$$-h\frac{\partial u_c^{num}}{\partial x} + \sum_{p=1}^L k_p u_p^{num} = 0$$
 (155)

and the following local truncation error:

$$e = -h\frac{\partial u_c}{\partial x} + \sum_{p=1}^{L} k_p u_p. \tag{156}$$

For simplicity, below we will use a uniform Cartesian mesh and L=9 grid points for the calculation of the derivative $\frac{\partial u_r^{num}}{\partial x}$ at the central c=5 grid point in the 2-D case (see Fig. 3a and our paper [38]). Using the procedure described in Sect. 3.2.1 (but without the use of PDEs for the



calculation of the coefficients b_p) and zeroing the corresponding coefficients b_p in the Taylor series of the local truncation error e, we can show that $k_6 = 1/2$ and $k_4 = -1/2$ (all other $k_i = 0$, i = 1, 2, 3, 5, 7, 8, 9) yield the following optimal order of e in Eq. (156) with L = 9:

$$e = -\frac{h^3}{6} \frac{\partial^3 u_5}{\partial x^3} + O(h^4). \tag{157}$$

In this case we have the well-known finite-difference approximation of the derivative. In contrast to the third order of the local truncation error in Eq. (157), the new post-processing procedure with the use of PDES provides the the fourth order of the local truncation error for homogeneous materials and improves the accuracy of the spatial derivative of by one order for the same 9-point compact stencils. We should also mention that the approximation given by Eq. (155) cannot be used for the stencils with interfaces (as those in Fig. 5a).

To summarize, the proposed post-processing procedure provides the optimal accuracy of the spatial derivatives of the displacements calculated at the grid points with the help of compact stencils. It can be developed with or without the use of PDEs. However, the use of PDEs improves the accuracy of the spatial derivatives for the given stencils. Despite the fact that we have applied the proposed post-processing technique to the stencils defined on Cartesian meshes, it can be also used for non-uniform meshes with the corresponding coefficients $r_{x,p}$, $r_{y,p}$ used in Eq. (64) (similar to OLTEM developed in our papers [25, 27, 28] for irregular boundaries). Finally, the post-processing procedure developed can be independently used with any known numerical technique (e.g., with finite elements).

6 OLTEM for the Calculation of the Primary Function and Its Derivatives at Any Point of the Domain

Here we will show that OLTEM can be used not only to the calculation of the spatial derivatives of the primary function at the grid points at post-processing as shown in Sect. 5 but also can be generalized for the calculation of the primary function and their derivatives at any point of the domain. We will explain the main idea of the new approach for the 3-D Poisson equation in the homogeneous media. Assume that the primary function is known at the grid points of a Cartesian mesh. Then, we will calculate the primary function and their derivatives at any point *P* of the domain using compact 27-point stencils shown in Fig. 4a. Without the loss of generality, let us consider any point *P*

of the 3-D 27-point cell of the dimensions 2hx2hx2h with the following coordinates:

$$x_P = x_{14} + r_{xP}h, y_P = y_{14} + r_{yP}b_yh,$$

 $z_P = z_{14} + r_{zP}b_zh,$ (158)

where the coefficients r_{xP} , r_{yP} and r_{zP} define the location of point P with respect to the central grid point with the coordinates x_{14} , y_{14} , z_{14} . For the calculation of the primary function $u_P(x_p, y_p, z_p)$ at point P, the following compact 27-point stencil can be used::

$$u_P^{num}(x_p, y_p, z_p) + \sum_{i=1}^{27} k_i u_i^{num} = \bar{f},$$
 (159)

where $\bar{f} = 0$ in the case of zero source f = 0 (or can be calculated in terms of non-zero source f), the unknown stencil coefficients k_i (i = 1, 2, ..., 27) are to be determined from the minimization of the local truncation error. The local truncation error e follows from Eq. (159) by the replacement of the numerical solution u_i^{num} by the exact solution u_P :

$$e = u_P(x_p, y_p, z_p) + \sum_{i=1}^{27} k_i u_i - \bar{f}.$$
 (160)

Similar to the derivations of OLTEM for the 3-D Poisson equation in our papers [27, 28, 36], a Taylor series of the local truncation error e in Eq. (160) can be written as:

$$e = b_{1}u_{14} + h\left(b_{2}\frac{\partial u_{14}}{\partial z} + b_{3}\frac{\partial u_{14}}{\partial y} + b_{4}\frac{\partial u_{14}}{\partial x}\right)$$

$$+ h^{2}\left(b_{5}\frac{\partial^{2}u_{14}}{\partial z^{2}} + b_{6}\frac{\partial^{3}u_{14}}{\partial z\partial y^{2}} + b_{7}\frac{\partial^{2}u_{14}}{\partial y^{2}} + b_{8}\frac{\partial^{3}u_{14}}{\partial z\partial x^{2}} + b_{9}\frac{\partial^{2}u_{14}}{\partial x\partial y}\right)$$

$$+ h^{3}\left(b_{10}\frac{\partial^{3}u_{14}}{\partial z^{3}} + b_{11}\frac{\partial^{3}u_{14}}{\partial z^{2}\partial y} + b_{12}\frac{\partial^{3}u_{14}}{\partial z\partial y^{2}} + b_{13}\frac{\partial^{3}u_{14}}{\partial y^{3}} + b_{14}\frac{\partial^{3}u_{14}}{\partial z^{2}\partial x} + b_{15}\frac{\partial^{3}u_{14}}{\partial z\partial y\partial x} + b_{16}\frac{\partial^{3}u_{14}}{\partial x\partial y^{2}}\right) + h^{4}\left(b_{17}\frac{\partial^{4}u_{14}}{\partial z^{4}} + \dots + b_{25}\frac{\partial^{4}u_{14}}{\partial x\partial y^{3}}\right)$$

$$+ h^{5}\left(b_{26}\frac{\partial^{5}u_{14}}{\partial z^{5}} + \dots + b_{36}\frac{\partial^{5}u_{14}}{\partial x\partial y^{4}}\right)$$

$$+ h^{6}\left(b_{37}\frac{\partial^{6}u_{14}}{\partial z^{6}} + \dots + b_{49}\frac{\partial^{6}u_{14}}{\partial x\partial y^{5}}\right) + O(h^{7})$$

$$(161)$$

where the coefficients b_p (p=1,2,...) are expressed in terms of the coefficients k_i (i=1,2,...,27) and r_{xP} , r_{yP} and r_{zP} . Here we should mention that the expression for the local truncation error, Eq. (161), includes only the first order derivatives with respect to x (the higher order derivatives with respect to x are excluded with the help of the Poisson equation; see our papers [27, 28, 36] for the details). If we zero the first 16 coefficients $b_i = 0$ (i=1,2,...,16) up to the third order with respect to h in Eq. (161) as well as the 6 coefficients $b_i = 0$ (i=17,18,19,21,23,24) of the the fourth order with



respect to h in Eq. (161) then the remaining 3 coefficients $b_i = 0$ (i = 20, 22, 25) of the fourth order become non-zero and the local truncation error in Eq. (161) can be written as:

$$e = \frac{1}{6}h^{4} \left[(r_{xP}r_{zP}^{3} - r_{xP}^{3}r_{zP}) \frac{\partial^{4}u_{14}}{\partial x \partial z^{3}} + r_{xP}r_{yP}(r_{yP}^{2} - r_{xP}^{2}) \frac{\partial^{4}u_{14}}{\partial x \partial y^{3}} + r_{yP}r_{zP}(r_{yP}^{2} - r_{zP}^{2}) \frac{\partial^{4}u_{14}}{\partial z \partial y^{3}} \right] + O(h^{5}),$$
(162)

i.e., the fourth order is the maximum possible order of accuracy for the local truncation error e of the stencil equation, Eq. (159). If we try to calculate the local truncation error e in Eq. (160) without the use of the Poisson equation, then a Taylor series of the local truncation error in Eq. (161) will include more terms due to the additional high-order derivatives of u_{14} with respect to x. In this case, the 27 stencil coefficients k_i allow to zero only the coefficients b_i up to the second order with respect to h. This means that the use of the partial differential equation (the Poisson equation) for the calculation of the primary function $u_P(x_p, y_p, z_p)$ at point P with the 27-point stencil increases the accuracy by one order. We should also mention that the stencil coefficients k_i in Eq. (159) can be calculated by the procedure described in our papers [27, 28, 36].

Similar to the primary function, we can also calculate its spatial derivatives at any point of the domain. In this case, the stencil equation, Eq. (159), should be modified as follows:

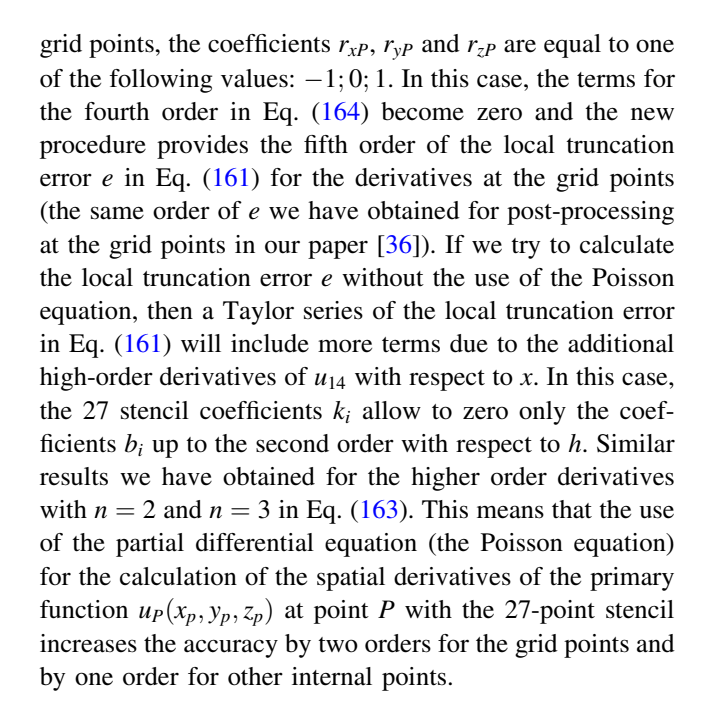
$$h^{n} \frac{\partial^{n} u_{P}^{num}(x_{p}, y_{p}, z_{p})}{\partial x^{n}} + \sum_{i=1}^{27} k_{i} u_{i}^{num} = \bar{f},$$

$$(163)$$

for any partial derivative with respect to x (similar modifications can be done for the derivatives with respect to y, z and the mixed derivatives). Similar to Eq. (159) for the primary function, the local truncation error for Eq. (163) can be represented in the form of Eq. (161). Then, we can zero the following coefficients $b_i = 0$ (i = 1, 2, ..., 21, 23, 24). The remaining 2 coefficients $b_i = 0$ (i = 22, 25) of the fourth order become non-zero. For the first order derivative $\frac{\partial u_P(x_p, y_p, z_p)}{\partial x}$, the local truncation error in Eq. (161) can be calculated as:

$$e = \frac{1}{6}h^{4} \left[\left(-3r_{xP}^{2}r_{zP} + r_{zP}^{3} \right) \frac{\partial^{4}u_{14}}{\partial x \partial z^{3}} + r_{yP} \left(r_{yP}^{2} - 3r_{xP}^{2} \right) \frac{\partial^{4}u_{14}}{\partial x \partial y^{3}} \right] + O(h^{5}),$$
(164)

i.e., the fourth order is the maximum possible order of accuracy for the local truncation error e of the stencil equation, Eq. (163). It is interesting to mention that for the



7 New Numerical High-Order Boundary Conditions for 'Quadratic' Elements

If the boundary cuts some regular grid points included into the stencil then we have the cut stencil with a smaller number of the internal grid points. In this case the cut stencils cannot usually provide the same high order of accuracy as that for the regular stencils. Let us consider this in more detail for the 2-D 25-point stencils ('quadratic' elements) with the Dirichlet and Neumann boundary conditions. For example, the grid point 13 in Fig. 7a is the closest internal grid point to the horizontal boundary and its stencil includes 15 internal grid points (in contrast to the regular stencil with the 25 internal grid points for the 'quadratic' elements; see Fig. 3c. The grid points 16, 17, ..., 25 in Fig. 7a are not included into this stencil because they are located outside the physical domain Ω or on the boundary. Without a special treatment of the boundary conditions, the 15-point cut stencil in the 2-D case (see Fig. 7a) cannot provide the order of accuracy of the regular 25-point stencil and this leads to the decrease in accuracy of the global system of equations that includes all regular and cut stencils. However, the order of accuracy of the cut stencil can be improved if the boundary conditions are also included into the expression for the local truncation error of the cut stencils; see the derivations below for the time-independent elasticity.

7.1 Dirichlet Boundary Conditions

Let us consider the 2-D time-independent elasticity equations given by Eq. (127) with the Dirichlet boundary



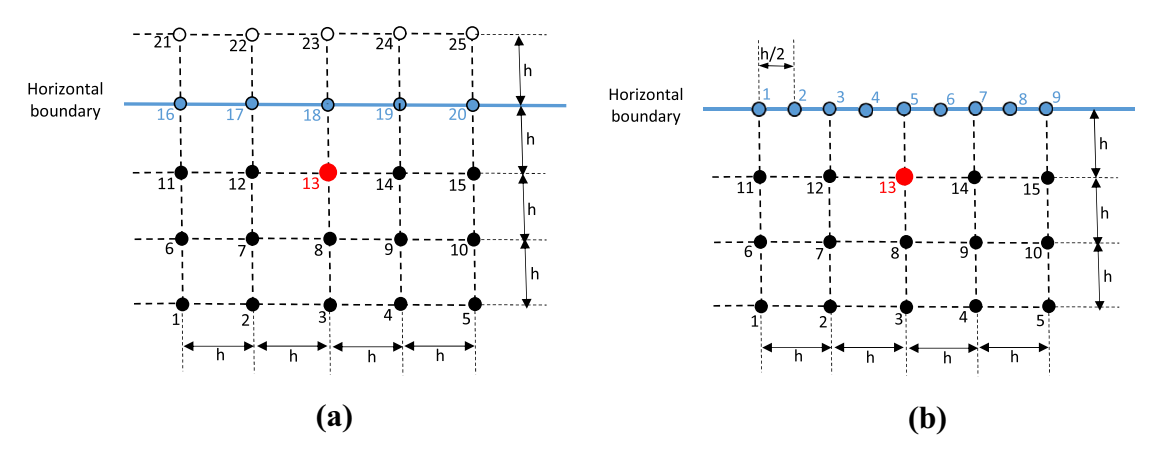


Fig. 7 a The regular 25-point stencil cut by the horizontal boundary. b The 15-point cut stencil with the 9 boundary points

conditions given by Eq. (128). Let us also consider OLTEM with the 25-point stencil equations given by Eq. (130) with L=25. In our paper [2] we have shown that OLTEM with the 25-point stencils and conforming Cartesian meshes provides the 12th order of the local truncation error or the 10th order of accuracy for the global solution. However, for the internal grid points located close to the boundary, a part of the stencil grid points are cut by the boundary. As an example, let us consider the cut stencil in Fig. 7a. This stencil includes 15 internal grid points located inside the domain, 5 boundary points on the horizontal boundary and 5 grid points located outside the domain. Here, we will show how to construct the 15-point stencil with the internal grid points that will provide a high accuracy due to the use of the boundary conditions. First, the case of the Dirichlet boundary conditions is analyzed. The considered cut stencil can be explicitly written using Eq. (130) as:

$$\sum_{i=1}^{L} k_{j,i} u_i^{num} + \sum_{i=1}^{L} \bar{k_{j,i}} v_i^{num} = \bar{f_j}, \qquad j = 1, 2$$
 (165)

with L=15. The local truncation error for the cut stencils, Eq. (165), with the inclusion of the Dirichlet boundary conditions at M_1 selected boundary points is given by Eq. (131) with $M_2=0$ and can be written as follows:

$$e_{j} = \sum_{i=1}^{L} k_{j,i} u_{i} + \sum_{i=1}^{L} \bar{k}_{j,i} v_{i} - \bar{f}_{j}$$

$$+ \sum_{i=1}^{M_{1}} q_{1,i} (g_{1,i} - u_{B,i}) + \sum_{i=1}^{M_{1}} \bar{q}_{1,i} (g_{2,i} - v_{B,i}).$$
(166)

with L=15. The analysis presented below shows that we can take $M_1=9$ boundary points uniformly distributed along the horizontal boundary over the interval 4h with the distance $h_1=h/4$ between the boundary points; see

Fig. 7b. The coordinates of the L = 15 internal grid points of the cut stencil (see Figs. 7b) with respect to the central grid point (x_{13}, y_{13}) can be written as follows:

$$x_p = x_{13} + d_{x,p}h, \quad y_p = y_{13} + d_{y,p}b_yh, \quad p = 1, 2, ..., L$$
 (167)

where the coefficients $d_{x,p}$ and $d_{y,p}$ can be easily defined. For example, for the internal grid point shown in Fig. 7 we can find that $d_{x,p} = i - 3$ and $d_{y,p} = j - 3$ for p = 5(j-1) + i with i = 1, 2, 3, 4, 5 and j = 1, 2, 3.

Similarly, we can describe the coordinates of the M_1 = 9 boundary points of the cut stencil (see Fig. 7b) with respect to the central grid point (x_{13}, y_{13}) :

$$x_{B,p} = x_{13} + r_{x,p}h,$$
 $y_{B,p} = y_{13} + r_{y,p}b_yh,$ $p = 1, 2, ..., M_1$
(168)

where the coefficients $r_{x,p}$ and $r_{y,p}$ can be easily defined after the selection of the location of the boundary points along the boundary.

In order to derive a Taylor series of the local truncation error given by Eq. (166), let us expand the exact solution at the L = 15 grid points and the selected $M_1 = 9$ boundary points in Eq. (166) into a Taylor series at small $h \ll 1$ in the vicinity of the central interface point (x_{13}, y_{13}) as follows:

$$\begin{split} w_{j} &= w_{13} + \frac{\partial w_{13}}{\partial x} [d_{xj}h] + \frac{\partial w_{13}}{\partial y} [d_{yj}b_{y}h] + \frac{\partial^{2}w_{13}}{\partial x^{2}} \frac{[d_{xj}h]^{2}}{2!} \\ &+ \frac{\partial^{2}w_{13}}{\partial y^{2}} \frac{[d_{yj}b_{y}h]^{2}}{2!} + 2 \frac{\partial^{2}w_{13}}{\partial x \partial y} \frac{[(d_{xj}h)[d_{yj}b_{y}h]}{2!} + ..., \qquad j = 1, 2, \dots, L(M_{1}). \end{split}$$

$$(169)$$

In Eq. (169) the function w_j is u_j or v_j for the internal and boundary points, the coefficients $d_{x,j}$, $d_{y,j}$ for the boundary points in Eq. (169) should be replaced by the coefficients $r_{x,j}$, $r_{y,j}$. The exact solution u_{13} and v_{13} to the elasticity equations, Eq. (127), at the central grid point with the coordinates $x_c = x_{13}$ and $y_c = y_{13}$ meets Eqs. (132)-(135).



Below, we consider the local truncation error for the first stencil equation, Eq. (166) with j=1. The derivations for the local truncation error and the stencil coefficients for the second stencil equation of Eq. (166) with j=2 can be similarly done (see also Sect. 4.3.1). Inserting Eqs. (169) and Eqs. (132)-(135) into Eq. (166) we will get the discretized load term $\bar{f_1}$ and the following local truncation error in space e_1 :

$$e_{1} = b_{1,1}u_{13} + b_{1,2}v_{13}$$

$$+ h \left(b_{1,3} \frac{\partial u_{13}}{\partial x} + b_{1,4} \frac{\partial v_{13}}{\partial x} + b_{1,5} \frac{\partial u_{13}}{\partial y} + b_{1,6} \frac{\partial v_{13}}{\partial y} \right)$$

$$+ h^{2} \left(b_{1,7} \frac{\partial^{2} u_{13}}{\partial x \partial y} + b_{1,8} \frac{\partial^{2} v_{13}}{\partial x \partial y} + b_{1,9} \frac{\partial^{2} u_{13}}{\partial y^{2}} + b_{1,10} \frac{\partial^{2} v_{13}}{\partial y^{2}} \right)$$

$$+ h^{3} \left(b_{1,11} \frac{\partial^{3} u_{13}}{\partial x \partial y^{2}} + \dots + b_{1,14} \frac{\partial^{3} v_{13}}{\partial y^{3}} \right)$$

$$+ h^{4} \left(b_{1,15} \frac{\partial^{4} u_{13}}{\partial x \partial y^{3}} + \dots + b_{1,18} \frac{\partial^{4} v_{13}}{\partial y^{4}} \right)$$

$$+ h^{5} \left(b_{1,19} \frac{\partial^{5} u_{13}}{\partial x \partial y^{4}} + \dots + b_{1,22} \frac{\partial^{5} v_{13}}{\partial y^{5}} \right)$$

$$+ h^{6} \left(b_{1,23} \frac{\partial^{6} u_{13}}{\partial x \partial y^{5}} + \dots + b_{1,26} \frac{\partial^{6} v_{13}}{\partial y^{5}} \right)$$

$$+ h^{7} \left(b_{1,27} \frac{\partial^{7} u_{13}}{\partial x \partial y^{6}} + \dots + b_{1,30} \frac{\partial^{7} v_{13}}{\partial y^{7}} \right)$$

$$+ h^{8} \left(b_{1,31} \frac{\partial^{8} u_{13}}{\partial x \partial y^{7}} + \dots + b_{1,34} \frac{\partial^{8} v_{13}}{\partial y^{8}} \right)$$

$$+ h^{9} \left(b_{1,35} \frac{\partial^{9} u_{13}}{\partial x \partial y^{8}} + \dots + b_{1,42} \frac{\partial^{10} v_{13}}{\partial y^{9}} \right)$$

$$+ h^{10} \left(b_{1,39} \frac{\partial^{10} u_{13}}{\partial x \partial y^{9}} + \dots + b_{1,42} \frac{\partial^{10} v_{13}}{\partial y^{10}} \right)$$

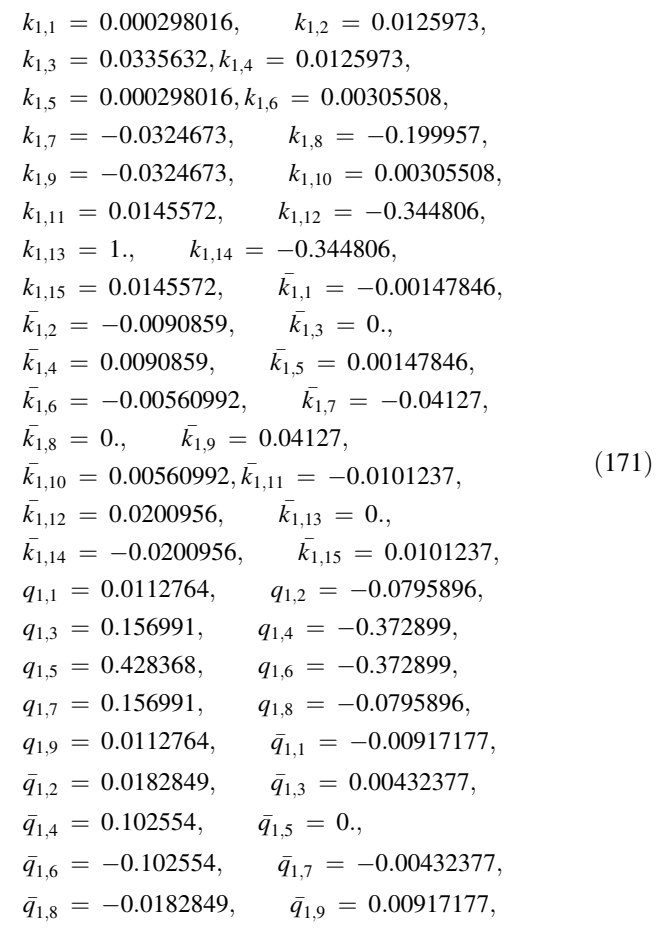
$$+ h^{11} \left(b_{1,43} \frac{\partial^{11} u_{13}}{\partial x \partial y^{10}} + \dots + b_{1,46} \frac{\partial^{11} v_{11}}{\partial y^{11}} \right)$$

$$+ h^{12} \left(b_{1,47} \frac{\partial^{12} u_{13}}{\partial x \partial y^{11}} + \dots + b_{1,50} \frac{\partial^{12} v_{12}}{\partial y^{12}} \right) + O(h^{13})$$

$$(170)$$

where the coefficients $b_{1,p}$ (p=1,2,...) are expressed in terms of the coefficients $k_{1,i}$, $\bar{k}_{1,i}$ and $q_{1,m}$, $\bar{q}_{1,m}$ (i=1,2,...,L, $m=1,2,...,M_1$). Here we should mention that the expression for the local truncation error e_1 , Eq. (170), includes only the first-order derivatives with respect to x (the higher order derivatives with respect to x are excluded with the help of Eqs. (132)-(135)).

By zeroing the first 46 coefficients $b_{1,i}=0$ $(i=1,2,\ldots,46)$ and assuming that $k_{1,13}=1$ (see Remark 1) and $\bar{k}_{1,13}=0$ (we also take $k_{2,13}=0$ and $\bar{k}_{2,13}=1$ in order to have the linearly independent first (j=1) and second (j=2) stencils) we can form a system of 48 algebraic equations for the first stencil. Solving this system, we will get the following 30 coefficients $k_{1,i}$, $\bar{k}_{1,i}$ as well as the 18 coefficients $q_{1,m}$, $\bar{q}_{1,m}$:



with the following local truncation error:

$$e_{1} = h^{12} \cdot 10^{-6} \left(6.54235 \frac{\partial^{12} v_{13}}{\partial x \partial y^{11}} - 4.72256 \frac{\partial^{12} u_{13}}{\partial y^{12}} \right) + O(h^{13}),$$

$$(172)$$

i.e., using the boundary conditions at the 9 selected boundary points, we can provide the 12-th order of the local truncation error for the 15-point cut stencil.

Let us also consider the new procedure for the 25-point stencils when the boundary cuts 15 grid points; see Fig. 8a. In this case we can use the stencil with the 9 internal grid points and the 15 boundary points uniformly distributed at distance $h_1 = 3h/7$ along the horizontal and vertical parts of the boundary as shown in Fig. 8b. The stencil equations for the grid point with the coordinate x_9 and y_9 (see Fig. 8b) and the corresponding local truncation error can be written in the form of Eqs. (165) and (166) with L = 9 and M = 15 (for convenience, we use a new numeration of the internal grid points from 1 to 9 in Fig. 8b). Repeating the derivations given by Eqs. (167) - (170) and zeroing the first 46 coefficients $b_{1,i} = 0$ (i = 1, 2, ..., 46) and assuming that $k_{1,9} = 1$ (see Remark 1) and $\bar{k}_{1,9} = 0$ (we also take $k_{2,9} = 0$ and $\bar{k}_{2,9} = 1$ in order to have the linearly independent first



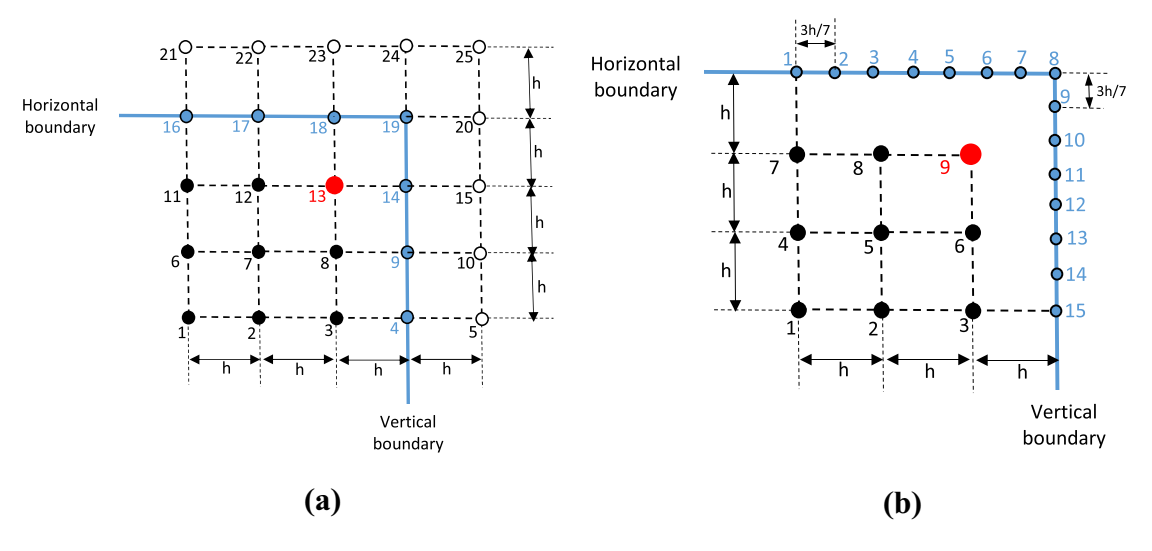


Fig. 8 a The regular 25-point stencil cut by the horizontal and vertical boundaries. b The 9-point cut stencil with the 15 boundary points

(j=1) and second (j=2) stencils) we can form a system of 48 algebraic equations for the first stencil. Solving this system, we will get the following 18 coefficients $k_{1,i}$, $\bar{k}_{1,i}$ as well as the 30 coefficients $q_{1,m}$, $\bar{q}_{1,m}$:

$$\begin{array}{lll} k_{1,1} &= -0.000323273, & k_{1,2} &= 0.00559361, \\ k_{1,3} &= 0.0185748, & k_{1,4} &= -0.00111318, \\ k_{1,5} &= -0.0477601, & k_{1,6} &= -0.16123, \\ k_{1,7} &= 0.008167, & k_{1,8} &= -0.32599, & k_{1,9} &= 1., \\ \bar{k}_{1,1} &= -0.00141205, & \bar{k}_{1,2} &= -0.0123643, \\ \bar{k}_{1,3} &= -0.0190124, & \bar{k}_{1,4} &= -0.00508834, \\ \bar{k}_{1,5} &= -0.0494195, & \bar{k}_{1,6} &= 0.0234136, \\ \bar{k}_{1,7} &= -0.00783463, & \bar{k}_{1,8} &= 0.0247765, \\ \bar{k}_{1,9} &= 0, & q_{1,1} &= -0.159342, \\ q_{1,2} &= -0.0752364, & q_{1,3} &= -0.0754087, \\ q_{1,4} &= -0.313099, & q_{1,5} &= 0.167508, \\ q_{1,6} &= -0.120758, & q_{1,7} &= 0.0538803, \\ q_{1,8} &= -0.000336028, & q_{1,9} &= 0.407694, \\ q_{1,10} &= -0.751422, & q_{1,11} &= 0.859015, \\ q_{1,12} &= -0.716692, & q_{1,13} &= 0.330017, \\ q_{1,14} &= -0.117431, & q_{1,15} &= 0.0156938, \\ \bar{q}_{1,1} &= -0.17299, & \bar{q}_{1,2} &= 0.355267, \\ \bar{q}_{1,3} &= -0.604681, & \bar{q}_{1,4} &= 0.614102, \\ \bar{q}_{1,5} &= -0.303421, \bar{q}_{1,6} &= 0.130629, \\ \bar{q}_{1,7} &= -0.00515474, & \bar{q}_{1,8} &= -0.00880635, \\ \bar{q}_{1,9} &= 0.0214342, & \bar{q}_{1,10} &= -0.112411, \\ \bar{q}_{1,11} &= 0.0525618, & \bar{q}_{1,12} &= 0.106248, \\ \bar{q}_{1,13} &= -0.0488856, \\ \bar{q}_{1,14} &= 0.0334346, & \bar{q}_{1,15} &= -0.0103847, \end{array}$$

with the following local truncation error:

$$e_{1} = h^{12} \\ \cdot 10^{-5} \left(2.45681 \frac{\partial^{12} u_{9}}{\partial x \partial y^{11}} + 2.69764 \frac{\partial^{12} v_{9}}{\partial x \partial y^{11}} - 1.8176 \frac{\partial^{12} u_{9}}{\partial y^{12}} + 2.87954 \frac{\partial^{12} v_{9}}{\partial y^{12}} \right) + O(h^{13}),$$

$$(174)$$

i.e., using the boundary conditions at the 15 selected boundary points, we can provide the 12-th order of accuracy for the local truncation error for the 9-point cut stencil. The regular 9-point stencil provides just the 4-th order of accuracy for the local truncation error.

7.2 Neumann Boundary Conditions

The derivation of the numerical high-order Neumann boundary conditions for cut stencils is similar to that for the Dirichlet boundary condition in the previous section 7.1. In order to show this, let us consider the cut stencil shown in Fig. 7. Similar to section 7.1, we will use the stencil equations given by Eq. (165) with L=15. The local truncation error e_j for these stencil equations can be described by Eq. (131) with $M_1=0$:

$$e_{j} = \sum_{i=1}^{L} k_{j,i} u_{i} + \sum_{i=1}^{L} \bar{k}_{j,i} v_{i} - \bar{f}_{j}$$

$$+ h \left[\sum_{i=1}^{M_{2}} q_{2,i} (\bar{g}_{1,i} - t_{x,B,i}) + \sum_{i=1}^{M_{2}} \bar{q}_{2,i} (\bar{g}_{2,i} - t_{y,B,i}) \right].$$

$$(175)$$

The Neumann boundary conditions are given by Eq. (129). We will also use the $M_2 = 9$ boundary points as shown in Fig. 7b. Repeating the derivation of section 7.1, we can find a Taylor series of the local truncation error for the first



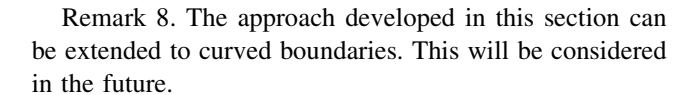
stencil in the form of Eq. (170). Due to the difference between Eq. (166) and Eq. (175), the expressions for the coefficients $b_{1,p}$ in Eq. (170) will be different for the Dirichlet and Neumann boundary conditions. By zeroing the first 46 $b_{1,i}=0$ coefficients $(i=1,2,\ldots,46)$ and assuming that $k_{1,13}=1$ (see Remark 1) and $\bar{k}_{1,13}=0$ (we also take $k_{2,13}=0$ and $\bar{k}_{2,13}=1$ in order to have the linearly independent first (j=1) and second (j=2) stencils) we can form a system of 48 algebraic equations for the first stencil. Solving this system, we will get the following 30 coefficients $k_{1,i}$, $\bar{k}_{1,i}$ as well as the 18 coefficients $q_{1,m}$, $\bar{q}_{1,m}$ in the case of the Neumann boundary conditions:

$$\begin{array}{lll} k_{1,1} = -0.00674247, & k_{1,2} = 0.0379803, \\ k_{1,3} = 0.126982, & k_{1,4} = 0.0379803, \\ k_{1,5} = -0.00674247, & k_{1,6} = -0.0819144, \\ k_{1,7} = -0.364449, & k_{1,8} = 0.173851, \\ k_{1,9} = -0.364449, & k_{1,10} = -0.0819144, \\ k_{1,11} = -0.259115, & k_{1,12} = 0.0238247, \\ k_{1,13} = 1., & k_{1,14} = 0.0238247, \\ k_{1,15} = -0.259115, & \bar{k}_{1,1} = -0.0236224, \\ \bar{k}_{1,2} = -0.137025, & \bar{k}_{1,3} = 0., & \bar{k}_{1,4} = 0.137025, \\ \bar{k}_{1,5} = 0.0236224, & \bar{k}_{1,6} = -0.129285, \\ \bar{k}_{1,7} = -0.27089, & \bar{k}_{1,8} = 0., & \bar{k}_{1,9} = 0.27089, \\ \bar{k}_{1,10} = 0.129285, \bar{k}_{1,11} = -0.286487, \\ \bar{k}_{1,12} = 1.11672, & \bar{k}_{1,13} = 0., & \bar{k}_{1,14} = -1.11672, \\ \bar{k}_{1,15} = 0.286487, & q_{1,1} = 0.113835, \\ q_{1,2} = -0.505557, & q_{1,3} = 1.32361, \\ q_{1,4} = -2.82079, & q_{1,5} = 2.8939, \\ q_{1,6} = -2.82079, & q_{1,7} = 1.32361, \\ q_{1,8} = -0.505557, & q_{1,9} = 0.113835, \\ \bar{q}_{1,1} = -0.0466458, & \bar{q}_{1,2} = -0.0820813, \\ \bar{q}_{1,3} = -0.251888, & \bar{q}_{1,4} = -0.0549269, \\ \bar{q}_{1,5} = 0., & \bar{q}_{1,6} = 0.0549269, & \bar{q}_{1,7} = 0.251888, \\ \bar{q}_{1,8} = 0.0820813, & \bar{q}_{1,9} = 0.0466458, \end{array}$$

with the following local truncation error:

$$\begin{split} e_1 &= h^{12} \cdot 10^{-5} \bigg(10.3145 \frac{\partial^{12} v_{13}}{\partial x \partial y^{11}} - 7.83087 \frac{\partial^{12} u_{13}}{\partial y^{12}} \bigg) \\ &+ O(h^{13}), \end{split} \tag{177}$$

i.e., using the boundary conditions at the 9 selected boundary points, we can provide the 12-th order of the local truncation error for the 15-point cut stencil.



8 Comparison of Accuracy of OLTEM and FEM

Here we shortly summarize the results related to the order of accuracy of OLTEM for different PDEs considered in the previous Sections as well as we compare the order of accuracy of OLTEM and FEM at similar stencil equations. In contrast to finite elements, the maximum possible order of accuracy of OLTEM with similar stencils is different for different PDEs, see Table 1, 2, 3 for the regular, cut and heterogeneous stencils. As can be seen from Table 1, OLTEM with the regular stencils for the scalar PDEs provides a higher order of accuracy than that for FEM at similar stencils. It it interesting to note that for the Poisson and Helmholtz equations, the order of accuracy of OLTEM on square meshes is higher than that on rectangular meshes. Moreover, for the Poisson equation OLTEM with the 2-D $5 \times 5 = 25$ -point stencils and 3-D $5 \times 5 \times 5 = 125$ -point stencils (these stencils corresponds to those for quadratic finite elements) yields the different orders of accuracy in the 2-D and 3-D cases (however, the increase in the order of accuracy for OLTEM in the 2-D and 3-D cases is huge compared to that for finite elements, e.g., by 8 orders in the 3-D case and by 12 orders in the 2-D case on square meshes).

For a system of the elasticity PDEs, OLTEM with the 2- $3 \times 3 = 9$ -point stencils and with the $3 \times 3 \times 3 = 27$ -point stencils (similar to those for linear finite elements) provides the same order of accuracy as that for linear finite elements, i.e., linear elements provide the optimal order of accuracy. However, OLTEM with the 2-D $5 \times 5 = 25$ -point stencils with the 3-D and $5 \times 5 \times 5 = 125$ -point stencils (similar to those for quadratic finite and isogeometric elements) provides a much higher order of accuracy than that for quadratic finite and isogeometric elements (a huge increase by 6 orders for elastostatics and by 2 orders for elastodynamics); see Table 1.

As we mentioned in Sect. 7, currently we have implemented the new numerical high-order boundary conditions for 'quadratic' elements with cut stencils for the simple boundaries corresponding to regular domains. Therefore, Table 2 shows only the accuracy of OLTEM on irregular boundaries with the 9-point (2-D) and 27-point (3-D) stencils corresponding to 'linear' elements. As can be seen from Table 2, for the scalar PDEs with the Dirichlet boundary conditions, OLTEM with cut stencils provides the same accuracy of global solutions on irregular domains



Table 1 The comparison of the order of accuracy of global solutions obtained by OLTEM with regular stencils and by FEM in the case of homogeneous materials and regular domains

Governing Equations	Stencils	Order of accuracy		Order increase with OLTEM
		Conventional finite and isogeometric elements	OLTEM	OLIEW
Time-dependent wave and heat equations	9-point (2D) and 27-point (3D) stencils	2	4	4 - 2 = 2
	25-point (2D) and 125-point (3D) stencils	4	8	8 - 4 = 4
2. Poisson Equation	9-point (2D) and 27-point (3D) stencils	2	4 (rectangular meshes)	4 - 2 = 2 (rectangular meshes)
			6 (square meshes)	6 - 2 = 4 (square meshes)
	25-point (2D) and 125-point (3D) stencils	4 (rectangular meshes)	14 (rect. meshes)-2D	14 - 4 = 10 (rect.meshes)-2D
			10 (rect. meshes)-3D	10 - 4 = 6 (rect.meshes)-3D
		6 (square meshes)	18 (square meshes)-2D	18 - 6 = 12 (square meshes)-2D
			14 (square meshes)-3D	14 - 6 = 8 (square meshes)-3D
3. Time-independent Helmholtz equation	9-point (2D) and 27-point (3D) stencils	2	4 (rectangular meshes)	4 - 2 = 2 (rectangular meshes)
			6 (square meshes)	6 - 2 = 4 (square meshes)
4. Time-dependent elasticity equations	9-point (2D) and 27-point (3D) stencils	2	2	0
	25-point (2D) and 125-point (3D) stencils	4	6	6 - 4 = 2
5. Time-independent elasticity equations	9-point (2D) and 27-point (3D) stencils	2	2	0
	25-point (2D) and 125-point (3D) stencils	4	10	10 - 4 = 6

as that on regular domains in Table 1. However, for the scalar PDEs with the Neumann boundary conditions, the accuracy of OLTEM on irregular domains is one order smaller than that for the Dirichlet boundary conditions and is one order higher than that for linear finite elements. For a system of the elasticity PDEs, OLTEM with the 2-D $3 \times 3 = 9$ -point stencils and with the 3-D $3 \times 3 \times 3 = 27$ -point stencils (similar to those for linear finite elements) on irregular domains provides the same order of accuracy as that for linear finite elements. We should also mention that due to the minimization of the leading terms for the local truncation error in OLTEM, it provides a much high accuracy than linear and high-order finite elements even if OLTEM and finite elements have the same orders of accuracy.

The accuracy of OLTEM for heterogeneous materials with irregular interfaces and its comparison with the accuracy of finite elements is shown in Table 3. OLTEM with the 9-point (2-D) and 27-point (3-D) stencils ('linear' elements) for heterogeneous materials with irregular

interfaces yields the same order of accuracy as that on irregular domains (see the results in Tables 2 and 3). For 'quadratic' elements, OLTEM significantly exceeds the accuracy of quadratic finite elements at similar stencils despite unfitted meshes. For example, OLTEM yields a huge increase in accuracy by 8, 7 and 3 orders for the Poisson, elastostatics and elastodynamics equations, respectively (see Table 3).

Below, we present only two numerical examples from our papers [3, 27] related to the comparison of OLTEM with unfitted meshes and FEM with conforming meshes used for the solution of the 3-D scalar wave equation on an irregular domain and the 2-D elastostatics equations for heterogeneous materials with an irregular interface. For these two examples, we used the method of manufactured solutions with exact solutions. Much more 2-D and 3-D numerical examples solved by OLTEM can be found in our papers mentioned in the Introduction.

For the first problem we consider a prism *ABCDOPQR* with a spherical hole (see Fig. 9a). Figures 9b and 10 show



Table 2 The comparison of the order of accuracy of global solutions obtained by OLTEM with cut stencils and by FEM in the case of homogeneous materials and irregular domains

Governing equations	Stencils	Order of accuracy	Order increase with OLTEM	
		Conventional finite and isogeometric elements	OLTEM with unfitted Cartesian meshes	- Will OBIEM
Time-dependent wave and heat equations	9-point (2D) and 27-point (3D) cut stencils	2	4 (Dirichlet boundary conditions)	4 - 2 = 2
			3 (Neumann boundary conditions)	3 - 2 = 1
2. Poisson Equation	9-point (2D) and 27-point (3D) cut stencils	2	4 (Dirichlet boundary conditions)	4 - 2 = 2
			3 (Neumann boundary conditions)	3 - 2 = 1
3. Time-independent Helmholtz equation	9-point (2D) and 27-point (3D) cut stencils	2	4 (Dirichlet boundary conditions)	4 - 2 = 2
			3 (Neumann boundary conditions)	3 - 2 = 1
4. Time-dependent elasticity equations	9-point (2D) and 27-point (3D) cut stencils	2	2	0
5. Time-independent elasticity equations	9-point (2D) and 27-point (3D) cut stencils	2	2	0

examples of an unfitted Cartesian mesh for OLTEM and a conforming tetrahedral finite element mesh generated by the commercial finite element code 'COMSOL'. The comparison of accuracy for the numerical results obtained by OLTEM with the 27-point stencils and by linear and high-order (up to the 5-th order) finite elements are presented in Fig. 11 for the maximum relative errors in displacement e_u^{max} (a, b) and in velocity e_v^{max} (c, d); see our paper [27] for the details. As can be seen from Fig. 11, at the same numbers of degrees of freedom N, OLTEM with 'linear' elements yields much more accurate results than those obtained by conventional linear and high-order finite elements including quadratic, cubic, quartic, quintic tetrahedral finite elements with much wider stencils and greater computational costs. It is also interesting to note that at accuracy of 5%, the new approach reduces the number of degrees of freedom by a factor of greater than 1000 compared to that for linear finite elements with similar stencils (e.g., compare curves 1 and 2 in Fig. 11a at $Log_{10}e_u^{max} =$ -1.3). This leads to a huge reduction in computation time for OLTEM at a given accuracy. This reduction in computation time will be even greater if a higher accuracy is needed, e.g., 1% or less.

The second numerical example is related to the 2-D elastostatics problem for a square domain with an elliptical inclusion (see Fig. 12a) solved by OLTEM with the 25-point stencils ('quadratic' elements) and unfitted meshes as well as by finite elements with conforming meshes; see the examples of the corresponding meshes in Fig. 12b,c. The

comparison of accuracy for the numerical results obtained by OLTEM with the 25-point stencils ('quadratic' elements) and by linear and high-order (up to the 5-th order) finite elements are presented in Fig. 13 for the maximum relative errors and for the relative errors in the L_2 norm for the three stress components s_x , s_y and s_{xy} ; see our paper [3] for the details. We should also mention that for OLTEM we used the new post-processing procedure for the stress calculation described in Sect. 5. As can be seen from Fig. 13, at the same numbers of degrees of freedom N, OLTEM yields much more accurate results than those obtained by conventional high-order finite elements with much wider stencils and greater computational costs. Moreover, OLTEM with the 25-point stencils ('quadratic' elements) provides the 10-th order of accuracy for stresses at mesh refinement; see curves 1 in Fig. 13.

9 Concluding Remarks

In this paper, we review OLTEM published in our papers [1, 2, 22–38] as well as we consider some new developments of OLTEM. In contrast to our published papers on OLTEM, here we use slightly different derivations for the imposition of the boundary conditions. Now the boundary and interface conditions are uniformly imposed at a small number of the selected boundary and interface points as additional constraints with Lagrange multipliers. Some modifications are also used for the derivations of OLTEM



Table 3 The comparison of the order of accuracy of global solutions obtained by OLTEM and FEM for heterogeneous materials with irregular interfaces

Governing Equations	Stencils	Order of accuracy		Order increase with OLTEM
		Conventional finite elements and conforming meshes	OLTEM with unfitted Cartesian meshes	with OLILW
Time-dependent wave and heat equations with irregular interfaces	9-point (2D) and 27-point (3D) stencils	2	3	3 - 2 = 1
2. Poisson equation with irregular interfaces	9-point (2D) and 27-point (3D) stencils	2	3	3 - 2 = 1
	25-point (2D) and 125-point (3D) stencils	3	11	11 - 3 = 8
3. Time-independent elasticity equations with irregular interfaces	9-point (2D) and 27-point (3D) stencils	2	2	0
	25-point (2D) and 125-point (3D) stencils	3	10	10 - 3 = 7
4. Time-dependent elastodynamics equations with irregular interfaces	9-point (2D) and 27-point (3D) stencils	2	2	2 - 2 = 0
	25-point (2D) and 125-point (3D) stencils	3	6	6 - 3 = 3
		3 (lumped mass matrix)	4 (lumped mass matrix)	4 - 3 = 1

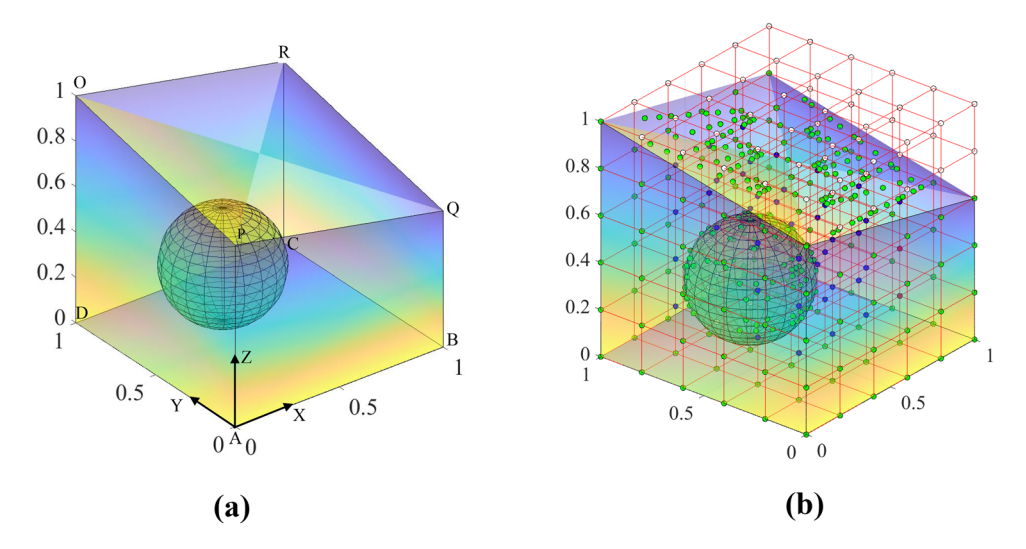


Fig. 9 a A 3-D prism ABCDOPQR (A(0, 0, 0), B(1, 0, 0), C(1, 1, 0), D(0, 1, 0), O(0, 1, 1), P(0, 0, 0.8), Q(1, 0, 0.6), R(1, 1, 0.8)) with a spherical hole of radius 0.25 centered at (0.4, 0.6, 0.3). **b** An unfitted Cartesian mesh for OLTEM

for the time-dependent PDEs for which we first replace the time derivatives by the spatial derivatives in the stencil equations using PDEs and then we consider a Taylor series of the local truncation error for the calculation of the stencil coefficients (in our published papers except paper [38] we applied PDEs after a Taylor series expansion). In contrast to our previously published papers on OLTEM for

heterogeneous materials, the more general interface conditions with the jumps for the function and fluxes are used in this paper. These small modifications simplify the understanding and the derivations of OLTEM. We do not use any weak formulations for the derivation of the discrete equations of OLTEM. The structure of the discrete equations in OLTEM is assumed or can be taken from any



Fig. 10 a An example of a conforming tetrahedral finite element mesh generated by the commercial software COMSOL for the discretization of the 3 -D prism ABCDOPQR with the spherical hole (see Fig. 9a). **b** shows a part of the mesh in the vicinity of the spherical hole

 $\log_{10} e_u^{max}$

-2

-3

0

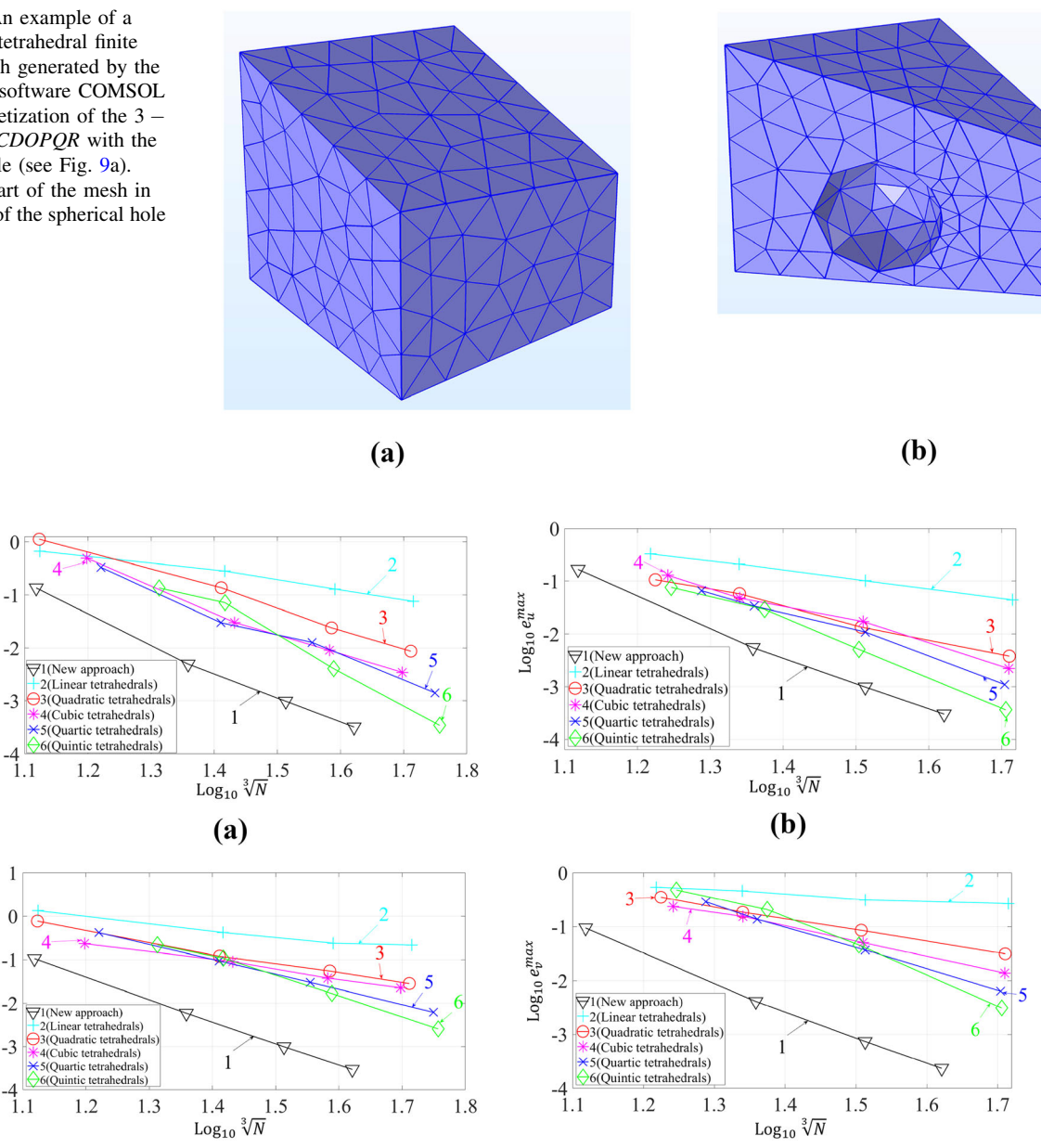


Fig. 11 The maximum relative errors in displacement e_u^{max} (**a**, **b**) and in velocity e_v^{max} (**c**, **d**) as a function of $\sqrt[3]{N}$ at mesh refinement in the logarithmic scale. N is the number of degrees of freedom. The numerical solutions of the 3-D scalar wave equation with zero (\mathbf{a} , c) and non-zero (b, d) loading functions for the prism with the spherical hole (see Fig. 9a) are obtained by OLTEM on unfitted cubic

(c)

 $(b_y = b_z = 1)$ Cartesian meshes (curve 1) and by conventional linear (curve 2), quadratic (curve 3), cubic (curve 4), quartic (curve 5) and quintic (curve 6) tetrahedral finite elements. Symbols ∇ , +, \bigcirc , \star , \times and \diamond correspond to the results for the different N used in the calculations

(d)

known numerical method. The main idea of OLTEM consists in the fact that if the unknown function/functions in a discrete equation should meet PDE or a system of PDEs then the coefficients of the discrete equation can be calculated by the minimization of the local truncation error and they will provide the maximum possible accuracy for the discrete equation.

The main features and advantages of OLTEM can be summarized as follows:

Many difficulties of existing numerical techniques for irregular geometry (e.g., finite elements, spectral element, isogeometric elements, the finite volume method, and many others) are related to complicated mesh



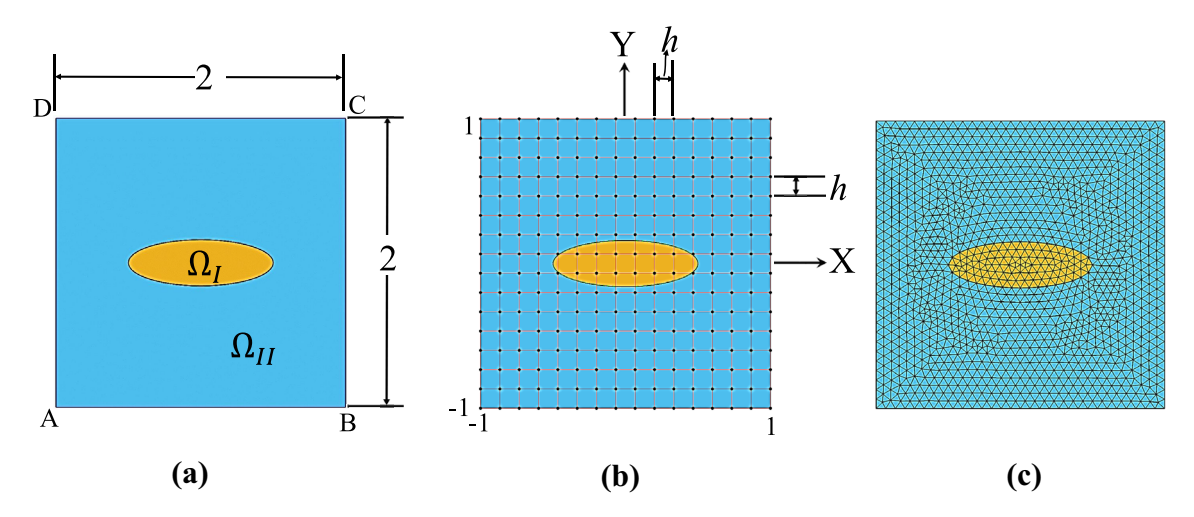


Fig. 12 A square plate ABCD with an elliptical interface centered at point (0, 0) (a). Examples of an unfitted square Cartesian mesh for OLTEM (b) and of a conforming triangular finite element mesh generated by COMSOL (c)

generators and the poor accuracy of 'bad' elements (e.g., the elements with small angles). In contrast to these techniques, OLTEM is based on simple unfitted Cartesian meshes with a trivial procedure for the formation of the compact stencils for 2-D and 3-D complex irregular geometry as well as OLTEM with unfitted meshes provides a much higher accuracy than the above-mentioned techniques on conforming meshes with similar stencils (similar computational costs), e.g., see Tables 1,2,3 for the comparison of accuracy of OLTEM and FEM.

- In contrast to the Taylor series expansion-based methods such as the generalized finite difference methods and others (e.g., see paper [39] and reference there), OLTEM does introduce additional unknowns on irregular boundaries and interfaces, does not change the width of stencil equations as well as provides a much higher accuracy than the above-mentioned techniques with similar stencils (similar computational costs), e.g., OLTEM with $5 \times 5 = 25$ -point stencils for the 2-D Poisson equation provides the 18-th order of accuracy (see Table 1 and our paper [1]). The implementation of the Dirichlet and Neumann boundary conditions as well as the interface conditions for OLTEM on unfitted meshes is simple and straightforward.
- A very effective and accurate OLTEM post-processing procedure has been developed for the calculation of the spatial derivatives of the primary function at grid points that is based on the application of the original PDEs. It uses the compact stencil equations similar to those in basic computations with the similar procedure for the calculation of the optimal stencil coefficients that provide a high accuracy of the spatial derivatives. For example, we have obtained the 10-th order of accuracy for stresses for 2-D elastostatics problems with

- heterogeneous materials and irregular interfaces calculated by OLTEM with the 25-point stencils; see our paper [3]. In this case, the use of the elastostatics PDEs increases the accuracy of stresses by 6 orders compared to the post-processing without the use of PDEs.
- As we mentioned above, despite unfitted meshes, OLTEM provides a very high accuracy of numerical solutions especially when the 25-point (2-D) and 125-point (3-D) stencil equations (similar to those for quadratic finite elements) are used. For example, OLTEM with 'quadratic' elements yields a huge increase in accuracy by 8, 7 and 3 orders for the Poisson, elastostatics and elastodynamics equations with irregular interfaces, respectively (see Table 3).
- Even at the same order of accuracy, OLTEM yields much more accurate results than finite elements due to the minimization of the leading terms of the local truncation error in OLTEM. Numerical results from our papers show that at the engineering accuracy, OLTEM can reduce the number of degrees of freedom by 1000-1000000 times compared to that for finite elements at similar stencils. This leads to a huge reduction in the computation time.
- OLTEM with 'quadratic' elements provides very accurate results for the elasticity equations with nearly incompressible materials (e.g., with Poisson ratio 0.4995), e.g., see our papers [2, 3, 24].
- For time-dependent PDEs, OLTEM offers a rigorous approach for the calculation of the diagonal mass matrix that is based on the accuracy considerations. For the internal grid points located far from the boundary and interfaces, the diagonal mass matrix can be calculated in terms of the coefficients of the stiffness matrix, e.g., see Eqs. (29) and (75) (similar formulas



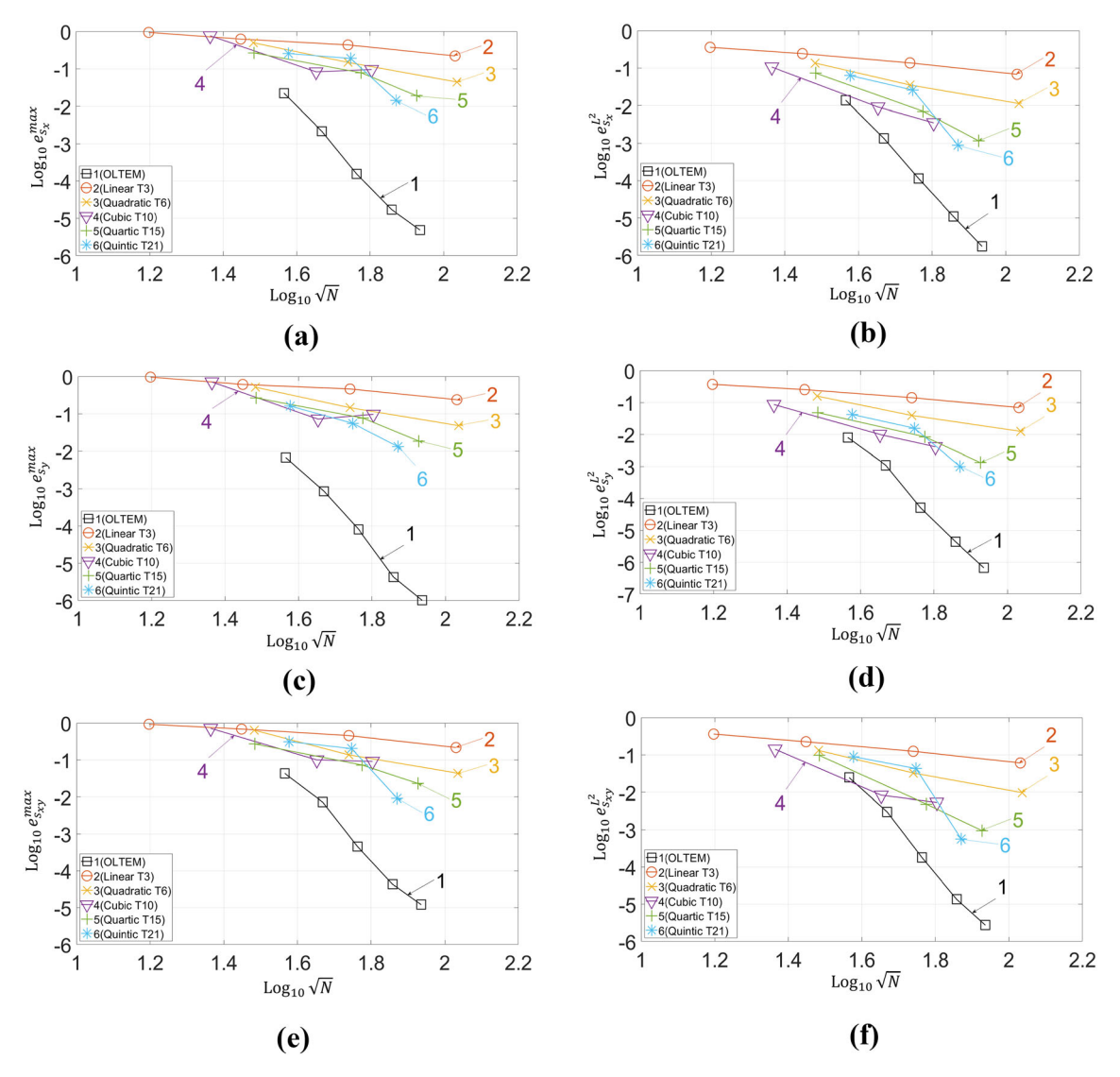


Fig. 13 The maximum relative errors in stresses $e_{s_x}^{max}$ (**a**), $e_{s_y}^{max}$ (**c**), $e_{s_y}^{max}$ (**e**) as well as the errors in stresses $e_{s_x}^{L^2}$ (**b**), $e_{s_y}^{L^2}$ (**d**), $e_{s_y}^{L^2}$ (**f**) in the L^2 norm as a function of the number N of degrees of freedom in the logarithmic scale. The numerical solutions for the plate with the

elliptical interface are obtained by OLTEM (curve 1) and by conventional triangular finite elements (curves 2-6). Curves (2,3,4,5,6) correspond to linear, quadratic, cubic, 4-th order and 5-th order finite elements, respectively

can be derived for the elastodynamics equations as well as for heterogeneous materials, e.g., see our paper [38]).

- New numerical high-order boundary conditions for cut stencils have been developed for OLTEM with 'quadratic' elements. They offer the same very high accuracy of cut stencils as that for OLTEM with regular stencils.
- A new post-processing procedure for the calculation of the spatial derivatives of primary functions at the grid points has been generalized in this paper. We have developed a new approach for the calculation of the primary functions and their derivatives at any point of the domain. This approach is based on the optimization of accuracy of the approximation formulas that includes the use of the original PDEs. For example, the new
- approximation technique can be used for accurate data transfer between different meshes.
- OLTEM can be easily combined with other numerical techniques by the replacement of the stencil equations for some selected grid points with the stencil equations of OLTEM. For example, in our papers [1, 24] the stencils of OLTEM were used for the grid points of one subdomain while the finite element stencils equations were used for for the grid points of another subdomain.
- OLTEM does not require time consuming numerical integration for finding the coefficients of the stencil equations, e.g., as for high-order finite, spectral and isogeometric elements. The stencil coefficients are calculated analytically or numerically (for irregular



geometry) by the solution of small local systems of linear algebraic equations. Numerical experiments show that the solution of these small local systems of algebraic equations is fast. Moreover, these local systems are independent of each other and can be efficiently solved on a parallel computer.

In the future we plan the development of OLTEM with adaptive mesh refinement similar to the h- and prefinement for finite elements. This will include special 'transition' stencils for quadtrees/octrees meshes that allow a simple refinement strategy with Cartesian meshes. We will also study the possibility of the development of the symmetric global matrices for OLTEM by the increase in the number of the selected boundary and interface points for the cut and heterogeneous stencils of OLTEM (currently, the global matrices for OLTEM are non-symmetric due to the cut and heterogeneous stencils). Research on the use of preconditioners for the solution of the global systems of discrete equations of OLTEM is also planned (for the results presented in our papers on OLTEM, we use direct solvers and the built-in iterative MATLAB solver 'gmres'). Similar to different finite-different techniques on irregular geometry, the rigorous proof of stability of OLTEM is an open problem (currently we solve problems by OLTEM using a large number (1000-2000) of different unfitted meshes with very different locations of grid points with respect to irregular boundary and interfaces in order to numerically show stability of OLTEM). The extension of OLTEM to other PDEs for homogeneous and heterogeneous materials as well as to non-linear PDEs will be also considered in the future.

Acknowledgements The research has been supported in part by the NSF grant CMMI-1935452, by Sandia (contract 2416989) and by Texas Tech University. I would also like to thank my former and current PhD students, Dr. B. Dey and Mr. M. Mobin for the numerical experiments with OLTEM and FEM. The views and conclusions contained in this paper are those of the author and should not be interpreted as representing the official policies.

References

- Idesman A, Dey B (2020) New 25-point stencils with optimal accuracy for 2-d heat transfer problems. Comparison with the quadratic isogeometric elements. J Comput Phys 418:109640
- Idesman A, Dey B (2020) Compact high-order stencils with optimal accuracy for numerical solutions of 2-d time-independent elasticity equations. Comput Methods Appl Mech Eng 360:112699
- Idesman A, Dey B, Mobin M (2022) The 10-th order of accuracy of 'quadratic' elements for elastic heterogeneous materials with smooth interfaces and unfitted Cartesian meshes. Eng Comput 38:4605–4629
- Vos P, van Loon R, Sherwin S (2008) A comparison of fictitious domain methods appropriate for spectral/hp element discretisations. Comput Methods Appl Mech Eng 197(25–28):2275–2289

- Burman E, Hansbo P (2010) Fictitious domain finite element methods using cut elements: I. A stabilized Lagrange multiplier method. Comput Methods Appl Mech Eng 199(41–44): 2680–2686
- Rank E, Kollmannsberger S, Sorger C, Duster A (2011) Shell finite cell method: a high order fictitious domain approach for thin-walled structures. Comput Methods Appl Mech Eng 200(45–46):3200–3209
- Rank E, Ruess M, Kollmannsberger S, Schillinger D, Duster A (2012) Geometric modeling, isogeometric analysis and the finite cell method. Comput Methods Appl Mech Eng 249–252:104–115
- May S, Berger M (2017) An explicit implicit scheme for cut cells in embedded boundary meshes. J Sci Comput 71(3):919–943
- Main A, Scovazzi G (2018) The shifted boundary method for embedded domain computations. Part I: Poisson and stokes problems. J Comput Phys. https://doi.org/10.1016/j.jcp.2017.10. 026
- Song T, Main A, Scovazzi G, Ricchiuto M (2018) The shifted boundary method for hyperbolic systems: Embedded domain computations of linear waves and shallow water flows. J Comput Phys 369:45–79
- Kreisst H-O, Petersson NA (2006) An embedded boundary method for the wave equation with discontinuous coefficients. SIAM J Sci Comput 28(6):2054–2074
- Kreiss H-O, Petersson NA (2006) A second order accurate embedded boundary method for the wave equation with Dirichlet data. SIAM J Sci Comput 27(4):1141–1167
- Kreiss H-O, Petersson NA, Ystrom J (2004) Difference approximations of the Neumann problem for the second order wave equation. SIAM J Numer Anal 42(3):1292–1323
- McCorquodale P, Colella P, Johansen H (2001) A Cartesian grid embedded boundary method for the heat equation on irregular domains. J Comput Phys 173(2):620–635
- Johansen H, Colella P (1998) A Cartesian grid embedded boundary method for Poisson's equation on irregular domains. J Comput Phys 147(1):60–85
- Zhang Q, Babuska I (2020) A stable generalized finite element method (SGFEM) of degree two for interface problems. Comput Methods Appl Mech Eng 363:112889
- Guo R, Lin T (2019) A higher degree immersed finite element method based on a Cauchy extension for elliptic interface problems. SIAM J Numer Anal 57(4):1545–1573
- Xiao Y, Xu J, Wang F (2020) High-order extended finite element methods for solving interface problems. Comput Methods Appl Mech Eng 364:112964
- Cheung J, Gunzburger M, Bochev P, Perego M (2020) An optimally convergent higher-order finite element coupling method for interface and domain decomposition problems. Results Appl Math 6:100094
- Neiva E, Badia S (2021) Robust and scalable h-adaptive aggregated unfitted finite elements for interface elliptic problems. Comput Methods Appl Mech Eng 380:113769
- Badia S, Neiva E, Verdugo F (2022) Linking ghost penalty and aggregated unfitted methods. Comput Methods Appl Mech Eng 388:114232
- Idesman A, Dey B (2017) The use of the local truncation error for the increase in accuracy of the linear finite elements for heat transfer problems. Comput Methods Appl Mech Eng 319:52–82
- Idesman A (2018) The use of the local truncation error to improve arbitrary-order finite elements for the linear wave and heat equations. Comput Methods Appl Mech Eng 334:268–312
- Idesman A, Dey B (2020) Accurate numerical solutions of 2-d elastodynamics problems using compact high-order stencils. Comput Struct 229:106160
- Idesman A (2020) A new numerical approach to the solution of PDEs with optimal accuracy on irregular domains and Cartesian



meshes. Part 1: the derivations for the wave, heat and Poisson equations in the 1-D and 2-D cases. Arch Appl Mech 90(12):2621–2648

- Dey B, Idesman A (2020) A new numerical approach to the solution of PDEs with optimal accuracy on irregular domains and Cartesian meshes. Part 2: numerical simulation and comparison with FEM. Arch Appl Mech 90(12):2649–2674
- Idesman A, Dey B (2019) A new 3-D numerical approach to the solution of PDEs with optimal accuracy on irregular domains and Cartesian meshes. Comput Methods Appl Mech Eng 354:568–592
- 28. Idesman A, Dey B (2020) The treatment of the Neumann boundary conditions for a new numerical approach to the solution of PDEs with optimal accuracy on irregular domains and Cartesian meshes. Comput Methods Appl Mech Eng 365:112985
- Idesman A, Dey B (2020) A new numerical approach to the solution of the 2-D Helmholtz equation with optimal accuracy on irregular domains and Cartesian meshes. Comput Mech 65:1189–1204
- Idesman A, Dey B (2022) The numerical solution of the 3D Helmholtz equation with optimal accuracy on irregular domains and unfitted Cartesian meshes. Eng Comput 38:4979–5001
- Idesman A, Dey B (2022) Optimal local truncation error method to solution of 2-D time-independent elasticity problems with optimal accuracy on irregular domains and unfitted Cartesian meshes. Int J Numer Methods Eng 123(11):2610–2630
- Idesman A, Dey B (2022) Optimal local truncation error method for 2-D elastodynamics problems on irregular domains and unfitted Cartesian meshes. Int J Numer Anal Methods Geomech 46(16):3096–3120
- 33. Idesman A, Dey B (2020) A high-order numerical approach with Cartesian meshes for modeling of wave propagation and heat transfer on irregular domains with inhomogeneous materials. Comput Methods Appl Mech Eng 370:113249
- 34. Idesman A, Dey B (2021) Optimal local truncation error method for solution of wave and heat equations for heterogeneous materials with irregular interfaces and unfitted Cartesian meshes. Comput Methods Appl Mech Eng 384:113998
- 35. Idesman A, Dey B (2022) 3-rd and 11-th orders of accuracy of 'linear' and 'quadratic' elements for the Poisson equation with

- irregular interfaces on unfitted Cartesian meshes. Int J Numer Methods Heat Fluid Flow 32:2719-2749
- 36. Idesman A, Mobin M (2022) Optimal local truncation error method for solution of 3-D Poisson equation with irregular interfaces and unfitted Cartesian meshes as well as for post-processing. Adv Eng Softw 167:103103
- Idesman A, Dey B, Mobin M (2023) Optimal local truncation error method for solution of elasticity problems for heterogeneous materials with irregular interfaces and unfitted Cartesian meshes. Mech Adv Mater Struct 30(2):356–372
- Idesman A, Mobin M (2023) Optimal local truncation error method for solution of 2-D elastodynamics problems with irregular interfaces and unfitted Cartesian meshes as well as for postprocessing. Mech Adv Mater Struct. https://doi.org/10.1080/ 15376494.2022.2162639
- Jacquemin T, Tomar S, Agathos K, Mohseni-Mofidi S, Bordas SPA (2020) Taylor-series expansion based numerical methods: a primer, performance benchmarking and new approaches for problems with non-smooth solutions. Arch Comput Methods Eng 27(7):1465–1513
- Zienkiewicz O. C, Zhu J. Z (1992) The superconvergent patch recovery and a posteriori error estimates. Part 1: the recovery technique. Int J Numer Methods Eng 33(7):1331–1364
- Zienkiewicz O. C, Zhu J. Z (1992) The superconvergent patch recovery and a posteriori error estimates. Part 2: error estimates and adaptivity. Int J Numer Methods Eng 33(7):1365–1382
- 42. Kumar M, Kvamsdal T, Johannessen KA (2017) Superconvergent patch recovery and a posteriori error estimation technique in adaptive isogeometric analysis. Comput Methods Appl Mech Eng 316:1086–1156 (Special Issue on Isogeometric Analysis: Progress and Challenges)

Publisher's Note Springer Nature remains neutral with regard to jurisdictional claims in published maps and institutional affiliations.

Springer Nature or its licensor (e.g. a society or other partner) holds exclusive rights to this article under a publishing agreement with the author(s) or other rightsholder(s); author self-archiving of the accepted manuscript version of this article is solely governed by the terms of such publishing agreement and applicable law.

